INSTITUTO POLITÉCNICO
DE BRAGANÇA

NUMERICAL PREDICTION OF THERMAL AND DYNAMIC CHARACTERISTICS OF A FIRE-INDUCED CEILING-JET

Mohamed Seddik Khetata

Final Report of the Thesis Presented to the

School of Technology and Management

Polytechnic Institute of Bragança

To the Fulfilment of the Requirements for the Master of Science Degree in

Industrial Engineering

(Mechanical Engineering branch)

July 2016

This page was intentionally left in blank

NUMERICAL PREDICTION OF THERMAL AND DYNAMIC CHARACTERISTICS OF A FIRE-INDUCED CEILING-JET

Mohamed Seddik Khetata

Final Report of the Thesis Presented to the

School of Technology and Management

Polytechnic Institute of Bragança

To the fulfilment of the Requirements for the Master of Science Degree in

Industrial Engineering

(Mechanical Engineering branch)

Supervisor at IPB: Prof.Dr.Paulo Alexandre Gonçalves Piloto

Supervisor at UHBC: Prof.Dr. Abdallah Benarous

July 2016

This page was intentionally left in blank

ACKNOWLEDGMENT

My thanks go especially to my parents Ahmad Khetata and HakimaBoumaza who supported me from the beginning and without their i would not be where i am today.

I would like to thank my major professor at IPB, Dr Paulo Alexandre Gonçalves Piloto for his expertise and guidance and his important advices not just in my work even in all domains of my life experience in Portugal. I must also express my gratitude to professor Luis Mesquita and all the staff of the Instituto Politécnico de Bragança (IPB) for all the facilities provided for allowing studies in perfect conditions. Special thanks to Dr Augusta Mata for her pedagogic and social assistance.

My kind acknowledgements to my supervisor at the Hassiba Benbouali University (UHBC) of Chlef (Algeria), Pr Abdallah Benarous for his support and guidance and all the key persons of the ERASMUS+ program, especially Pr. Dr Lamri Belkacem and Mr Kada Abdelhak. A special thanks to Pr. Dr Mahmoudi Hacene from UHBChlef.

I thank also my sisters, Nadia and Ihcene, my friends and colleagues from IPB Portugal for the good times

This page was intentionally left in blank

ABSTRACT (EN)

The aim of this thesis is to test the ability of some correlative models such as Alpert correlations on 1972 and re-examined on 2011, the investigation of Heskestad and Delichatsios in 1978, the correlations produced by Cooper in 1982, to define both dynamic and thermal characteristics of a fire induced ceiling-jet flow. The flow occurs when the fire plume impinges the ceiling and develops in the radial direction of the fire axis. Both temperature and velocity predictions are decisive for sprinklers positioning, fire alarms positions, detectors (heat, smoke) positions and activation times and back-layering predictions. These correlative models will be compared with a 3D numerical simulation software CFAST. For the results comparison of temperature and velocity near the ceiling. These results are also compared with a Computational Fluid Dynamics (CFD) analysis, using ANSYS FLUENT.

Key words

Fire, CFAST, Correlative models, ANSYS FLUENT, Ceiling jet

This page was intentionally left in blank

ABSTRACT (PT)

O objetivo desta tese é testar a capacidade de alguns modelos de correlação, tais como o modelo de Alpert definido em 1972 e redefinido em 2011, a investigação de Heskestad e Delichatsios em 1978 e as correlações produzidas por Cooper em 1982, para definir as características dinâmicas e térmicas de um fluxo de gases tipo jato produzido junto ao teto induzido por fogo. O fluxo ocorre quando a chama de fogo atinge o teto e se desenvolve na direção radial em relação ao eixo do fogo. Ambas as previsões de temperatura e velocidade são decisivas para posicionamento de “sprinklers”, posicionamento de detetores de incêndio, posicionamento de detetores de calor e fumo, tempos de ativação de alarmes e previsões de estratificação de camadas de escoamento. Estes modelos correlativos serão comparados com um modelo 3D de um programa de simulação numérica CFAST, para a comparação dos resultados de temperatura e da velocidade perto do teto. Estes resultados são ainda comparados uma análise de dinâmica de fluidos computacional CFD, utilizando ANSYS FLUENT.

Palavras chave

Incêndio, CFAST, Modelos correlativos, ANSYS FLUENT, Escoamento de jato no teto

This page was intentionally left in blank

INDEX

LIST OF FIGURES

LIST OF TABLES

LIST OF TABLES OF ANNEX A

LIST OF TABLES OF ANNEX B

LIST OF TABLES OF ANNEX C

LIST OF TABLES OF ANNEX D

NOTATION

Latin lower case letters

g_z	Components of acceleration due to gravity [m/s^2]
$\dot{h}$	Heat flux [w/m^2]
$\dot{h}_{net}$	Net heat flux[w/m^2]
$\dot{m}_p$	Plume mass flow rate [kg/s]
r	Radial coordinate of plumes and ceiling jets [m]
t	Time [min]

Latin upper case letters

C_p	Specific heat at constant pressure [kJ/(kg K)]
D	Diameter of fir source [m]
E	Energy of combustion [MJ]
H	Height of the compartment [m]
H_f	Vertical distance between the floor and the ceiling [m]
H_s	Distance between the fire source of the car and the floor
$K_{xx,yy,zz}$	Thermal conductivity in x,y,z directions
L_f	Flame height [m]
L_h	Horizontal flame length
Q_V	Volumetric heat source
$\dot{Q}$	Total heat release rate (HRR) [kW]
$\dot{Q}_c$	Convective heat release rate [kW]
Q_D^*	Heat release coefficient related to the diameter of the local fire
Q_H^*	Non-dimensional hate release rate [W]
T	Gas temperature [°C]
T_{max}	Maximum temperature in the jet flow [°C]
T_m	Surface temperature of the member [°C]
$T_{(z)}$	Plume temperature along the symmetrical vertical flame axis [°C]
T_∞	Ambient temperature [°C]

V	Velocity vector
V_{max}	Maximum velocity [m/s]
$V_{x;y;z}$	Velocity in x,y,z directions
Z	Vertical distance [m]
Z_0	Height of virtual source above burning item [m]
Z'	Vertical position of the virtual heat source [m]

Greek letters

α	Convection
α_c	Coefficient of heat transfer by convection
ε	Emissivity
ε_f	Emissivity of fire
ε_m	Surface emissivity of the member
σ	Stephan Boltzmann constant =5.67×10^{-8} w/m^2k^2
∅	Configuration factor
δ	Thickness of ceiling jet [m]
λ	Thermal conductivity [kW/(m °C)]
ρ	Density [kg/m^3]
ρ_∞	Ambient air density[kg/m^3]
∇	Del operator

1- INTRODUCTION

One of the most interesting issues in fire engineering and fire safety is the rapidity of detecting fire using fire detection systems which operate in function of the hot gases and smoke. Our study case is fire induced the ceiling jet.

The velocity and temperature of the hot gases due the fire in compartment are two major values that we must take in consideration in the studies of fire, the main goal of this work is doing different numerical simulations using two commercial software, which are CFAST(Consolidated Model of Fire and Smoke Transport), an advanced calculation method based on the two zone models: and CFD (Computational fluid dynamics). Also simple calculation methods, based on the correlative models devoted to fire plumes and ceiling jets were used to compare results of temperature and velocity near the ceiling which is considering unconfined in six radial positions of a localized fire. Five car categories in different fire scenarios of burning car in open car parking were considered for analysis.

After the different numerical simulation and calculation there are a set of results which are discussed in this work, showing in which region of targets positions the results correlate and are in agreement between them, or exist a relative difference.

These kind of results give us more information about the activation time of fire detectors which can be sprinklers or heat alarms. By this way the fire will be sufficiently small and easily controlled.

1.1- State of the art

This work presents the analysis of a fire induced ceiling jet and a comparison between correlative models and two zone models. The main objective is to compare the temperature and velocity of the gas near the ceiling for different ratio parameter (r/H). The radial coordinate of plumes and ceiling jets (r) and the height if the compartment (H).

On May 18th, 1972 in Philadelphia, at the 76th Annual Meeting of the National Fire Protection Association there was a presentation about the calculation of response time of Ceiling-Mounted Fire Detectors [1]. Measurements of gas temperature have been made with a burning fuel during the fire tests in order to determine how gas temperature T, varies with the vertical distance Z, below the ceiling at several radial positions, from the plume axis. In each case outside of fire plume the maximum gas temperature occurs just near the ceiling. Experiments show that gas temperature decreases with vertical distance Z, below the ceiling.

however the value of T_{max} refers to maximum temperature in the jet flow close to the ceiling. Therefore at all radial positions, especially close to the fire plume gas temperature decreases as the ceiling height increases. Measurements of gas velocity have been made in similar fire tests, using different radial positions, including the fire plume. The gas velocity is nearly constant in the fire plume but decreases sharply with radial distance beyond the fire plume.

In 1979, at the Seventeenth Symposium (International) on Combustion, the Factory Mutual Research Corporation, Norwood, Massachusetts presented an investigation about the initial convective flow in fire [2]. This study concerns physical modelling of the initial fire environment generated by fire in an enclosure. The experiments were conducted in a large test building located in West Glocester. With two floor-to ceiling. The substructure within the building volume contains office space, observation rooms, shop areas, stairways, and special-purpose rooms. All apertures communicating with the test volume (windows, doors) were closed during the experiments, and there was no forced ventilation. The compartment was equipped with sprinkler piping mounted below ceiling level. The fire source (wood-crib) rested on a load table, and centred on a square wood platform on the side. The platform either rested on the floor or was mounted on an electrically powered elevating device which accurately positioned the platform. Ceiling instrumentation was mounted at stations along from the geometric fire axis. Each station incorporated two types of anemometers (pressure-differential type and hot wire), one thermocouple, one optical density meter and five types of fire detectors. The sensing level of all instruments was below ceiling level sections of the sprinkler piping, that were temporarily removed for the experiments. The building was cleared of smoke between experiments. As results from these experiments, the recorded gas velocities varied in magnitude from a fraction of one [m/s] near the ignition time, caused by normal drafts in the test building, to several [m/s] late in an experimental fire and close to the fire axis. Velocity data were accepted from each instrument station at the earliest time that the recorded signal showed systematic change due to fire activity. The flow axis of the fire plume was well centred on the geometric fire axis and the four temperature measurements were averaged into a single value to represent the radius. For fires growing with the second power of time, explicit relations have been determined for non-dimensional temperatures and velocities in the hottest layer under large flat ceilings. The local gas velocity in the hottest layer under flat ceilings can be related directly to the local temperature rise and ceiling clearance, regardless of time from ignition, fire-growth rate and, possibly, fire-growth behaviour [2].

In 1981, the National Bureau of Standards Centre for Fire Research completed an investigation about the structure and heat transfer properties of fire and fire plumes in horizontal ceiling [3]. The experiment used natural gas as fire source with a specific diameter, and emphasized two different heating release rates. The profiles of the average velocity and temperature were defined and compared with predictions of differential and integral results. The integral model provides good results for average velocity, temperature and composition in both combustion and non-combusting plumes, also for analysing plume properties, which could be extended to treat the properties of the ceiling jet. Some compromises were also dictated by the need to ultimately extend the approach to the ceiling-jet region. Estimates of radiative heat fluxes, however, were less satisfactory. Measurements reported by Alpert, Zukoski and co-workers were evaluated and presented investigation for a reasonable prediction of both flow properties and ceiling heat fluxes. There have been numerous attempts to model the properties of natural fires, integral models are typified by Wilcox and Taminini. Alpert has developed a comprehensive model describing this flow, and also provides some data on the ceiling of heat transfer rate and temperature and velocity. The previous work about flame impingement on a ceiling, measurements of the structure of the flow have been very limited. Predicting radiation in turbulent combustion flows represents a significant theoretical problem in its own right, even when the flow structure is known [3].

In 1984, on Twentieth Symposium International Combustion, the National Bureau of Standards Washington, DC, U.S.A. done a research about a buoyant source in the lower of two, homogeneous, stably stratified layers [4]. A point source of buoyancy is located at a specified elevation within the lower of two, homogeneous, stably stratified layers. Fire scenario was presented by Cooper. The concept of an "extended upper layer equivalent point source" is combined with the unconfined ceiling analysis of Cooper. The plume dynamics in the upper layer is described as being generated by a point source fire of strength Q', located a distance H' below the ceiling, and in an infinite "ambient" environment of temperature, T_{up}. The values Q’ and H’ are computed by invoking a principle of continuity which conserves plume mass and enthalpy flux across the upper layer interface. With Q' and H' in hand, the unconfined ceiling solution of Cooper is used to predict heat transfer to the ceiling. This method gave analytic results which were compared favourably to experimental data reported by Zukoski and Kubota. Set of model equations to describe the plume dynamics in enclosure fire scenarios was defined. Although the model equations and their solutions are remarkably simple, they were found to provide useful predictions to plume centreline temperatures, and to convective ceiling heat transfer fire scenarios [4].

In January 1986, a master thesis submitted to the Worcester Polytechnic Institute in Fire Protection Engineering shows how to use the fire plume theory in the design and analysis of fire detector and sprinkler [5]. The correlations for t^2 fires were developed using data from a series of wood crib burn tests. In their updated paper, Heskestad and Delichatsios also provided correlations for ceiling jet temperature and velocity from t^2 fires, based only on the convective heat release rate. The test fires had a convective heat release fraction of approximately 75%. Modelling fuels having different convective fractions will produce some degree of error. This thesis demonstrates how the response of fire detection and automatic sprinkler systems can be designed or analysed. National Bureau of Standards furniture calorimeter test data is compared to heat release rates predicted by a power-law fire growth model. The test was a burning tray with alcohol, located in the centre of a test room, with presence of sprinkler devices located on the ceiling in a square array. Other tests were done at the West Glocester facility to measure the effects of ceiling height and fire growth rate on the response of fire detectors. These tests included only open flaming fires and no smouldering fires. All tests were conducted under a large, flat ceiling with no walls. Three ceiling heights were selected for the tests. The height of the ceiling above the fuel surface changed with each different fuel configuration. Fire growth rate was varied by using three different wood crib configurations. This gives nine possible combinations of fire growth rate and ceiling height. Several of the tests were repeated to help determine the repeatability of the testing procedures. As result, equations were presented to calculate fire gas temperatures and velocities. The equations were proposed by Heskestad and Delichatsios to model temperatures and velocities along a flat ceiling with no walls [5].

On July 1991, the U.S. Department of Commerce and the National Institute for Standards and Technology Building and Fire Research Laboratory, published a report about the characterization of the confined ceiling jet in the presence of an upper layer in transient and Steady-State Conditions [6]. This report is the result of the analysis of data collected by Motevalli for confined smooth ceiling jets in transient and steady-state conditions. Comparison with the unconfined study by Motevalli and Marks (1990) is also made. The data collected for the unconfined case is extensive and detailed. A more limited set of data were collected for the confined case, however, a good comparison can be made between the data collected for the two cases. The same apparatus was used to test both cases, but modified for the second case to create a confined ceiling by adding a one half meter curtain wall to the perimeter of the ceiling. Examination and comparison of the two cases helped to define the confined ceiling jet characteristics and the effect of the developing upper layer. The results

can be used to aid in the development and verification of compartment fire models and to improve the design and placement of heat detectors and sprinklers. Results from the steady-state unconfined ceiling jet have been used to predict the ceiling jet characteristics for confined ceiling jets at early times in the fire. The basis for comparison is the fact that the unconfined ceiling jet has been studied extensively. Using the unconfined ceiling jet allowed the study of the jet characteristics alone without any interference from the developing upper layer. The unconfined ceiling jet simulates a condition where the walls are much further from the plume centreline [6].

In 1991, the Centre for Fire Safety Studies and Mechanical Engineering Department at the Worcester Polytechnic Institute and Mechanical Engineering Department from the University of Maryland completed the reassessment about characterizing the unconfined ceiling jet under steady-state conditions [7]. Detailed velocity and temperature measurements using cross-correlation velocimetry were obtained for unconfined ceiling jets under ceiling transient and steady-state conditions. Small fires were produced with a premixed methane-air burner. These measurements represent one of the most detailed studies of unconfined ceiling jets to date and seem to be in general agreement with large-scale data. Wall-jet studies of Glauert and Poreh, et. al. have established the ceiling jet to be a boundary-layer type flow. The ceiling jet is characterized using detailed temperature and velocity measurements as a function of respective maximum values, vertical distance from the ceiling (Z), and radial distance from the plume impingement point (r). Previous studies from Alpert, Veldman et al, You and Faeth and Heskestad and Delichatsios have produced correlations for the ceiling jet maximum ve1ocity and temperature. Alpert assumed a Gaussian behaviour for the velocity and temperature profiles and has developed an integral model for the boundary layer thickness. Beyler has also compiled and compared a list of ceiling jet correlations. The comparisons demonstrate that the agreement between the empirical models presented is not always as good as desired and no correlations defining the velocity and temperature profiles exist. Furthermore, very 1imited ceiling jet velocity measurements have been obtained. The experimental apparatus considers a ceiling, built with thick fibre board material, and the back face of the ceiling was insulated. The surface of the ceiling was painted and the emissivity was measured. A premixed methane-air burner with inside diameter was used. Small steady fires in the range were produced using this burner. This ensured a blue, short flame producing a nearly pure buoyant plume. The burner mouth was placed flush with an artificial floor whose distance to the ceiling could be modified in order to vary the floor to ceiling height. Fire strengths were used and measurements were made for two heights at r/H locations due to

the 1imited number of thermocouple pairs and their distribution, each experiment was repeated 3 to 4 times. Each time, the probe was positioned at a different distance from the ceiling. This provided enough data to complete velocity and temperature profiles. By default, this procedure also demonstrated the high degree of repeatability obtained. It is concluded that there is a general agreement between the different correlative models. Poreh et al used model that agrees well with Heskestad and Delichatsios at one of the radial position, but overestimates the data by 30% and 50% when r/H is smaller than 0.7. Cooper's model predicts an unreasonably high V_{max} at small r/H values and probably is not accurate in that range (r/H<0.4). Alpert's data were obtained using a hot-wire probe while Heskestad's measurements were made employing a bidirectional probe. The empirical equation from this work seems to closely agree with that of Alpert is in a general agreement with Heskestad and Delichatsios's correlation, both of which are for large-scale experiments. The velocity measurements by the authors are also much more detailed than those by other investigators. You and Faeth concluded that Alpert's integral model generally underestimates the measured maximum temperature, Heskestad and Delichatsios also show lower temperature in their large-scale experimental results. In addition, accurate determination of the location of maximum temperature requires very detailed measurements [7].

In 1995 the Society for Fire Protection Engineers (SFPE) update the Handbook of Fire Protection Engineering. Chapter 4, contains a research about ceiling jet flows [8]. Early studies at the Fire Research Station in Great Britain, and more recently at Factory Mutual Research Corporation, the National Institute of Standards and Technology (NIST), and at other research laboratories, have sought to quantify the gas temperatures and velocities in the hottest portion of the flow produced by steady fires beneath smooth, unconfined horizontal ceilings. Gas temperatures, and the depth of steady fire-driven ceiling jet flows has been developed by Alpert. This work involved the use of several idealizations in the construction of the theoretical model, but results are likely to provide reasonable estimates over radial distances of one or two ceiling heights from the point of fire plume impingement on the ceiling. His work quantified the maximum gas temperature and velocity at a given position in a ceiling jet flow produced by a steady fire. The correlations apply only during times after fire ignition when the ceiling flow may be considered unconfined. Experiments have shown that, unless great care is taken to ensure that the fuel perimeter is in contact with the wall surfaces, the method of reflection used to estimate the effects of the walls on ceiling jet temperature will be inaccurate. Generally, the results of Heskestad and Delichatsios predict larger temperature rises and gas velocities than Alpert’s results. These predictive methods apply to

quantifying the maximum temperature and maximum velocity at a given position in the ceiling jet flow and apply to situations where the flow can be considered unconfined. These methods are the basis for acceptable design [8].

In March 2002, National Institute of Standards and Technology (NIST) and U.S. Department of Commerce and Technology Administration completed a research about Comparison of CFAST and FDS for Fire Simulation with the two tests [9]. This work uses three methods: hand calculations, a zone model code (CFAST), and a computational fluid dynamics code (FDS) [10], to examine both two fire tests. The two tests used different fuels, propane gas and a hydrocarbon solvent, and occurred in two quite different locations. CFAST has both a user's manual describing how to run the code and a theory manual describing the internal workings and theory behind the code, as conclusion about this tests. The first tool examined was the application of simple hand calculations to the two fire tests. Hand calculations cannot be expected to yield precise information on a fire investigation. However, one can expect that a hand calculation yields sufficient information regarding a fire to determine whether or not a more detailed analysis is needed. This work has clearly shown that CFAST is in need of significant improvements if it is to be used in a performance-based code regime for analysing entire compartments. Far-field mass flows, temperature changes, and propagation of gas species are not well predicted by CFAST. Even near-field predictions of temperatures and mass flows can be in substantial error. FDS, as well as other Computational Fluid Dynamics (CFD) methods in general, is a relative newcomer to fire protection. CFD models such as FDS are not easy to use. Furthermore, their computational requirements greatly limit their applicability [9].

In 2006, the Department of Fire Protection Engineering of the University of Maryland presented a thesis about the characterization of fire induced flow transport along ceilings using salt-water modelling [11]. In these studies, salt-water modelling measurements were compared to following correlations recommended by Zukoski and al. Once the plume impinges on a ceiling, it turns to form a radially expanding ceiling jet. Alpert performed an analytical and experimental study developing the theory and associated scaling laws for fire induced ceiling jets. His analysis successfully predicted the maximum temperature distributions in the ceiling jets and is widely used in hazard analysis. Based on his analysis, he provided relationships for dimensionless ceiling layer thickness, velocity, and temperature, which compares favourably with measurements. He suggested that credible small-scale fire experiments could be conducted at ceiling heights down to 0.6 m. Motevalli and Marks conducted small-scale experiments of ceiling jet heat transfer, which generally compared

favourably with other ceiling jet data and analysis. The velocity and temperature measurements were obtained for unconfined ceiling jets under ceiling transient and steady-state conditions. These experimental and mathematical modelling studies have provided the necessary understanding to predict some of the general transport behaviour in fires based on empirical correlations. The results of these investigations have advanced the understanding of fire phenomena and improved the design of fire protections systems. However, detailed measurements in well controlled experiments are required for model development. In particular, characterizations of the velocity field in fire plume configurations are notably absent [11].

In 2010 on The fifth Fire Seat Event, Alpert presented a research about the fire-induced ceiling-jet (revisited) [12]. Data on near-maximum gas velocity and excess temperature in the ceiling jet induced by large-scale fires that were used to obtain well-known ceiling-jet formulas published in 1972 have been re-examined in light of knowledge on the virtual plume origin and the convective component of the fire heat release rate. Although the original formulas were presented without any experimental evidence, these relations seemed to be accepted as fact by many fire protection practitioners and even some researchers. One reason for this acceptance was an internal technical report that had already been widely distributed to fire researchers in the USA and internationally in 1971. This report described the ceiling jet model, a few data points from a full-scale fire test and sample data from small-scale (yet mostly turbulent) laboratory experiments. Subsequent to this report, the author examined available data from a variety of full-scale fire tests, with the resultant correlations of these data, inspired by the ceiling jet model, for excess gas temperature and velocity, respectively. Gas temperatures and velocities were measured by thermocouples and hot-wire anemometers, respectively, at several radial locations and at a few distances below the ceiling to be able to estimate maximum values. Most of such measurements were finally made at about 150 mm or less below the ceiling. The heat release rate used in the ordinates was the product of measured mass loss rate from a load platform (or heptanes flow rate in the case of the nozzle array) and an estimate of the actual value for heat of combustion during a typical fire, what is often now called the chemical heat of combustion. The length scale used for the correlation was the ceiling height above the top surface of the fuel, which for the heptanes sprays, was the height above the plane of the spray nozzles. Measurements were made in a very large test building facility in order to minimize the effects of ambient drafts and the accumulation of combustion products in a descending smoke layer. It can be seen that, except for the power of r/H in the gas velocity correlation, the new regression fit is nearly identical to

the original. The original power of r/H may have been selected with some degree of arbitrariness to obtain the rational number. Accordingly, a re-examination of data underlying the 1972 ceiling jet formulas has produced new regression fits that should be more reliable than the original formulas. Such algebraic formulas are useful for predicting detection and activation times of ceiling mounted devices, e.g., fire sprinklers. To determine what mass flux of agent droplets from these activated sprinklers arrives at the fire source [12].

In 2013, during the thirteenth international interflam conference, a paper about simple ceiling jet correlation derived from numerical simulation was presented [13]. Numerical simulations were used in this paper for two purposes. Firstly, an evaluation of previously derived correlations for ceiling jet excess temperatures and velocities was performed. Secondly the numerical simulations were used to demonstrate how computer simulations could be used as a complement to actual fire experiments in fire science research. Correlations to estimate temperatures and velocities in the hot gases beneath a ceiling in a fire are cited. These types of correlations are often used in fire safety engineering in order to get an estimate of sprinkler or heat detector activation in enclosure fires. Alpert assumed an axisymmetric and unconfined fire induced flow beneath a flat, horizontal ceiling, the ceiling jet divided into two regions. Thus two sets of correlations were defined. The maximum excess temperature and maximum velocity were defined in the turning region where the plume impinges the ceiling and these formulas are independent of the radial distance of the plume. The second set of correlations is valid in the far field and is dependent on the radial distance from the plume centre line. A total of 90 numerical simulations have been carried out in order to gather data. The numerical simulations were performed with the CFD model from FDS software. The heat release rate, room height and ceiling surface properties were varied in the numerical simulations. The heat release per unit area was kept constant but the fuel area varied which created 12 different constant heat release rates. The radiation fraction was kept constant in all the simulations. Seven different room heights were defined. The unobstructed and unconfined ceiling surface was either inert (a non-reacting solid boundary whose temperature is constantly fixed at initial ambient temperature or adiabatic non-reacting solid boundary with a calculated wall temperature). The domain of the fire compartment was sufficient large to avoid any board effect from this dimensions. All vertical sides of the domain were modelled as open to the surroundings. Two different properties of ceiling were used, inert or adiabatic, in the numerical simulations. The predicted temperature is presented in order to compare these two boundary conditions. A comparison of the temperature calculated with equation for maximum temperature of Alpert and the maximum and average temperature in FDS is

presented for two ratio parameters (r/H=0.5 and 0.9) from the plume centreline. The average temperature is derived as the mean of the temperature in the four cells just below the ceiling. The temperature gradient in the ceiling jet is also analysed. The maximum temperature in FDS is roughly 30-50% higher than predicted with equation for maximum temperature of Alpert. The difference is a bit less for the inert case. The maximum temperature was almost always located in the cell closest to the ceiling. This is regarded reasonable in regard to previous research on the location of the maximum temperature, because the cell closest to the ceiling covers 1-2%, depending on simulation, of the ceiling height. A comparison of the velocity calculated equation for maximum velocity of Alpert and the maximum and average velocity in FDS is presented for two ratio parameter distances (r/H=0.5 and 0.9) from the plume centre line. The average velocity is derived as the mean of the velocity in the four cells just below the ceiling. The velocity gradient in the ceiling jet is also analysed. The maximum velocity in FDS is roughly 70-80% higher than predicted with equation for maximum velocity of Alpert. There is a negligible difference between the inert and adiabatic case. Close to the plume there is a reasonable correspondence of the gas velocities. However, further way from the plume the average gas velocity was calculated with FDS roughly 10-25% higher than predicted with Alpert correlations [13].

In 2015, the SP Technical Research Institute of Sweden completed a report about fire-induced ceiling jet characteristics in tunnels under different ventilation conditions [14]. Theoretical analyses and experiments were conducted to investigate the ceiling jet characteristics in tunnel fires. A series of fire tests was carried out in two model tunnels with a scaling ratio, with varying heat release rates, ventilation velocities, fire source heights and tunnel geometries. Tests were carried out in two model tunnels to investigate the ceiling jet characteristics in SP's large fire hall. The model tunnel is constructed using thick Promptest L, with the exception of the lower part (50 %) of one side of the tunnel which is covered with a fire resistant window glaze, mounted in steel frames. The material is chosen according to the scaling theory proposed by Li and Hertzberg, to simulate concrete and rock used in tunnels (or a mixture of dense and medium dense concrete). A long tunnel section with grids was used as static box to smooth the flows. The end of the tunnel was set below a smoke hood through which the smoke was exhausted to the central exhaust cleaning system. The fire sources were placed in the centre of the model tunnels, the corresponding fire could be a car fire or a bus fire. An axial fan is attached to the end of the tunnel to produce a longitudinal flow in tests with longitudinal ventilation. For the tests with natural ventilation, the fan was removed. To investigate the fire spread to neighbouring objects or vehicles, wood and plastic

bricks were placed in the tunnel on the floor, one thermocouple and one heat flux meter were placed as targets on the floor. General conclusion about the results of this test and comparison between these results and some equations about the velocity and temperature near the ceiling are presented, being the equation proposed by Li et al very good to define gas velocities and temperatures for the test [14].

1.2- Ceiling jet fires

The studies about fire plume and ceiling jet are very important for improving fire detection system designs and practices, such as the designs of activation devices for heat alarm and many types of smoke and fire detectors.

The ceiling jet is created when there is an impingement between a buoyant plume and flat unobstructed ceiling where the hot gases spreads radially under the ceiling. Or it is the rapid flow of gas in a surface layer below the ceiling surface that is driven by the buoyancy of hot combustion products. Ceiling jet is formed when the plume (hot gas) touch the ceiling. When these hot gases rise vertically from a fire and entrain the surrounding air to form a plume, reaching underneath the ceiling, the plume turns sideways and forms a ceiling jet. The ceiling jet grows in thickness as the temperature and velocity decrease. The characteristic parameters of ceiling jets are based on are flame lengths, ceiling jet velocity, ceiling jet mass flow rate, gas temperatures, radiation and fire spread distance from the plume centreline axis to the point at which the ceiling jet properties are to be examined (r). Fire detectors and activators (sprinklers...) are placed near the ceiling surfaces, see Figure 1 The magnitude of the horizontal gas velocity and temperature in the ceiling jet determine if fire detectors and sprinklers can be actuated. The major factors controlling a ceiling jet are: the momentum, the buoyancy forces, the rate of entrainment, and the heat transfer to the ceiling [15]. The fire plume is formed when a mass of hot gases surrounded by a cold gas or when buoyancy happens. The difference in density will rise the hotter and less dense mass upward. There is an outline of ceiling jets and ceiling flames which are models tested for unconfined fire plume. The most commonly unconfined plume used in fire safety engineering, is buoyant axisymmetric plume which is the result of flame diffusion formed above the burning fuel, this plume contain three zones which are respectively: continuous flame or persistent flame, intermittent flame, than buoyant plume, as shown in Figure 2.

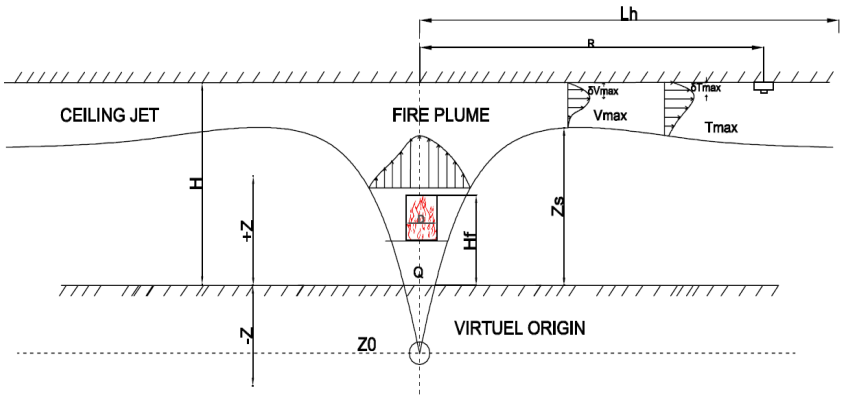

Figure 1-Schematic diagram for small localised fire

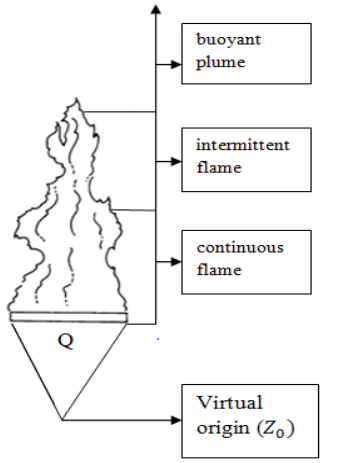

Figure 2- The three zones of the axisymmetric buoyant plume[16]

1.2.1- Fire plume characteristics

Hot products caused by buoyancy are generated in a fire to rise to the ceiling while mixing with room air to form a fire plume, which has the following properties : virtual origin, denoted Z_0 depends on the diameter of the fire source (D) and the total energy released ($\dot{Q}$). When Z_0 lie beneath the fuel source, it is negative and means that the area of the fuel source is large compared to the energy being released over that area. On the other hand, Z_0 is positive when located above the fuel source. So, the fuel releases high energy over a small area. Z_0 is given by:

$$Z_0 = 0.083\dot{Q}^{\frac{2}{5}} - 1.02D \quad (1)$$

The main parameter of the plume is the velocity. The biggest velocity is located at the centreline of the plume, denoted by U_0, and changes with height [16]. Then the plume

temperature is the other main parameter which can achieve the highest value near the centreline of the plume and is denoted by T_0. The third parameter is plume mass flow rate ($\dot{m}_p$). The plume mass flow increases steadily with height, since ambient air is continually entrained over the plume height [17]. The last parameter is the plume radius (r) that corresponds approximately to the point where the centreline temperature decreases to $0.5T_0$ [16] and the centreline velocity has decreased to $0.5U_0$.

1.2.2- Examples of ceiling jet fires

This section is going to present some examples about fires in unconfined ceiling jet. One famous example is the fire induced ceiling jet in tunnels. A buoyant smoke layer in a tunnel can be summarized into four phases or regions [17], the ceiling is impinging by the plume, then after impingement smoke under the ceiling spread radially which happening in the second region, on the third phase there is the interaction with side walls, and then the transition to the fourth phase which is one-dimensional spreading. In fire tunnels the smoke flow should be in two opposite directions. The complex heat transfer, including convective and radiative heat loss to the boundaries, when a smoke flow travels along the tunnel, there would be a boundary layer contacting the tunnel ceiling. The smoke flow temperature would decrease along the tunnel primarily due to the heat loss to the tunnel ceilings through this boundary layer [17].

Another typical case of ceiling jet fire can occur when fire happens in open car park. The basic characteristics of an open car park are Openings in external walls, limitation of the distance between façades, limitation of floor areas [18], may keep the fire limited on the ignition zone. In a fire event of a car it was observed that the flames extend out of the car, mainly through the windscreen and the rear window. The hot gases in the flames and above them move upward due to buoyancy, this flow of gases corresponds to the fire plume. The burning of a car is usually divided into two plumes which are called as the front and the rear fire plumes, and the summation of the heat releases included in the two fire plumes is equal to the heat release of the vehicle [19]. Several details about this case of ceiling jet fire will be given in a dedicate section.

1.3- Plan of thesis

Chapter one presents the state of the arte, contains different experimental investigation done by the researchers and comparison of the results for the temperature and velocity of the gas near the ceiling for different parameters. This chapter also includes an introduction about ceiling jet fire.

Chapter two contains a definition of different fire scenarios in open car parking, using a localized fire for the event of a car fire. Different car classes burning events will be presented with the results of the Heat Release rate (HRR) for each class.

Chapter three provides a general definition of heat transfer with discussion of the different modes of heat transfer which are included in this phenomenon.

Chapter four presents different correlative models (Alpert, Cooper, Heskestad and Delichatsios) to estimate the maximum temperature and velocity near the ceiling. The results are compared for different fire events and different fire compartments.

Chapter five is dedicated to the numerical simulation using CFAST software. A brief definition of CFAST will be presented followed by a discussion of the results about the maximum temperature and velocity between this simulation and results from the correlative models.

Chapter six is dedicated to the computational fluid dynamics, where this fire event is going to be simulated, based on specific solution for equations.

Chapter seven presents the conclusions and the future research about fire induced ceiling jets.

2- FIRE EVENTS AND DYNAMICS

In order to define some fire scenarios, a typical car fire inside a compartment was chosen. Different fire events were defined, taking into consideration the class of the car. The compartment was fixed and will be explained in this chapter. The ability to predict the dynamics of the fire and protect the compartment from fire damage is of great importance.

2.1- Fire in open car park

A car park may be considered as open if for every parking level, the ventilation areas in the walls are situated in at least two opposite facades, equal at least 1/3 of the total surface area of all the walls and correspond to at least 5% of the floor area of one parking level. The burning car is divided into two plumes which are called as the front fire plume and the rear fire plume [18]. Due to many causes of fire in car park that will be discussed on the next paragraph, the flames extend out of the car burning from the windscreen and the rear window, the hot gases move upward due to buoyancy and the fire plume impinges the ceiling of the car park. The burning car is divided into two plumes where the heat release rate included is equal to the heat release by the vehicle. See Figure 3.

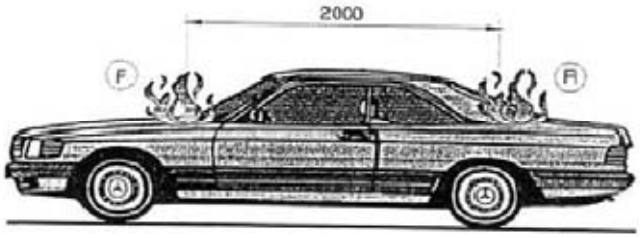

Figure 3- Front (F) and rear (R) fire plume [19]

The main causes of vehicle fire inside a car park can be related with the source of the combustible materials in a vehicle. For example in the passenger cabin, the interior lining, the rubber tires and the fuel, hot exhaust components, overheating of mechanical components, careless use of smoking materials can be responsible for this behaviour. Other causes can be related with electrical short circuit with the availability of amount of oxygen in car parks, the fire can be sustained. The fire spread between parked vehicles is dependent on the geometry of the building, more the compartment effect of fire can increase the likelihood of fire spread.

2.2- Different fire scenarios in car parks

The fire scenario (position and number of the vehicles) should represent the most unfavourable situation for the elements in the compartment (or substructure). The INERIS - Institut National de l'Environnement Industriel et des Risques, considers that fire scenarios with cars of class 3 should be used to evaluate the structural stability of the car park under fire. And the fire resistance of the structure should be ensured during the entire fire scenario, or at least, if allowed by National requirements, up to a certain resistance time R of the elements defined as for the standard ISO (International Organization for Standardization) curve. In addition, a scenario including a commercial vehicle (van containing 250 kg of highly flammable material: E =19 500 MJ) corresponds to an extreme situation and should only be used to check the global behaviour of the structure, assuming local collapse, without progressive collapse [18]. There are basically two approaches available when determining the fire design for a given scenario. One is based on knowledge of the amount and type of combustible materials in the compartment of fire origin.

2.2.1- Classification of cars (car classes)

The cars type used in fire scenario are classified depending on their theoretical energy of combustion (E). The different classes are presented in table one of annex A. According to statistical studies of actual fires in car parks, 90% of the vehicles involved in a fire are classified as class 1, 2 or 3 [19].

2.2.2- Fire scenarios

Scenario 1: assuming that one car burning at mid-span under the beam (corresponding to the maximum bending moment position), it is unrealistic to have two cars improperly parked in the same time which are burning beneath the steel beams and at mid-span assuming that the source of heat is defined by the burning of one car, see next figure. The relative position between the fire source and the limits of the compartment are assumed to be 0.3m above the ground floor and within an area equivalent to a circle with a diameter of 2m.

Scenario 2: involving two burning cars, one on each side of the element of the structure (column). This fire event was considered being the most dangerous for the columns. The time between the ignition of the first car and the second car can be assumed equal to15

minutes [18]. The heat release rate of this scenario can be determined by the envelope of both fire events, considering the fire travelling time.

Scenario 3: may link seven class 3-cars, having the possibility of a commercial vehicle in a special position of each fire event. The heat release rate of this scenario can be determined by the envelope of all fire events, considering the fire travelling time.

Scenario 4: may involves four class 3-cars parked face to face, with the possibility to have a commercial vehicle in each position. For all scenarios, the fire spread time from a vehicle to another may be considered equal to12 minutes, but the initial document by ECCS (European Convention for Constructional Steelwork) recommended a time delay equal to 15 minutes [19].

Scenario 5: involving three cars -class3, parked side by side. The scenario of three cars class 3 involved in a fire is an envelope scenario of around 98.7% of all possible scenarios [19]. The uses of fire scenarios is to define the curve of the real heat release rate of burning car. The five scenarios are represented in Figure 4.

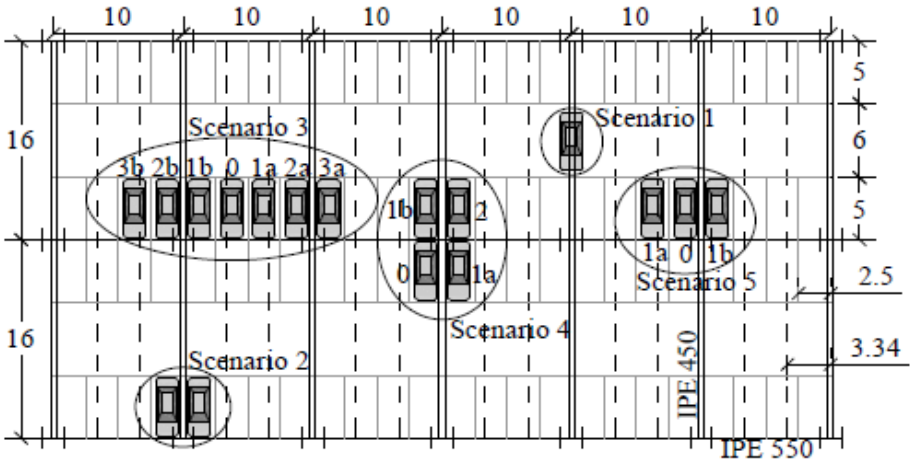

Figure 4- Fire scenarios in open car park (Dimensions given in m) [19]

2.2.3- Localized fires

By definition, localized fire is an event that involves only a limited area of the fire load in the compartment [20]. The determination of the thermal action of localised fires depends on the height of the flame close to the ceiling. A localised fire can be defined for two types of fire (small fires and large fires). For these two kinds of fire, two different correlative models can be applied, with some conditions. The first correlative model allows the calculation of the temperature of the flame, and the second correlative model allows the calculation of the heat flux. This two types of fire can be consider localised if the diameter of

fire D is smaller or equal to 10 m and if the heat release rate $\dot{Q}$ is smaller or equal than 50 MW.

2.2.3.1- Small fires

From Figure 5, the highest temperature is located at the vertical flame axis, which is called the plume centreline (plume zone). This temperature decreases from the source to the edge of the flame in Z direction. It is roughly constant in the continuous flame region and represents the mean flame temperature. The temperature decreases sharply above the flames as an increasing amount of ambient air is entrained into the plume. The design formula to calculate the temperature in the flame, for small localised fire, was proposed by Heskestad, see Eurocode EN1992-1-2. Considering a localised fire as shown in Figure 5, the flame height L_f is given by [20-21]:

$$l_f = -1.02D + 0.0148\dot{Q}^{(\frac{2}{5})} \quad (2)$$

When the flame is not impacting the ceiling of a compartment (l_f< H), or in case of fire in open air, the temperature $T_{(z)}$ in [°C] in the plume along the symmetrical vertical flame axis is given by [21]:

$$T_{(z)}=20+0.25\dot{Q}_c^{\,2/3}(Z - Z_0)^{(-\frac{5}{3})} \leq 900 \quad (3)$$

where

$$Z_0 = -1.02 + 0.00524\dot{Q}^{2/5} \quad (4)$$

And $\dot{Q}_c$ is the convective part of the rate of heat release [kW], with $\dot{Q}_c \approx 0{,}76\,\dot{Q}$ by default. Z_0 is defined as the virtual origin of the fire.

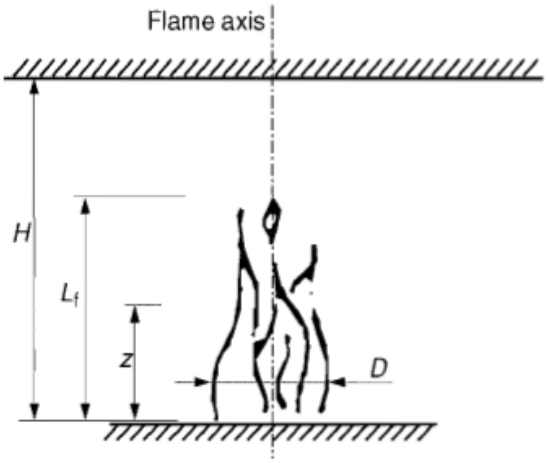

Figure 5- Schematic fire for small localised fire [20]

2.2.3.2- Large fires

In this case the fire plume impinges on the ceiling of the compartment ($l_f \geq H$), the flame turns and moves horizontally beneath the ceiling due to the ceiling surface. Using design formulation based on fire model developed by Hasemi, which is a simple tool for the calculation of the localised effect on horizontal elements located above the fire [21]. A schematic diagram of localised fire when the flame impinges the ceiling is represented in Figure 6, for the case of unconfined ceiling jet. The gas flows from the plume and continuous moving radially outward, loosing heat to the cooler zone of the compartment and also to the ceiling. The maximum temperature and maximum velocity occurs relatively close to the ceiling. When $l_f \geq H$, the horizontal flame length (L_h) in [m] is given by the equation 5, using formulas from [20] to determine the heat flux received by the surface area at the ceiling level, but not for calculation the ceiling jet temperature [21].

$$L_h = (2.9H(Q_H^*)^{0.33}) - H \tag{5}$$

Where Q_H^* in [w] is non-dimensional hate release rate and is given by:

$$Q_H^* = \frac{\dot{Q}}{1.11 \times 10^6 \times H^{2.5}} \tag{6}$$

The virtual origin Z_0 of the axis is given by:

$$Z_0 = -1.02D + 0.00524\dot{Q}^{2/5} \quad (7)$$

When the flame is impacting the ceiling ($l_f \geq H$; see Figure 6) the heat flux $(\dot{h})$ in [w/m^2] received by the fire exposed unit surface area at the level of the ceiling is given by [20]:

$$\dot{h} = 100000 \quad y \leq 0.30 \quad (8)$$

$$\dot{h} = 136300 - 121000\, y \quad 0.30 < y < 1.0 \quad (9)$$

$$\dot{h} = 15000\, y^{-3.7} \quad y \geq 1.0 \quad (10)$$

Where (y) is a parameter [-] given by:

$$y = \frac{r + H + Z'}{l_h + H + Z'} \quad (11)$$

Where (r) is the horizontal distance [m] between the vertical axis of the fire and the point along the ceiling where the thermal flux is calculated, see Figure 6, (Z') is the vertical position of the virtual heat source [m] and is given by:

$$Z' = 2.4D(Q_D^{*\frac{2}{5}} - Q_D^{*\frac{2}{3}}) \quad Q_D^* < 1.0 \quad (12)$$

$$Z' = 2.4D(1.0 - Q_D^{*\frac{2}{5}}) \quad Q_D^* \geq 1.0 \quad (13)$$

Where Q_D^* is heat release coefficient related to the diameter of the local fire

$$Q_D^* = \dot{Q}/(1.11 \times 10^6 \times D^{2.5}) \quad (14)$$

The net heat flux $(\dot{h}_{net})$ [W/m^2] received by the element exposed per surface area at the level of the ceiling, is given by:

$$\dot{h}_{net} = \dot{h} - \dot{\alpha}_c \times (T_m - 20) - T\varepsilon_m\varepsilon_f\sigma[(T_m + 273)^4 - (239)^4] \quad (15)$$

Hasemi´s method is a simple tool for the thermal evaluation of the localized effect of a fire on horizontal elements located above the fire [19].

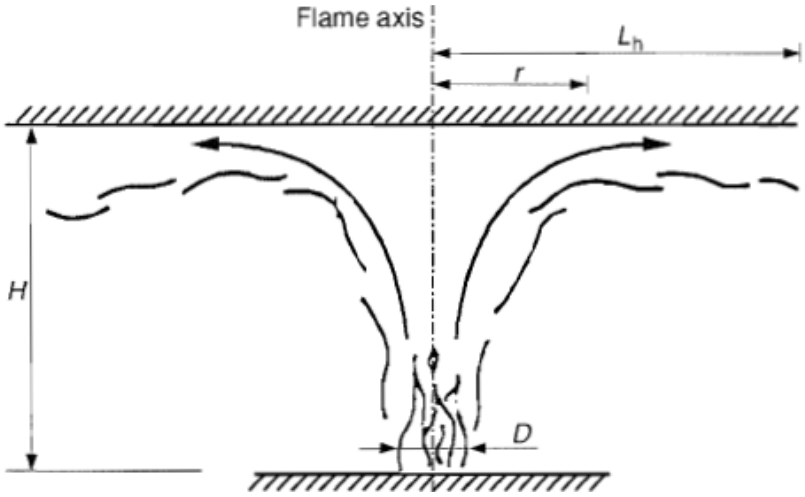

Figure 6- Localised fire impacting on ceiling of compartment [20]

Taking an example of a localised fire in open car park and assuming that fire scenario number 1 was selected, see Figure 7, the main parameters of the fire induce ceiling jet are represented. For this case it is assumed that this fire is equivalent to a pool fire with a diameter D=2 m, an elevation surface Hs equivalent to 0.3 m above the ground and a remaining distance H up to the ceiling equals 2.7 m.

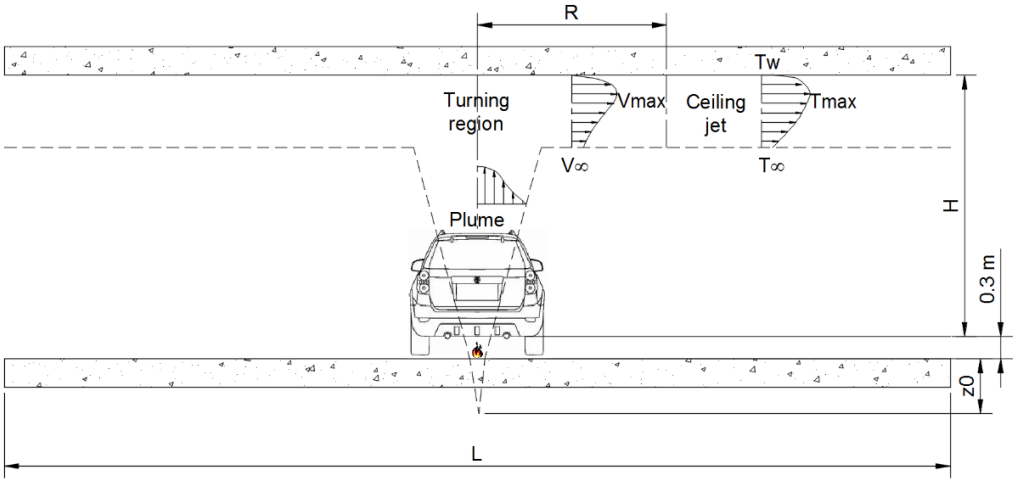

Figure 7- The geometry of the compartment for localized fire vehicle

2.3 - Definition of fire (HRR)

2.3.1- General definition of fire

Fire is a physical and chemical phenomenon that is strongly interactive by nature. The interactions between the flame, the fuel, and the compartment can be nonlinear, and the quantitative estimation of the processes involved is very complex. The burning and the

processes of interest in an enclosure fire mainly involve mass and heat fluxes. The combustion and therefore the fire cannot happen without meeting of the three elements simultaneously: the presence of a fuel or flammable Material, which can be solid (wood, coal, paper....), liquid (gasoline, alcohol ...) or gas (propane, butane), the presence of the oxidizer (oxygen, air, peroxide) and also the ignition source, which is necessary to start burning (spark, flame). The study of fire or combustion includes a number of disciplines such as: heat and mass transport, fluid mechanics, and chemical kinetics.

A fire is as a source of heat which is released at a specified rate. This heat may be defined by the product of enthalpy (the conversion factor is the heat of combustion) and mass loss rate (the conversion factor is the yield of a particular species) as it burns. A fire is constrained if the enthalpy conversion depends on the oxygen concentration otherwise it is unconstrained. Burning can take place in the portion of the plume in the lower layer (if any), in the upper layer, or in a door jet. For an unconstrained fire, the burning will all take place within the fire plume. For a constrained fire, burning will take place where there is sufficient oxygen. When insufficient oxygen is entrained into the fire plume, unburned fuel will successively move into and burn in: the upper layer of the fire compartment, the plume in the doorway to the next compartment, the upper layer of the next compartment, the plume in the doorway to the third compartment, and so forth until it is consumed or gets to the outside [22].

2.3.2- Definition of heat release rate (HRR)

The Heat Release Rate (HRR) is an important parameter to characterise a fire compartment, called also energy release rate. The burning of objects (cars, building....) releases a certain quantity of energy per unit time, it is measured in W, usually noted by ($\dot{Q}$). Fire development is generally characterized in terms of HRR and time. Table 3 of annex A indicates that for many design purposes the design fire energy output could be in the range 100 kW to 50 MW [16]. The heat release rate depends on the type, quantity, and orientation of fuel. The driving force in terms of fire is the heat release rate which means that the production of undesirable effects of fire and its products also elevates with increased HRR. There is a relation between different types of fire hazards and heat release rate, which means that smoke and toxic gases increase in parallel with heat release rate.

2.3.3- Convective heat release rate

The convective heat transfer to ceilings during enclosure fires can be related to the heat transfer to unconfined ceiling surfaces from buoyant plume-driven ceiling jets [23]. This quantity is usually noted by ($\dot{Q}_c$) and is also expressed in power units [kW]. Conducting an energy balance of the combustion products, the HRR can be established from temperature measurements. Two measurements are required: the mass flow of combustion products and the variation of temperature through the calorimeter, $\dot{Q}_c \approx 0.76\dot{Q}$ convective heat flux to the member related to the difference between the bulk temperature of gas bordering the relevant surface of the member and the temperature of that surface [20].

2.3.4- Heat release rate from vehicles

To get results of the heat release rate (HRR) from car burning in car parking, a set of experiments were done. Car tests of VTT (Technical Research Centre of Finland Ltd) in (1991) and by the Fire Research Station in UK and INERIS (Institut national de l'environnement industriel et des risques) in France. A new series of tests performed at CTICM (Centre Technique Industriel de la Construction Métallique) Maizières-Lès-Metz - France within an European research project [24] was important to record rate of heat release by considering other parameters: new series of cars, real fire compartment which means real configuration of cars in a park (the ceiling exists above the car which is near to the wall, spread of fire from one car to another) with different ventilation conditions involving one or two cars burning in a single test. The experimental device is depicted up in Figure 8. The test cars were placed on a weighing park. Some steel members were placed in the calorimeter hood, platform. The combustion products were collected by a hood above the car [25]. All the tested cars were in normal use conditions, with fuel tank full at two-thirds. In the first seven tests, the car was ignited by a tray of petrol placed under the left front seat. The left front window was fully open, while the right front window was left half open. In the last two tests, the ignition was started with 1 litre of fuel under the gear box, being this a test procedure adopted by some car manufactures. The doors of cars were closed for all nine tests [25].

Figure 8- Experience of Calorimeter hood [26]

Considering the experimental data collected by this project, the report introduced an HRR reference curve shown in Figure 9. A “wave” theory was also proposed in this report to account for the fire spread between multiple vehicles in a closed car park. According to this “wave” assumption, the cars will burn one after another, with a delay time of 12 minutes. By examining the HRR reference curve, one can infer that the fire of first car will start to decay when third car starts to ignite at around 24 minutes. It was also concluded that the fire can be confined within single vehicle with the provision of sprinklers or reliable detection system combined with adequate fire-fighting equipment [25].

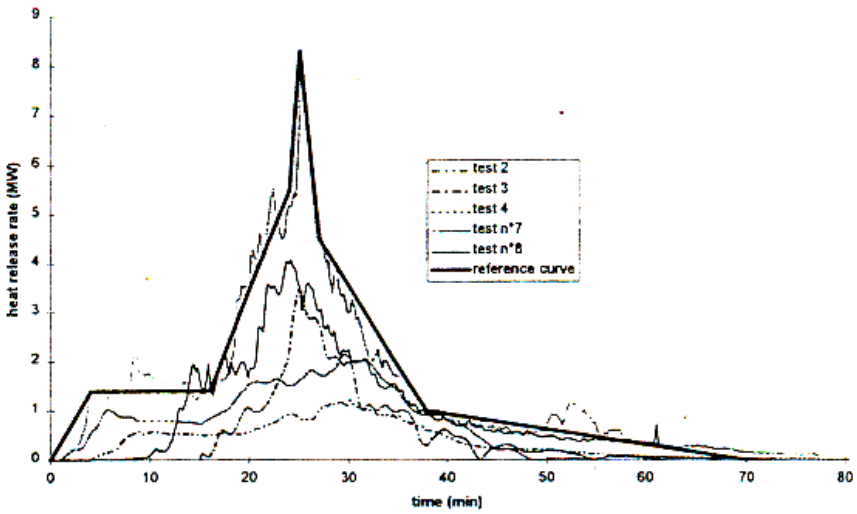

Figure 9- HRR (MW) vs. time (min) of five car fire tests and reference curve [26]

When there is a burning car for each class, this burning contains two plume regions, the front and the rear fire plumes, the total heat release rate of the vehicle is equal to the sum of the heat releases included in the two fires plume. The Table 1 shows the value of the total heat release rate (HRR) in [kW] of car class 1, class 2, class3, classe4 and 5 getting from tests of burning car in specific time which is in minutes. This classification was made in 1996 by European manufacturers and divide them into five categories.

Table 1- HRR of different car classes

Time Min	Time Sec	Class 1 HRR [KW]	Class 2 HRR [KW]	Class 3 HRR[KW]	Class 4 HRR[KW]	Class 5 HRR[KW]
0	0	0	0	0	0	0
4	240	884	1105	1400	1768	1768
16	960	884	1105	1400	1768	1768
24	1440	3474	4342	5500	6947	6947
25	1500	5242	6553	8300	10484	10484
27	1620	2842	3553	4500	5684	5684
38	2280	632	789	1000	1263	1263
70	4200	0	0	0	0	0

As we can see from the results of cars burning tests both car class 4 and 5 have the same values of HRR. The heat release rate curves of the different car classes for the new generations is depicted Figure 10 and shows a comparison between these curves. During any time dependent fire, such as a class 3 vehicle, the energy release rate (HRR) increases from zero to a maximum value for time equal to 25 minutes and decreases to zero at the end of the event.

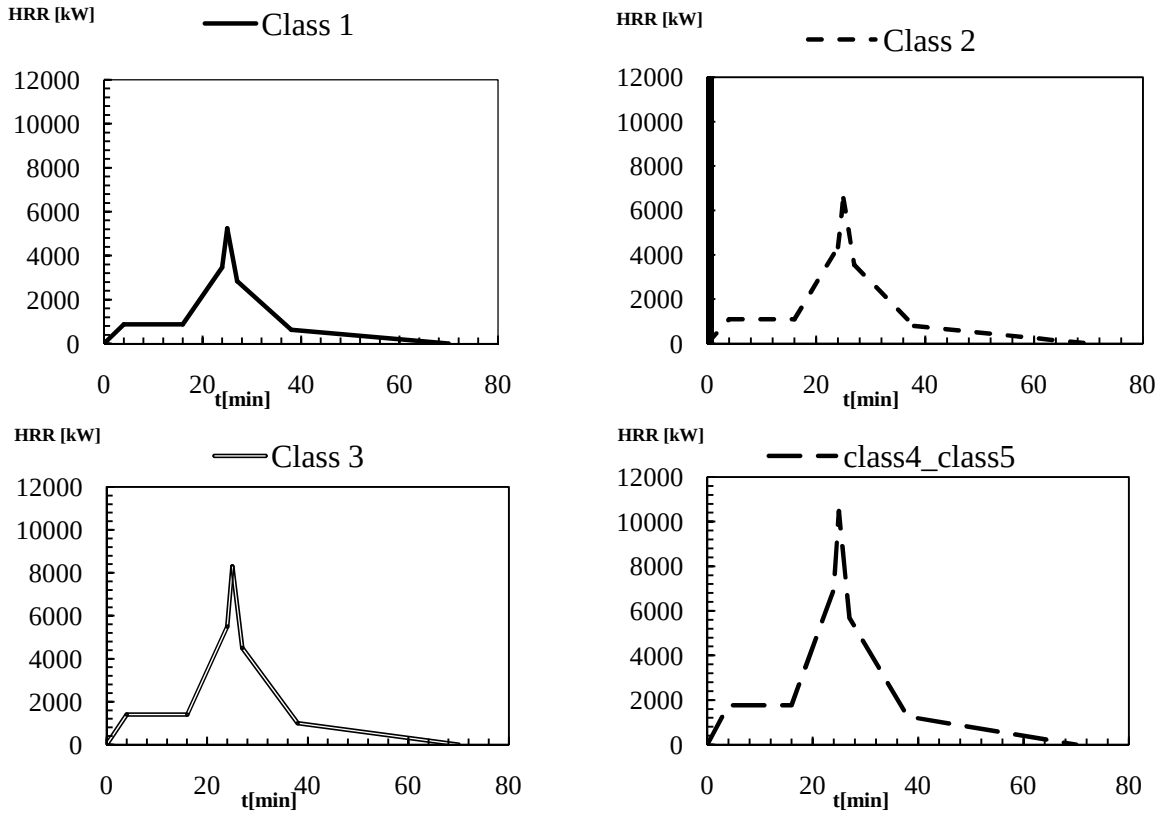

Figure 10- Curves of HRR for car classes1,2,3,4 and 5

2.4- Definition of fire compartment

Space within a building, extending over one or several floors, which is enclosed by separating elements such that fire spread beyond the compartment is prevented during the relevant fire exposure [20]. Fire compartment is a volume within a building which is completely surrounded with fire-resistant construction elements, which can be integrated right into the structure of the building. Fire compartments are not absolutely fire proof. Fire can work its way into or out of a fire compartment if it is intense enough, poorly managed, or not addressed quickly enough. Existing buildings can be retrofitted to create fire compartments. Movable barriers can be installed, or people can remodel parts of a building to create a fire compartment. Also known as a fire zone, a fire compartment can also sometimes address the potential of flood damage, as the same materials which keep fire out can sometimes keep water at bay as well. The fire compartments can consist of rooms or groups of rooms. When a fire starts inside a compartment, the sealed nature of the area can compartmentalize the fire, preventing it from spreading to other areas. The fire compartment used in this study represents a fire in open car park, being the dimensions defined in the next sections.

2.4.1- Phases of fires in compartment

The fire in compartment is characterized by four principal phases. The first phase is the fire development which is the evolution of the size of the fire from a small incipient fire. If there is no action to stop the fire, it will have the maximum size. In this situation the fire size will be controlled by the amount of existing fuel or by the amount of ventilation, see Figure 11.

The second phase is the flashover which is usually obvious to the observer of fire growth. When an object begins to burn in a compartment, gives rise to the appearance of a fire plume of hot gases and smoke. By natural convection rises to the ceiling, where it begins to spread horizontally, forming a layer. An unconfined flame tends to follow the initial growth period, a law in which the heat release rate is proportional to the square of time. Thus the layer next to the ceiling increases temperature and thickness because the plume continues to transport mass and energy from the burning material. The temperature increase of that layer makes the emission of radiation, being primarily directed downward, higher and higher. This radiation focuses on the existing objects in the compartment is partially absorbed and increases the temperature of these objects, which continue to produce volatile combustibles. When the upper layer reaches of 600°C order, the incident radiation is sufficient to ignite these released volatile combustibles, bringing simultaneously all objects under fire. This incident radiation has an estimation value of 20 kW/m^2 at ground level.

The third phase corresponds to the full development of the fire, which is affected by: a) the size and shape of the enclosure, b) the amount, distribution and type of fuel in the enclosure, c) the amount, distribution and form of ventilation of the enclosure and d) the form and type of construction materials comprising the roof (or ceiling), walls and floor of the enclosure [27].

The fourth phase corresponds to the cool down of the fire, and depends on the fire brigade intervention or the limitation on fuel or oxygen.

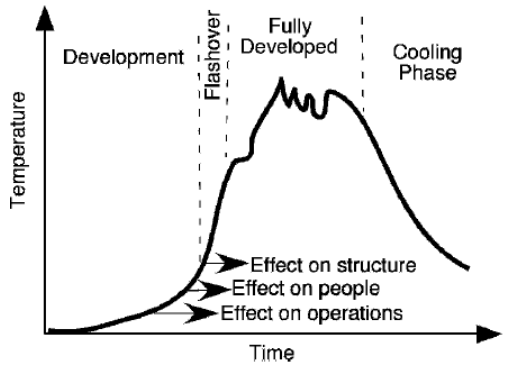

Figure 11- Phases of fire development [27]

2.4.2- Characteristics of fire compartment

The compartment in this study is named open car parking and has the following geometry characteristics: 10m width, 10m depth, height= 3m. Is characterized by the existence of concrete slabs. The compartment consists in two major walls, one ceiling and one floor. This compartment uses six targets to determine the temperature near the ceiling and six detectors to determine the velocity near the ceiling. The heat flows through the ceiling, walls, and floor of a compartment. The thermal properties of concrete and steel are presented in Table 2. Steel was considered to define the target material and concrete was considered to define the material of each element. Two zones are expected to define the fire compartment, which are the lower layer zone and upper layer zone. The compartment has also two major wall vents, with 0m for sill, 3m for soffit and 10m width.

Table 2- Thermal properties of Concrete and Steel

Thermal properties	concrete	steel
Density	2200 kg/m^3	7850 kg/m^3
Thermal conductivity	0.002 kW/(m °C)	0.053 kW/(m °C)
Specific heat	0.9 kJ/(kg °C)	0.425 kJ/(kg °C)
Emissivity	0.7	0.7

As mentioned in previous section, the fire event of a car may be consider represented by a pool fire with a specific diameter and with a high above the ground floor well defined. When the flame is higher than H, the flame impacts the ceiling and the Hasemi method is applied, see Figure 12.

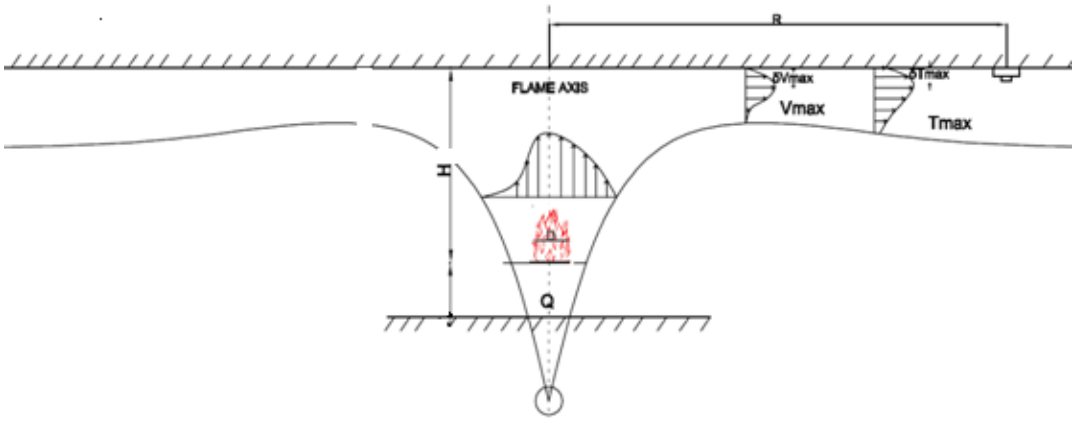

Figure 12- Localized fire of our case of study

2.5- Definition of different fire events

A "fire event" shall be defined as an occurrence in which extinguishing media was used to suppress fire. This may mean a portable fire extinguisher, water from fire department efforts, the activation of a kitchen vent hood, a building's sprinkler system, or any other fire suppression system within a building. On the rare occasion when evidence of fire is present, and the fire has self-extinguished, this will also be identified as a fire event. In this study, the fire even of a burning car was considered.

Many tests were done in previous years for calculate the heat release rate from car fire events. The first tests carried out in opened conditions were developed by Mangs and Keski-Rahkonenin the 90’s [19]. Ten tests of burning cars were done between 1995 and 1996, involving 15 cars old series (70ies/80ies) and a new generation series. (90ies) for cars class 3, with the performance of one car in five tests and two cars in the other five tests as shown in Figure 13. The graph of the comparison between the HRR of the two generation showed that the energy released by a car made in 1995 was twice that of a 1980’s car [26]. Some of the HRR results can be found in Figure 14.

Figure 13- The burning of old and new cars in open car park [24]

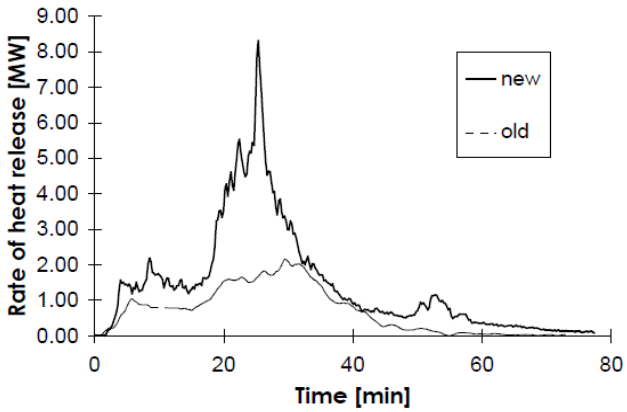

Figure 14- Heat released from cars of class 3, old and new generation [24]

Newer cars (1995) were used to simulate a fire event in an open car park. Based on these tests, reference curves of HRR for two class 3-cars (one car as fire source and another one subject to the spread of fire with 12 minutes of delay) were defined. These curves allow simulating multiple burning cars, Figure 15 presents the references curves for three consecutive burning class 3-cars, with maximum HRR of 8.3 MW, after 25 minutes. For commercial vehicles, CTICM suggests a maximum value of HRR equal to 18 MW. This value is considered as a "safe value" for design, but this is not a measured value [19]. Fires involving car are more severe with the current cars that they were in the 70's and 80's due to the strong increase of combustible products.

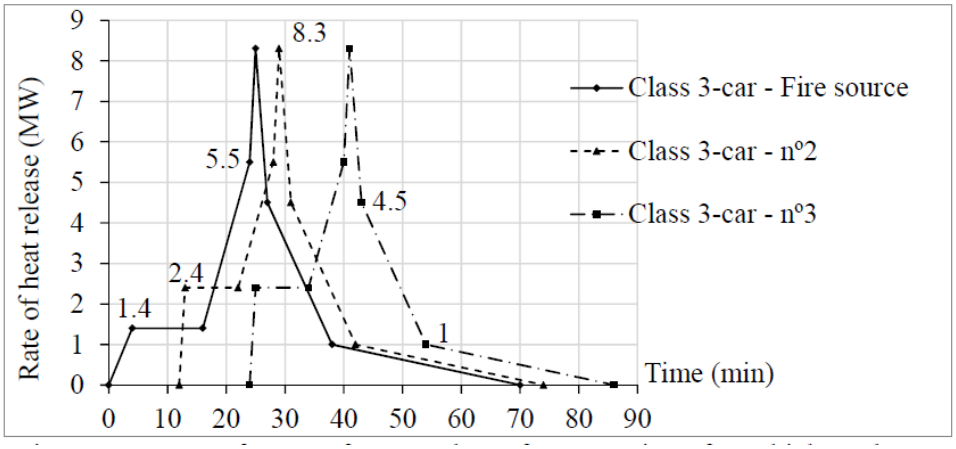

Figure 15- Curves of Rates of Heat Release from Burning of 3 Vehicles, Class 3 [19]

Four tests of pool fire under the vehicle where done on crash tested vehicles to study the spread of an under body fuel pool fire into the passenger compartment [26]. Using pool fire source for burning the cars, the measured HRR curve for each of these four tests is shown in Figure 16.

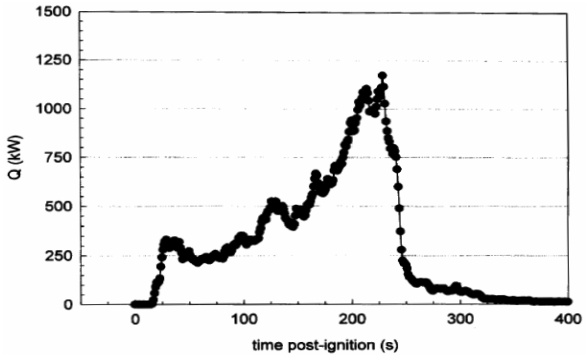

Test Part 6

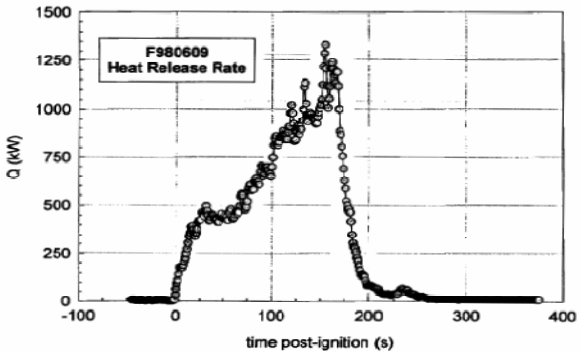

Test Part 9

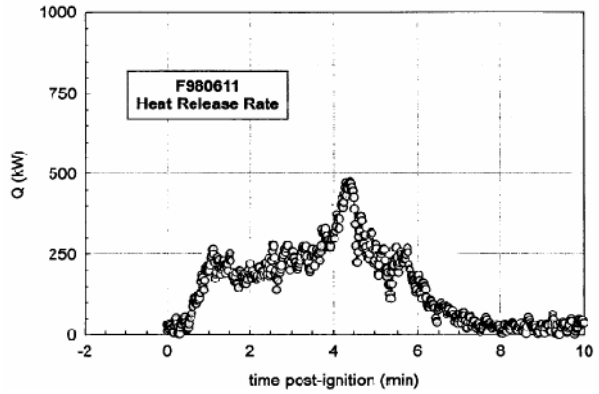

Test Part 10

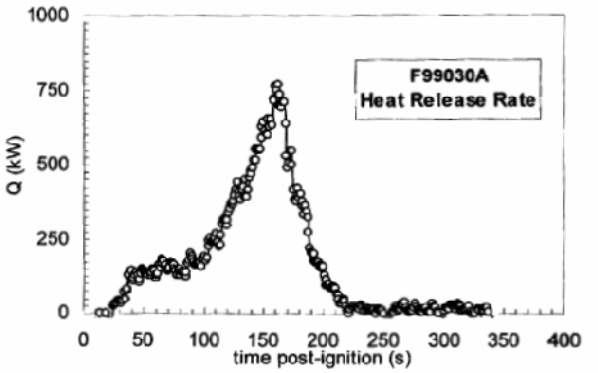

Test Part 12

Figure 16- HRR vs time for car fires initiated by fuel pool fire [26]

2.6- Fire detection

Detection is based upon heat transfer to the detector, plume and ceiling jet flow studies are important for improving fire detection system. Hot gases rise vertically from a fire and the surrounding air come in to form a plume. Upon reaching underneath the ceiling, the plume turns sideways and becomes a ceiling jet. The amount of air entrained to the fire plume will give the smoke production rate. Also, the magnitude of the horizontal gas velocities and temperature in the ceiling jet would determine whether fire detectors and sprinklers can be actuated [28]. For prediction of fire and prevent the damages caused by the fires whether be material or human damage, it necessary to use predictive fire systems or fire detectors or smoke detectors in the compartment. For instance if there is a fire in a room with the presence of the fire detectors, the fire will be sufficiently small to be easily controlled Sprinklers and heat alarms represent the most significant aspects of a fire management program, see Figure 17

Figure 17- Fire detectors: heat alarm (left), sprinklers (right) [29]

2.6.1- location of fire detectors systems in compartment

Ceiling-mounted fire detectors should be located so that the transfer of heat (thermally actuated) or mass (smoke actuated) to the detector is maximized in order to minimize the response time. It is thus necessary to calculate heat and mass transfer rates induced by a fire. Detector sensing elements are generally so small (compared to either the fire plume diameter or the total thickness of the near-ceiling flow outside the plume) that the heat transfer coefficient to a given sensing element will be nearly proportional to the square root of gas velocity, V, and independent of temperature [1].

The warning of fire by the heat detectors (alarms) is starting when the temperature in the area around the smoke detector reaches a certain level. Concerning the case of study, a burning car class 3 is considered in a compartment, which is consider an open car parking, with dimensions of 3m height, 10m for both of width and depth. The diameter of the fire is assume to be (D=2m). The distance between the fire source of the car and the floor (H_s = 0.3m). Six heat alarm positions were defined, corresponding to a ratio between radial position and height of r/H=0, 0.37, 0.74, 1.11, 1.48 and 1.85.

2.6.2- Rules for the perfect work of fire detectors

The location of fire detectors should be defined as a vertical distance below the ceiling of no more than six percent of the ceiling height. For optimum response time, fire detectors should be spaced at intervals of a quarter of the ceiling height. The fire design of a compartment should include the response time of thermally actuated fire detectors, under known conditions of ceiling height, detector spacing, and fire intensity (HRR). Detectors are ceiling-mounted, and ceilings should be smooth (vertical length of obstructions less than one

percent of ceiling height) The minimum wall to wall distance is 2 to 4 ceiling heights [1]. With the advantages of early fire detection, the time of warning the fire department is anticipated, the resolution of the fire event will be effective, and the fire control will be easier. This conditions will contribute to reduce the human and financial loss due to fire. Sprinklers in open car parking and the activation of these detectors system, in case of vehicle fire, will prevent the fire to spread between the neighbouring vehicles and protect the building structure.

3- HEAT TRANSFER

The most important thing for any fire hazard assessment is the ability to numerically estimate the quantity of heat transfer and fire gases coming from the fuel bed, and the surfaces in an enclosure. The heat transfer into the boundary surface of a compartment occurs by convection and radiation, and then flows through conduction to the walls. These three majors of heat transfer are the principal mechanisms by which heat is transferred between the gas layers and the enclosing compartment walls. Temperature and the flow of heat are the basic principles of heat transfer. The amount of thermal energy available is determined by the temperature, and the heat flow represents movement of thermal energy.

3.1- Convection

Convection is set of movements of groups or aggregates of molecules within fluids which can be gas, liquid through advection or through diffusion or as a combination of both of them. The phenomenon of convection does not exist in the solid body. Fluid movement during convection can be invisibly slow, or it can be rapid. Convection is also a major mode of mass transfer in fluids or gas and can be qualified as natural convection or forced convection. The gases emitted during combustion are hot, they tend to rise and expand especially if they encounter a horizontal barrier. When a temperature is in highest value, the hot gases that are prevalent or at higher levels, or other adjacent spaces may, in turn, ignite combustible materials. The convective heat transfer in fire with direct flame contact could convectively ignite objects. But we will see that the radiative component in turbulent fires and in fully developed compartment fires can be much more important, and can drown the convective contribution. For that reason, convective heat transfer is not a principal factor in fire heat transfer, but its presence cannot be overlooked. Convective heat transfer can be the dominating mechanism for the heating up of small devices such as detectors and temperature measuring devices. This mode of heat transfer is also important for heat transfer from a flame or hot gases impinging on a surface [16]. Most of natural fire and flows associated with fire are in the domain of natural convection which is considered one of important factor for fires for example forest fires.

3.2- Conduction

Known as diffusion heat transfer, the heat transfer by conduction is the flow or movement of thermal energy, represented by collisions of atoms and molecules and their immediate neighbours within solids and non-flowing fluids. The process of heat conduction depends on the cross-section of the material and the physical material properties.

3.3- Radiation

It is a phenomenon of transmission of energy in the form of waves or particles through space or through a material medium. Thermal radiation is the energy transfer between two bodies via electromagnetic waves. This form of energy transfer is exhibit by all bodies, and requires no medium for the heat to be transferred. It can even be seen to occur in a vacuum. The amount of energy that can be radiated by a surface is given by the Stefen-Boltzmann law.

When a fire started by meeting oxidant medium, a fuel and a source of heat, combustion produces heat, gas and smoke and fire tends to spread. Heat, often considerable, given off by the fire, fire can communicate with any fuel which is near; being spread by radiation. Flame shape and thickness, respectively, play a key role in these burning orientations [16]. Radiation heat transfer is very complex and depends on the temperature and soot distribution for fundamental computations.

4- CORRELATIVE MODELS

4.1- Definition of correlative models

The correlative models is a set of formulas to estimate temperatures and velocities of hot gases which are formed and diffused just beneath an unconfined ceiling the fire. These types of correlations are often used in fire safety engineering in order to get an estimate of sprinkler or heat detector activation, presented ground-breaking correlations for flow velocities and excess temperatures for steady and unconfined ceiling jets, which are widely used because of its easy uses [26]. These equations can be used for the estimations of damages on a ceiling material, to predict if the material ignite or to evaluate if the structural behaviour will be affected. The correlative models are implemented in different software such as CFAST. Many investigators have studied the fire induced ceiling jet. Detailed measurements of velocity and temperature were produced, such as Alpert correlations in 1972 and re-examined in2011, the investigation of Heskestad and Delichatsios in 1978, and the correlations produced by Cooper in1982.

4.2- Alpert correlations

Alpert has developed an integral model and also provides some data on ceiling heat transfer rates and temperature and velocity levels in the ceiling-jet region. Assuming an axisymmetric fire induced flow beneath a flat, horizontal ceiling that was unobstructed by walls and the ceiling jet was divided into two regions. Thus two sets of correlations were proposed, each one is valid for specific limits for the maximum excess of temperature (T_{max}) and maximum velocity(V_{max}). The measurements of velocity and temperature were done under various conditions of heat release rate of fire and ceiling height. The suggestions of Alpert were based on fire experiments and conducted at different ceiling heights. The correlations developed by Alpert are easy to use and are widely used in hazard analysis calculations. They have been employed by other researchers (Evans and Stroup) in the development of a generalized program for prediction of heat detector response [30]. The experiments were done with fuel arrays of wood and plastic pallets, cardboard boxes, plastic materials in cardboard boxes, and liquid fuels with energy release rates ranging from 668 kW to 98 MW under ceiling, with heights between 4.6 to 15.5 m. The correlations to quantify the maximum gas temperature and velocity are provided below.

IF r/H >0,18

$$T_{max} = T_{\infty} + \frac{5{,}38 \times (\frac{\dot{Q}}{r})^{\frac{2}{3}}}{H} \quad (16)$$

IF r/H≤0,18

$$T_{max} = T_{\infty} + \frac{16{,}9 \times \dot{Q}^{\frac{2}{3}}}{H^{\frac{5}{3}}} \quad (17)$$

IF r/H>0.15

$$V_{max} = 0.197 \times \frac{\dot{Q}^{1/3} H^{1/2}}{r^{5/6}} \quad (18)$$

F r/H≤0,15

$$V_{max} = 0.69 \times (\frac{\dot{Q}}{H})^{1/3} \quad (19)$$

T_{max} represents the maximum temperature given in [°C], T_{∞} is ambient temperature equal to 20°C, H is the ceiling height [m], and r is radial position given in [m], V_{max} represents the maximum velocity in [m/s].

These correlations are divided into two zones, one part applies to the region of impingement where the upward flow of gas in the plume turns to flow out beneath the ceiling horizontally. Equations 17 and 19 are independent of radius and are actually corresponding to axial plume flow temperatures and velocities, calculated at the ceiling height above the fire source. The other correlations apply outside of this turning region as the flow moves away from the impingement area [16]. Alpert correlations are valid after fire ignition and the ceiling must be considered unconfined and smooth. These correlations apply to a fire source located at least 1.8 H distant from walls. The thickness of ceiling jet δ is found to be within a range of approximately 5 to 12% of the ceiling height H. Furthermore, peaks of temperature and velocity occur within 1% of H measured from the ceiling. A1pert assumed a Gaussian behaviour for the velocity and temperature profiles and has developed an integral model for the boundary layer thickness. This layer position is defined from the ceiling at a distance of 0.01H.

4.2.1- Maximum Velocity and Temperature during the fire event

The results of the maximum velocity and temperature near the ceiling depends on the fire event (car class). The following conditions were assumed in the compartment (open car parking): T_{∞}=20°C, H=2.7m, D=2m. The maximum velocity and temperature was calculated for six target and sensors on the ceiling, corresponding to the radial position r/H=0, 0.37, 0.74, 1.11, 1.48 and 1.85, see Figure 18 and Figure 19

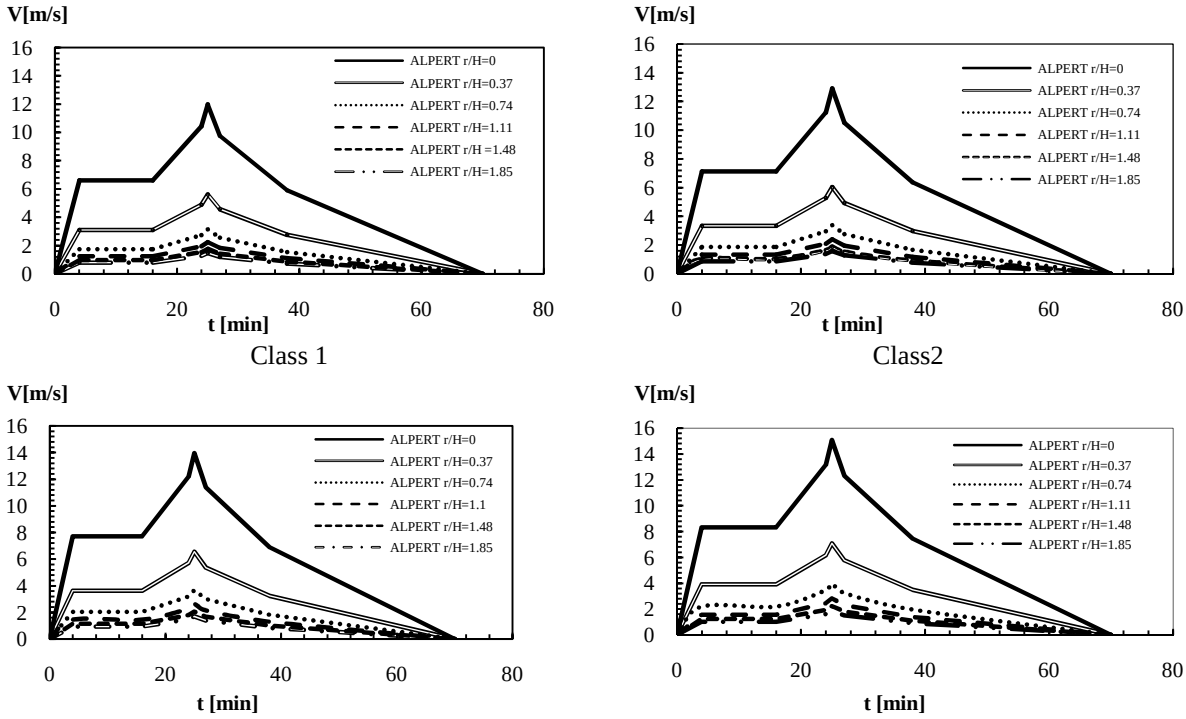

Figure 18- Velocity near the ceiling from Alpert correlations

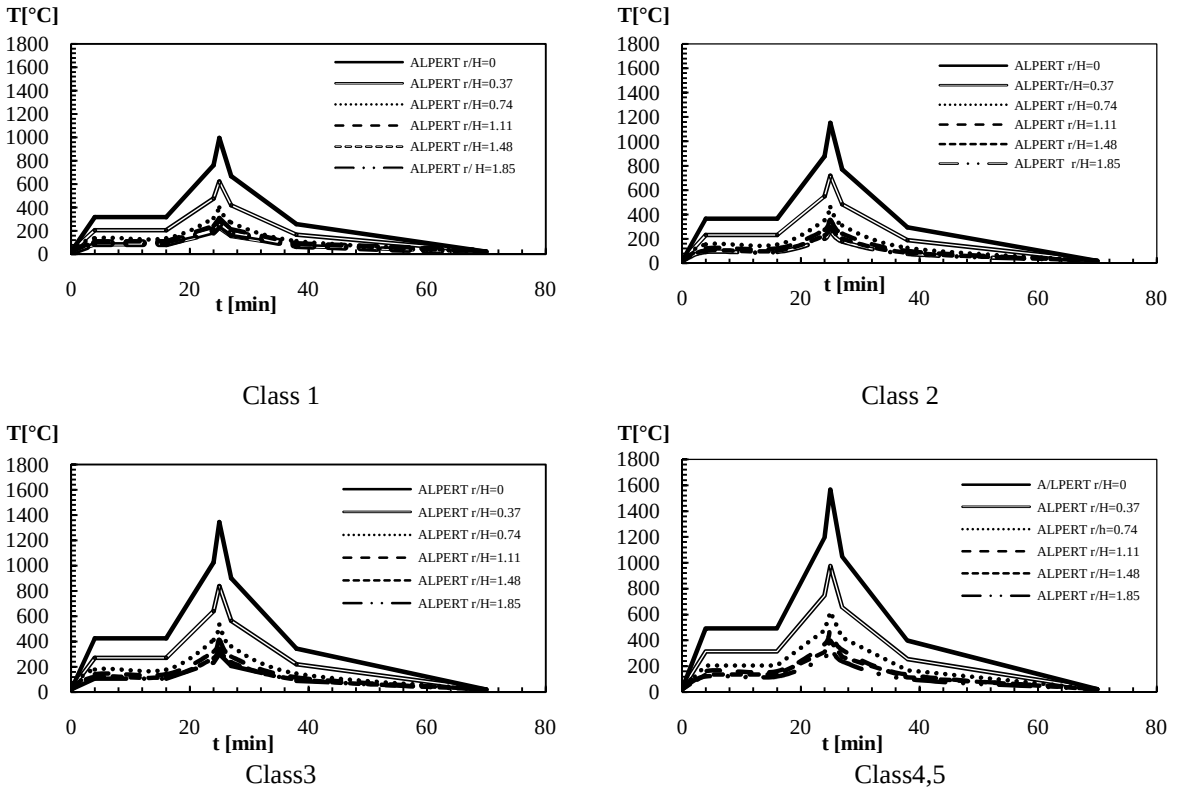

Figure 19- Temperature near the ceiling from Alpert correlations

4.2.2- Maximum Temperature and Velocity for different ratio r/H

From the results of velocity and temperature in the hot zone layer, calculated by the correlations developed by Alpert, the maximum dynamic characteristic were extracted from the event for time equal to 25 minutes (1500s). The curves of maximum velocity and temperature are shown in Figure 20 and Figure 21 respectively versus r/H in different positions for car class 1, 2 ,3 and 4, 5.

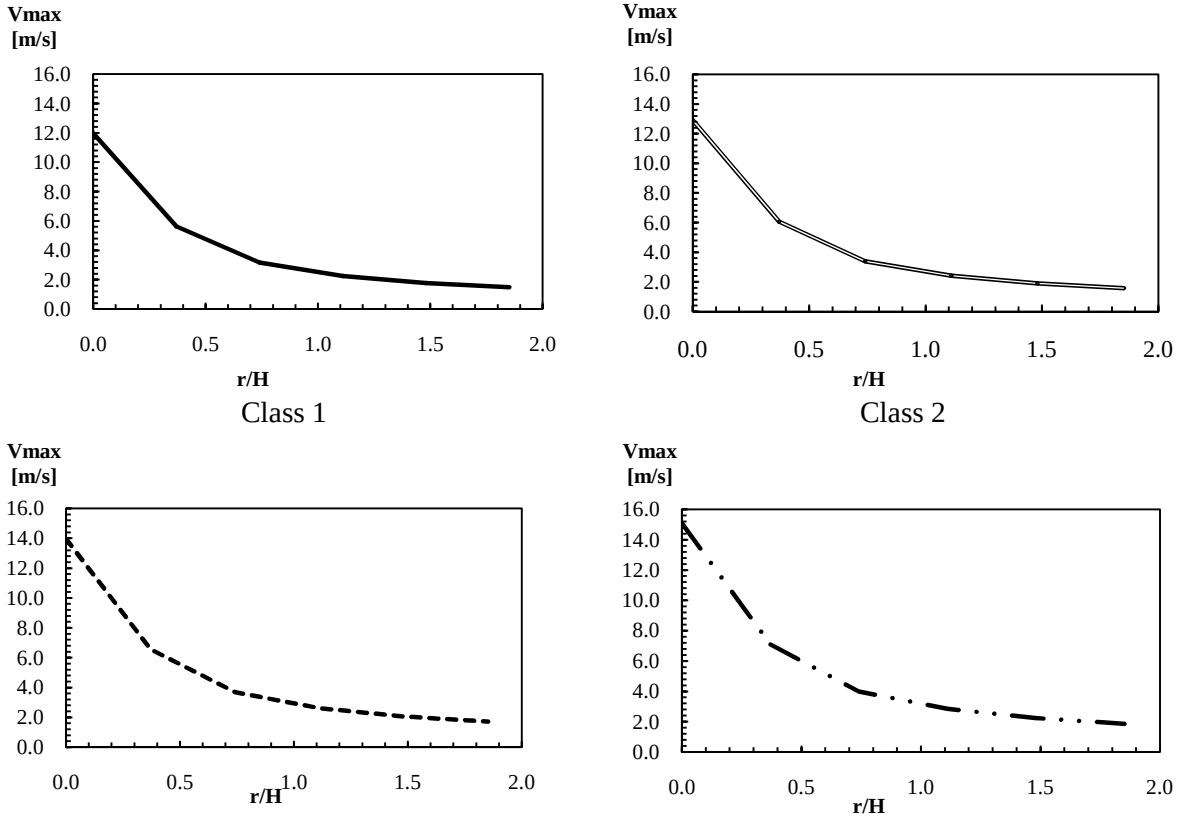

Figure 20- Vmax of all car classes calculated by Alpert correlations

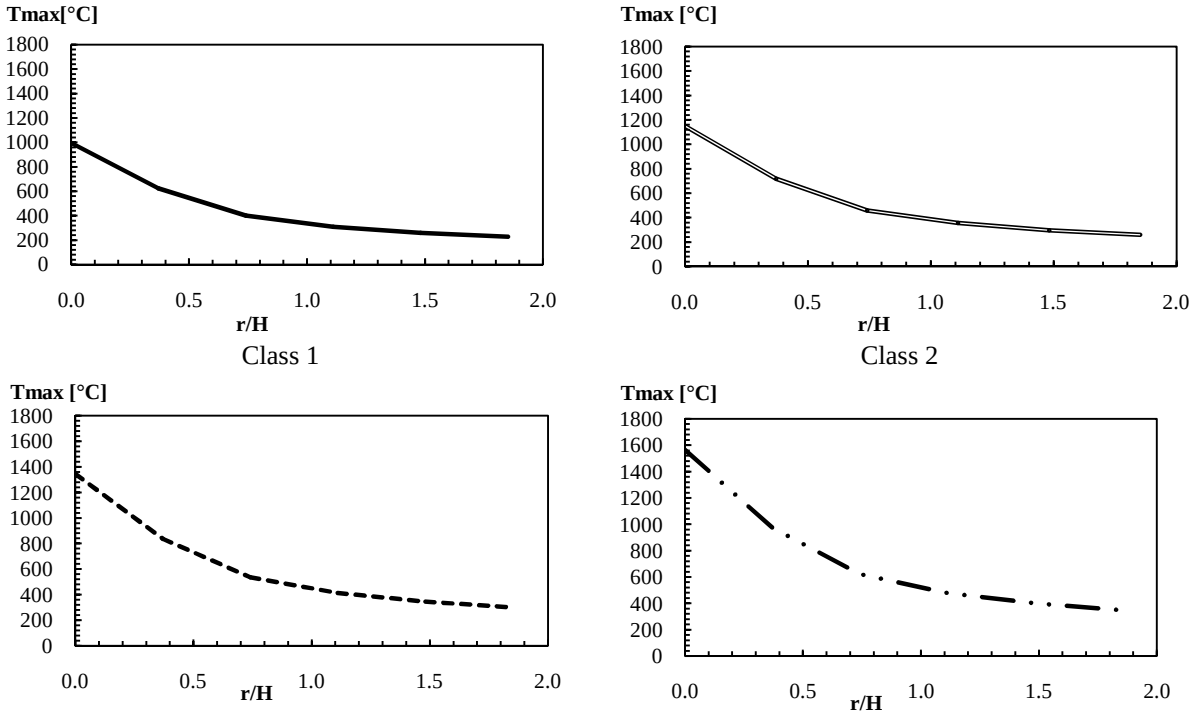

Figure 21- Tmax of all car classes calculated by Alpert correlations

Both maximum temperature and velocity decrease with the ratio r/H, as expected. These values also increase with the class of the fire event.

4.3- Cooper correlations

The investigations of Cooper were done in detail about a ceiling jet in a region r/H > 0.2, measured horizontally from the centre axis of the plume to the wall. Correlations for velocity and temperature have been derived [15]. Using steady-state and time varying heat release rates in full-scale multi-room fire scenarios to generate an experimental data base to use in mathematical fire simulation models. The tests focused on smoke filling and selected measurements of the increasing temperatures over time [23]. Cooper developed correlations for the maximum temperature and velocity with limits which are dependent on the ratio r/H, and defined in the following equations.

$0 \leq r/H \leq 0.75$ $$T_{max} = 28.1EXP(-1.77 \times \frac{r}{H}) \times \dot{Q}^{2/3} \times H^{-5/3} + T_{\infty} \quad (20)$$

If $0.75 \leq r/H \leq 4.0$ $$T_{max} = 5.77 \times (\frac{r}{H})^{-0.88} \times \dot{Q}^{\frac{2}{3}} \times H^{-\frac{5}{3}} + T_{\infty} \quad (21)$$

If $0.2 \leq r/H \leq 4.0$ $$V_{max} = 0.26 \times (\frac{r}{H})^{-1.1} \times \dot{Q}^{1/3} \times H^{-1/3} \quad (22)$$

4.3.1- Maximum Velocity and Temperature during the fire event

The same calculation was done using Cooper correlative model, using the same data, the same dimensions of event, and the same positions for targets and sensors. Figure 22 and Figure 23 present the results for the velocity and the temperature of the hot gases, near the ceiling in a location expected to have maximum values.

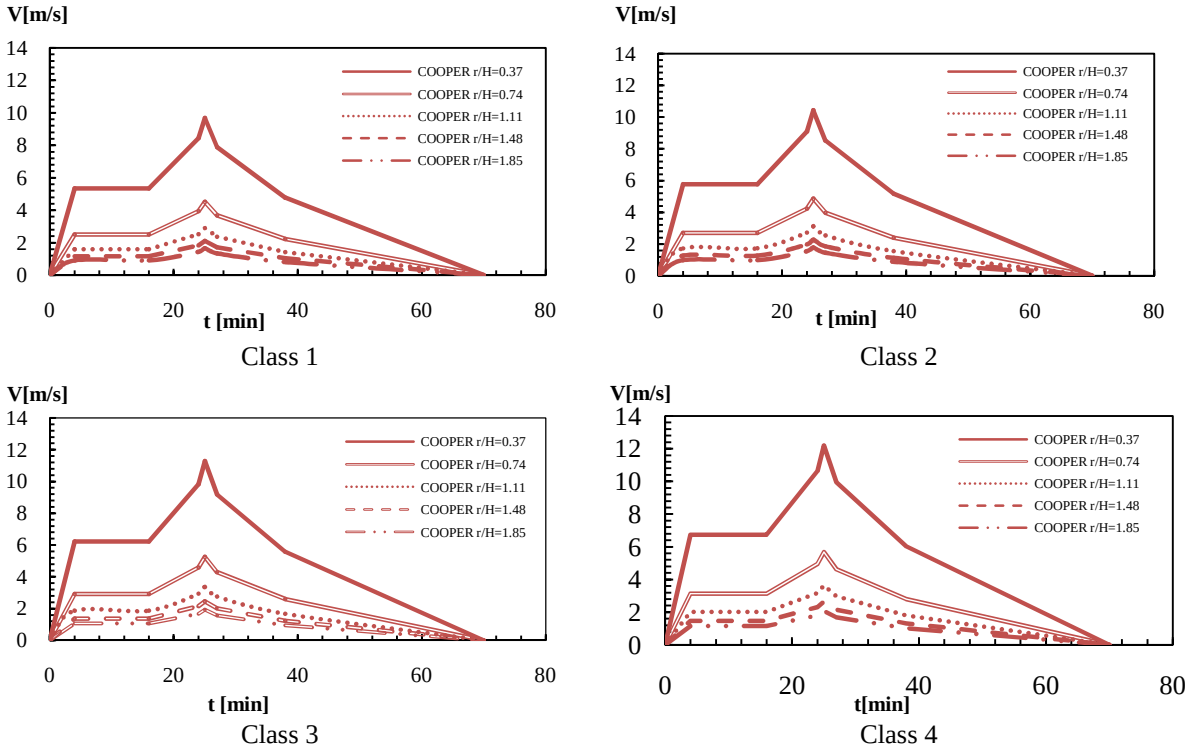

Figure 22- Velocity near the ceiling from Cooper correlations

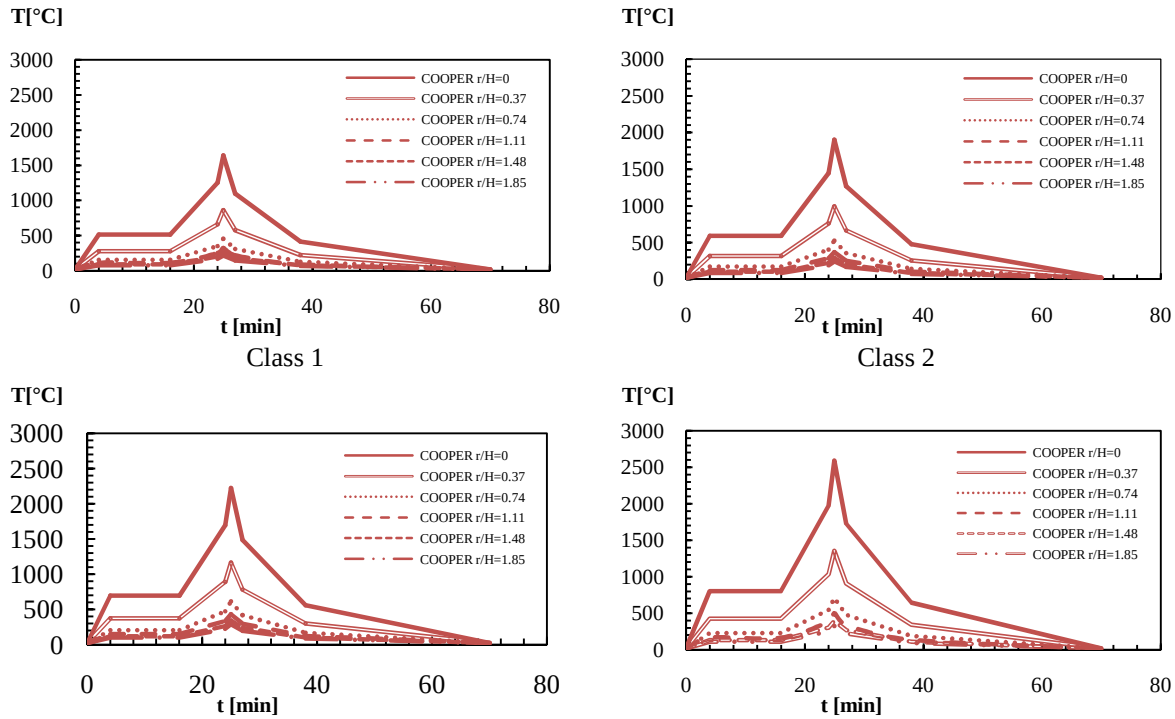

Class 1 Class 2

Class 3 Class 4,5

Figure 23- Temperature near the ceiling from Cooper correlations

4.3.2- Maximum Temperature and Velocity for different ratio r/H

The values of velocity and temperature of the gases near the ceiling are considered as maximum when the time is equal to 25 min. The variation of the maximum values during the event is plotted against the ratio r/H, depending of the fire class in Figure 24 and Figure 25.

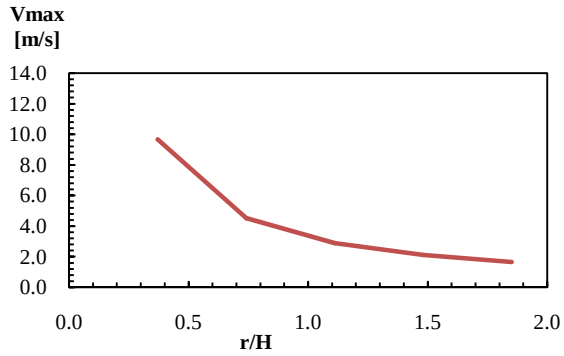

Class1

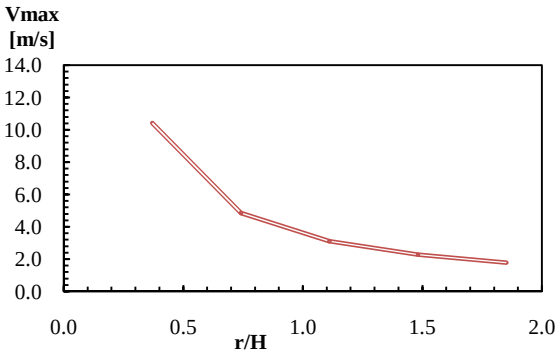

Class 2

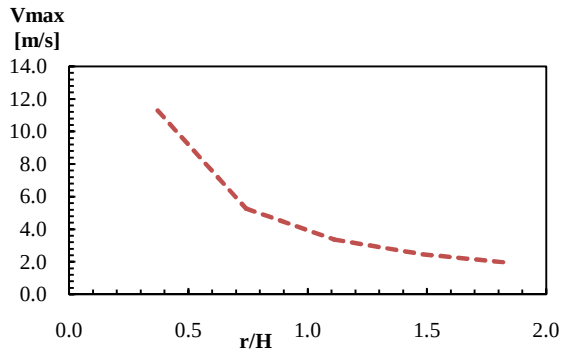

Class 3

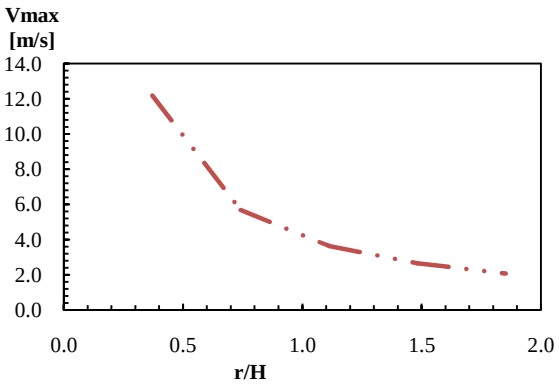

Class 4,5

Figure 24- Vmax of all car classes calculated by Cooper correlations

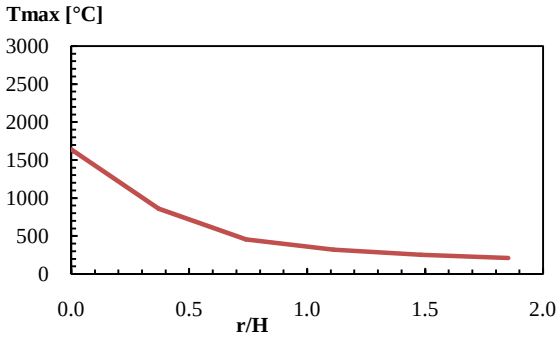

Class 1

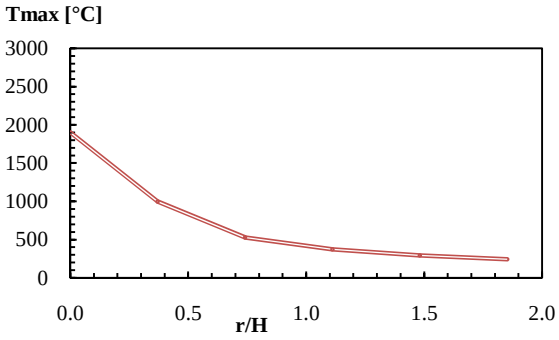

Class 2

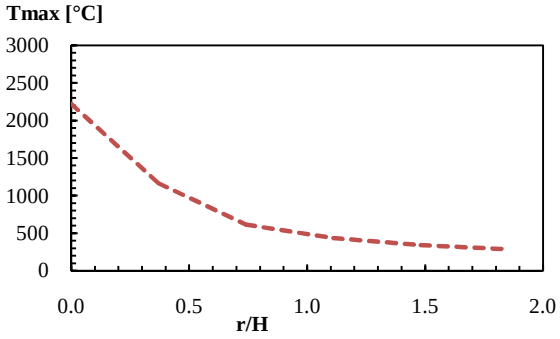

Class 3

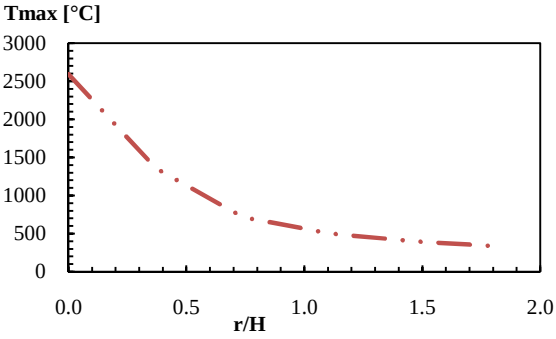

Class 4,5

Figure 25- Tmax of all car classes calculated by Cooper correlations

Both maximum temperature and velocity decrease with the ratio r/H, as expected. These values also increase with the class of the fire event. This conclusion is in agreement with the results obtained by Alpert correlative model.

4.4- Heskestad and Delichatsios correlations

Hekestad and Delicatsios made a sets of experiments or tests with three different ceiling heights under an extensive flat ceiling for a total of nine experimental configurations. Their results are now beginning used extensively for predicting gas temperatures and velocities over growing fire [31]. These authors developed some work concerning the physical modelling of the initial fire environment generated by fire in an enclosure. This event persists up to that time in a fire when recirculation of combustion products begins to influence the further yield of products. Three wood-crib fires of different fire-growth rates were combined with three different ceiling heights under large fiat ceilings for a total of nine experimental configurations [3]. Heskestad assumed a point source and introduced a virtual origin at height Z_0, see Figure 1 and Figure 2 and see equation 1, in account the fact that some plume properties depend on the convective energy release rate $\dot{Q}_c$. Heskestad examined experimental data and found that the plume radius, centreline temperature, and centreline velocity in the plume zone obey the following relations, valid above the flame height.

$$V_{max}=1.0\left(\frac{\dot{Q}_C}{(H-Z_0)}\right)^{1/3} \quad (23)$$

$$T_{max} = 2.5\left(\frac{\dot{Q}_C^{2/5}}{(H-Z_0)}\right)^{5/3} \quad (24)$$

Where $(\dot{Q}_C)$ is the convective energy release rate in [kW], H is the height in [m], $(\dot{Q})$ is the total heat release rate HRR in [kW], (Z_0) is the virtual origin given in equation 1.

$0<r/H\leq 8$ $\quad V_{max}=0.179\times(r/H)^{-0.63} \times (0.188 + 0.313 \times r/H)^{-2/3}\times\dot{Q}^{1/3}H^{-1/3}$ (25)

$0<r/H\leq 8$ $\quad T_{max} = 2.75 \times (0.188 + 0.313 \times r / H)^{-4/3}\times\dot{Q}^{2/3}H^{-5/3} + T_\infty$ (26)

4.4.1- Maximum Velocity and Temperature during the fire event

The results of the maximum velocity and temperature obtained from the simple correlative models of Heskestad and Delichatsios are depicted in Figure 26 and Figure 27. Results agree with previous conclusions used for the other correlative models.

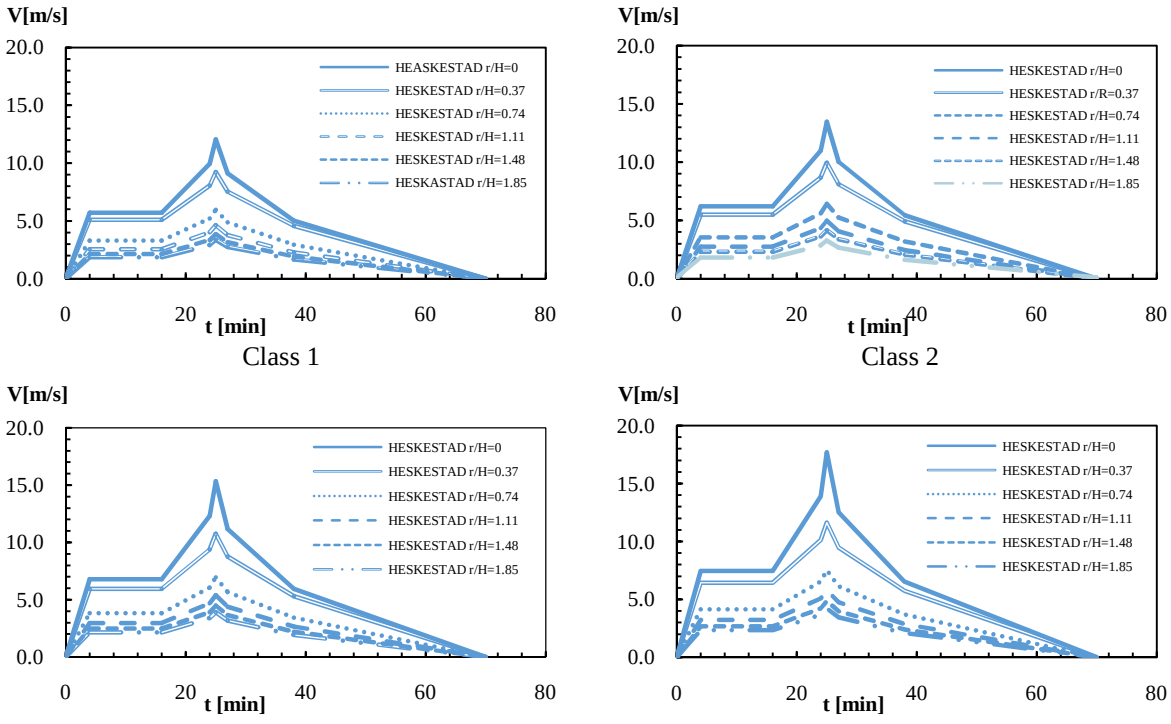

Figure 26- Velocity near the ceiling from Heskestad and Delichatsios correlations

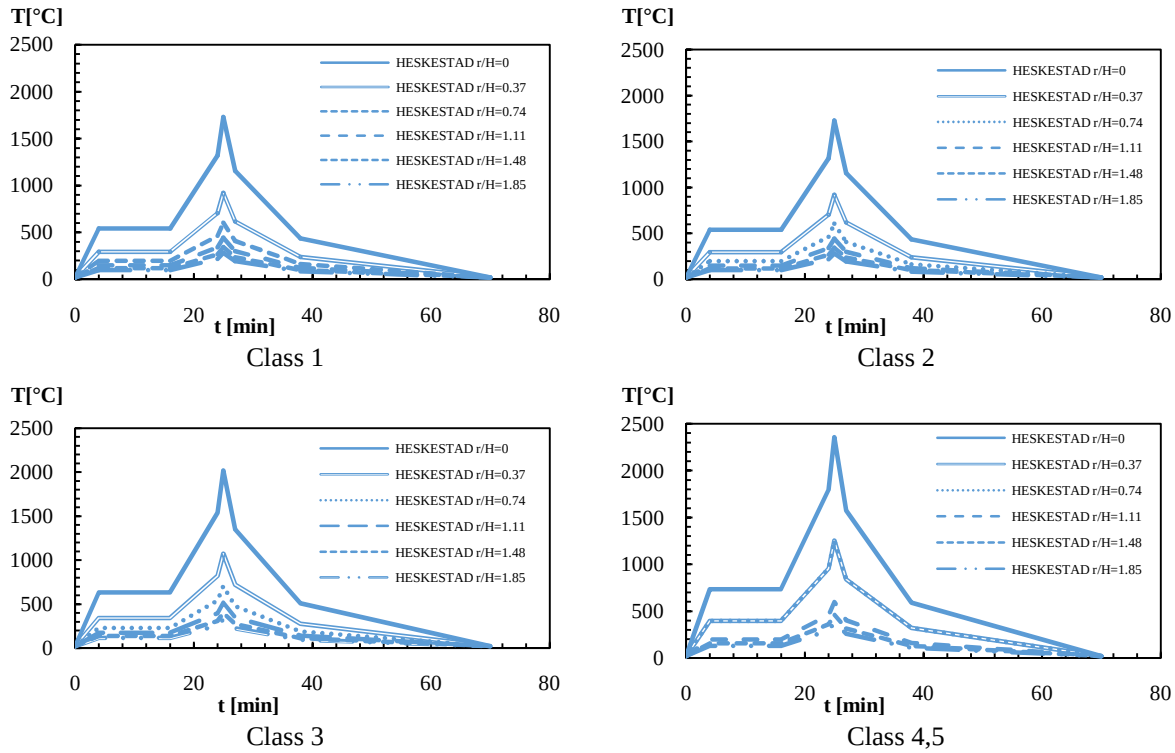

Figure 27- Temperature near the ceiling from Heskestad and Delichatsios correlations

4.4.2- Maximum Temperature and Velocity for different ratio r/H

The maximum values of temperature and velocity of the hot gases near the ceiling were calculated from Heskestad and Delichatsios correlations, using the same time as reference (t=25 minutes). Figure 28 and Figure 29 present the variation of each dynamic parameter.

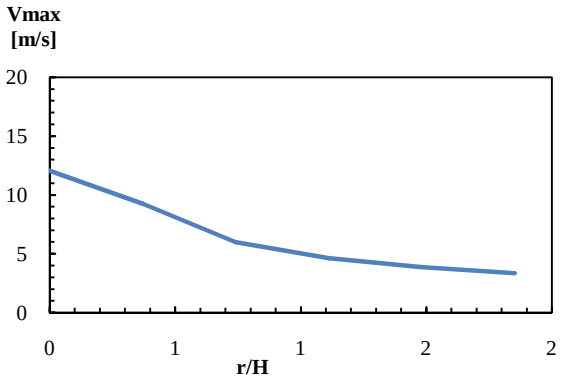

Class 1

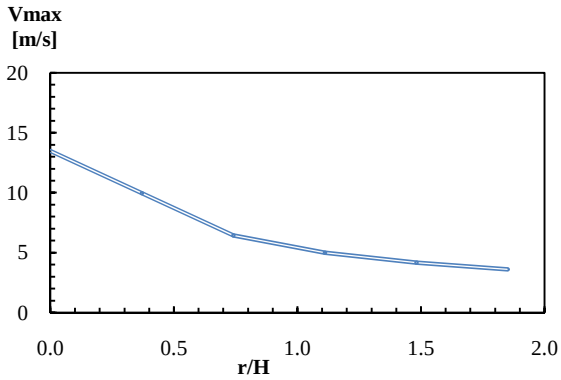

Class 2

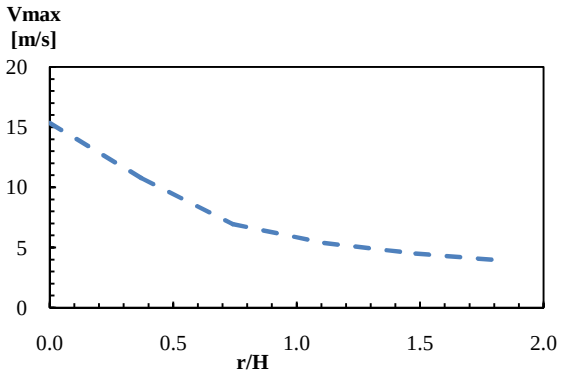

Class 3

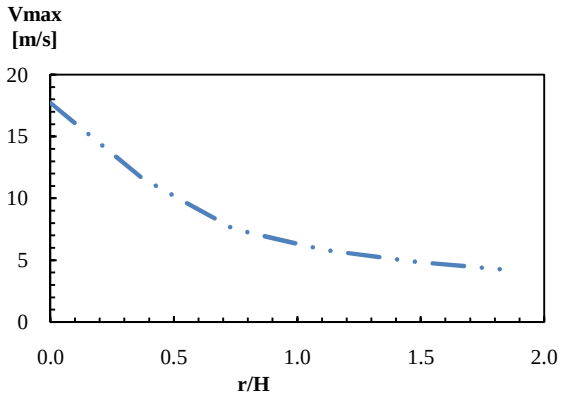

Class 4,5

Figure 28- Vmax of car classes from Heskestad and Delichatsios correlations

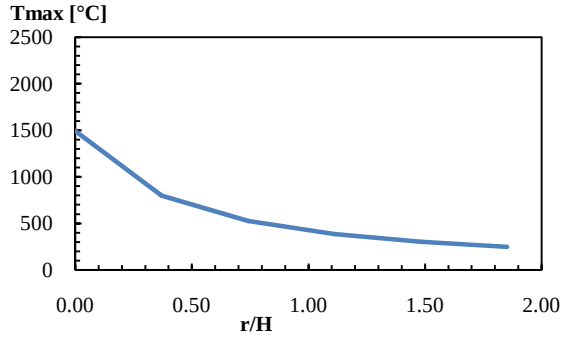

Class 1

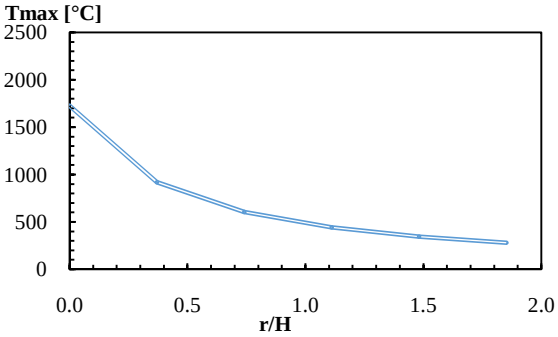

Class 2

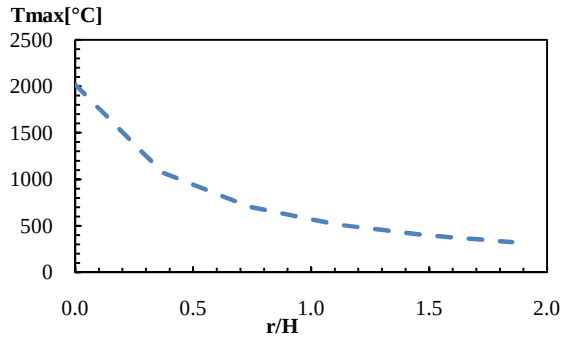

Class 3

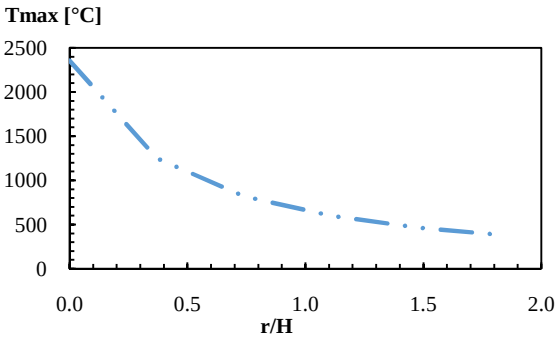

Class 4,5

Figure 29- Tmax of car classes from Heskestad and Delichatsios correlations

4.5- Comparison of results

Temperature and velocity are two major quantities that should be calculated in order to decide about any sensor position or activation system (sprinklers, heat alarm), during any time dependent fire. In all classes of vehicles, the energy release rate (HRR) increases from zero to a maximum value and decreases to zero at the end of the fire. The correlative models (Alpert, Cooper, Heskestad and Delichatsios) are used to compare the velocity and temperature near the ceiling for six target positions, corresponding to r/H=0, 0.37, 0.74, 1.11, 1.48 and 1.85, based on an integration process over the volume of each layer (lower and upper). The ordinary differential equations for the conservation of mass and energy, are solved in each layer.

4.5.1- Maximum temperature comparison for class 1

Figure 30 represents the comparison between different correlative models. The maximum temperature decreases with the increase of the ratio r/H, being the results obtained from Heskestad and Delichatios positioned between the other correlative models. After the ratio value of r/H=0.74, this correlative model overestimates the maximum temperature in comparison to Alpert and Cooper models.

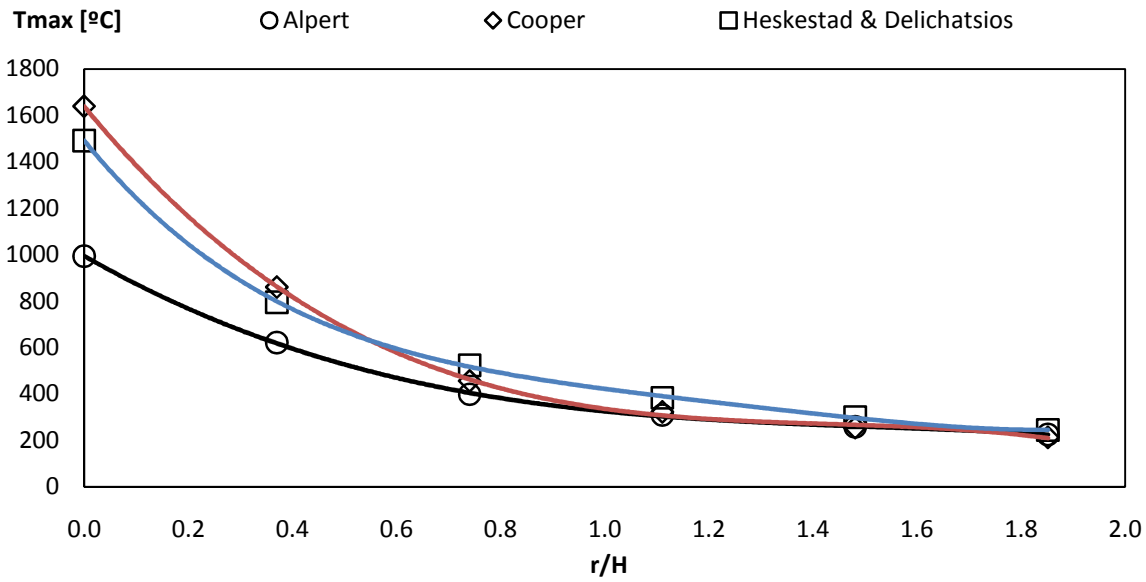

Figure 30- Comparison of the value of T_{max} from the correlative models for class 1

Cooper 's model seems to correlate well with Alpert correlations for r/H greater than 1.1, with difference between them below 5%. The results of the maximum temperature obtained from Heskestad and Delichatsios do not agree with Alpert, being these results approaching together when r/H is greater than 1.85. For this ratio the relative difference is 8.8%. Cooper's model seems to underestimate the maximum temperature, in comparison to Heskestad and Delichatsios results for ratio r/H greater than 0.5.

The following trend lines are based on the correlative results which are the Cooper approximation for T_{max} (Eq 27), the Heskestad and Delichatsios approximation for T_{max} (Eq 28), and Alpert's approximation for T_{max} (Eq 29).

$$T_{max}= -429.9 \left(\frac{r}{H}\right)^3+1849 \left(\frac{r}{H}\right)^2- 2721 \frac{r}{H} + 1638 \quad (27)$$
$$R^2=0.999$$

$$T_{max}= 293.9\left(\frac{r}{H}\right)^4 - 1490\left(\frac{r}{H}\right)^2+2869 \left(\frac{r}{H}\right)+1491 \quad (28)$$
$$R^2=0.999$$

$$T_{max}= - 172.2 \left(\frac{r}{H}\right)^3 + 789.1 \left(\frac{r}{H}\right)^2 - 1286 \frac{r}{H} + 994.8 \quad (29)$$
$$R^2= 0.999$$

The approximation fits well the variation of T_{max} with respect to r/H. The curve fitting was developed with the R^2 coefficient being always greater than 0.999.

4.5.2-Maximum temperature comparison for class 2

Figure 31 represents the evolution of the maximum temperature for a class 2 fire event. The maximum temperature decreases with the increase of the ratio r/H, being the relative results obtained by all the correlative model in agreement with previous fire event class car. The maximum temperature increases with the class of the fire event.

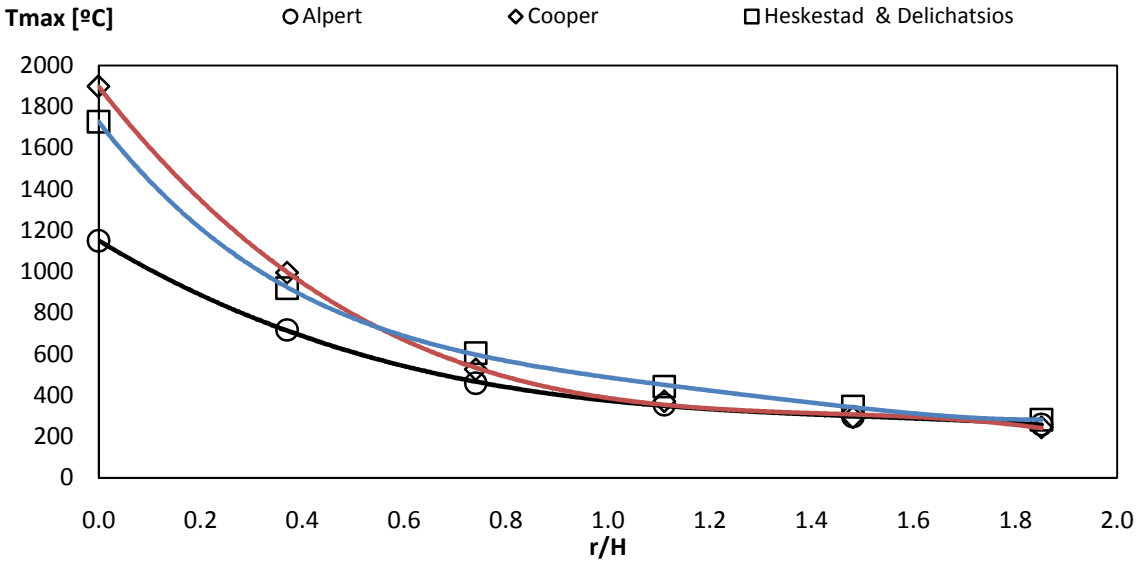

Figure 31- Comparison of the value of T_{max} from the correlative models for class 2

Cooper model's correlate very well with Alpert model (we are taking Alpert results as reference) when the ratio of r/H is greater than 1.1, with relative deference between them below 5%. There is a good approximation between the Alpert and Cooper model when r/H>0.74 with relative difference smaller than 14.5%.

An approximation is noticed between the correlative models of Heskestad and Delichatsios, and Cooper at the region when the ratio r/H approaches 0.5. A best fitted approximation to the simulated results was done, for each correlation. The following equations are based on the correlative results which are the Cooper approximation for T_{max} (Eq 30), the Heskestad and Delichatsios approximation for T_{max} (Eq 31), and Alpert's approximation for T_{max} (Eq 32).

$$T_{max} = -489.9\left(\frac{r}{H}\right)^3 + 2145\left(\frac{r}{H}\right)^2 - 3157\left(\frac{r}{H}\right) + 1898 \quad (30)$$
$$R^2 = 0.999$$
$$T_{max} = 341\left(\frac{r}{H}\right)^4 - 1792\left(\frac{r}{H}\right)^3 + 3330\left(\frac{r}{H}\right)^2 - 3181\left(\frac{r}{H}\right) + 1727 \quad (31)$$
$$R^2 = 0.999$$
$$T_{max} = -199.8\left(\frac{r}{H}\right)^3 + 915.7\left(\frac{r}{H}\right)^2 - 1492\left(\frac{r}{H}\right) + 1151 \quad (32)$$
$$R^2 = 0.999$$

4.5.3- Maximum temperature comparison for class 3

Figure 32 represents the evolution of the maximum temperature for a class 3 fire event. The maximum temperature decreases with the increase of the ratio r/H, being the

relative results obtained by all the correlative model in agreement with previous fire event class car. The maximum temperature increases with the class of the fire event.

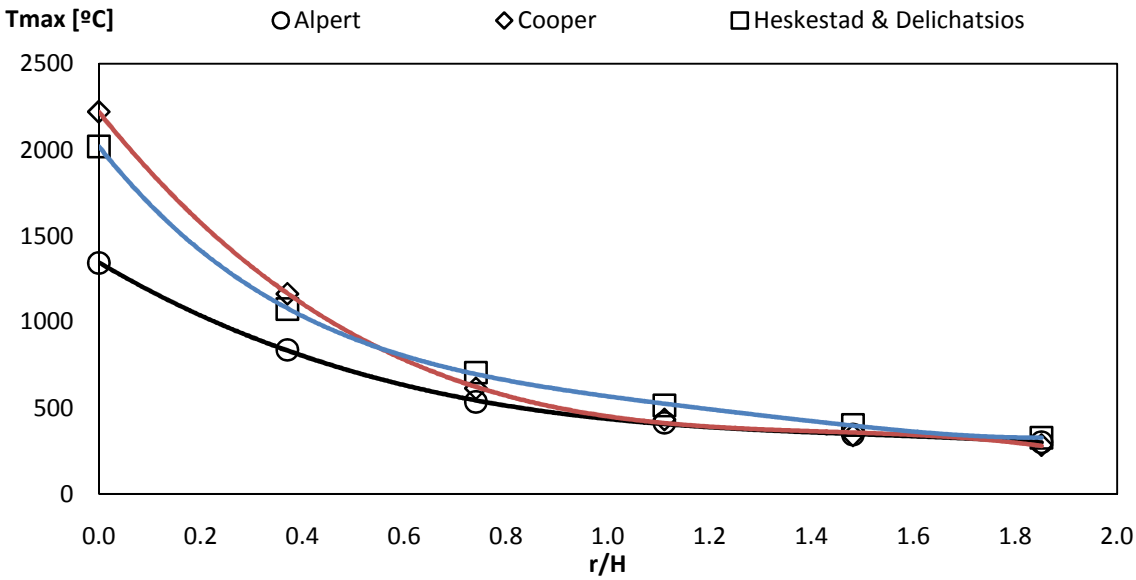

Figure 32- Comparison of the value of T_{max} from the correlative models for class 3

The maximum temperature decreases with the ratio r/H, as previous mentioned for the other fire class events. The same approximation was developed, using trend lines with very good approximation coefficient $R^2 \approx 1$. The following equations are proposed, based on the correlative results, which are the Cooper approximation for T_{max} (Eq 33), the Heskestad and Delichatsios approximation for T_{max} (Eq 34), and Alpert's approximation for T_{max} (Eq 35).

$$T_{max} = -584.1\left(\frac{r}{H}\right)^3 + 2512\left(\frac{r}{H}\right)^2 - 3696\left(\frac{r}{H}\right) + 2218 \quad (33)$$
$$R^2 = 0.999$$
$$T_{max} = 399.2\left(\frac{r}{H}\right)^4 - 2024\left(\frac{r}{H}\right)^3 + 3898\left(\frac{r}{H}\right)^2 - 3724\left(\frac{r}{H}\right) + 2018 \quad (34)$$
$$R^2 = 0.999$$
$$T_{max} = -233\left(\frac{r}{H}\right)^3 + 1072\left(\frac{r}{H}\right)^2 - 1747\left(\frac{r}{H}\right) + 1344 \quad (35)$$
$$R^2 = 0.999$$

4.5.4- Maximum temperature comparison for class 4 and 5

Figure 33 represents the evolution of the maximum temperature for the fire event of class 4 and class 5. Higher values are expected, because the HRR used for these fire events is higher. Once again the maximum temperature decreases with the ratio r/H.

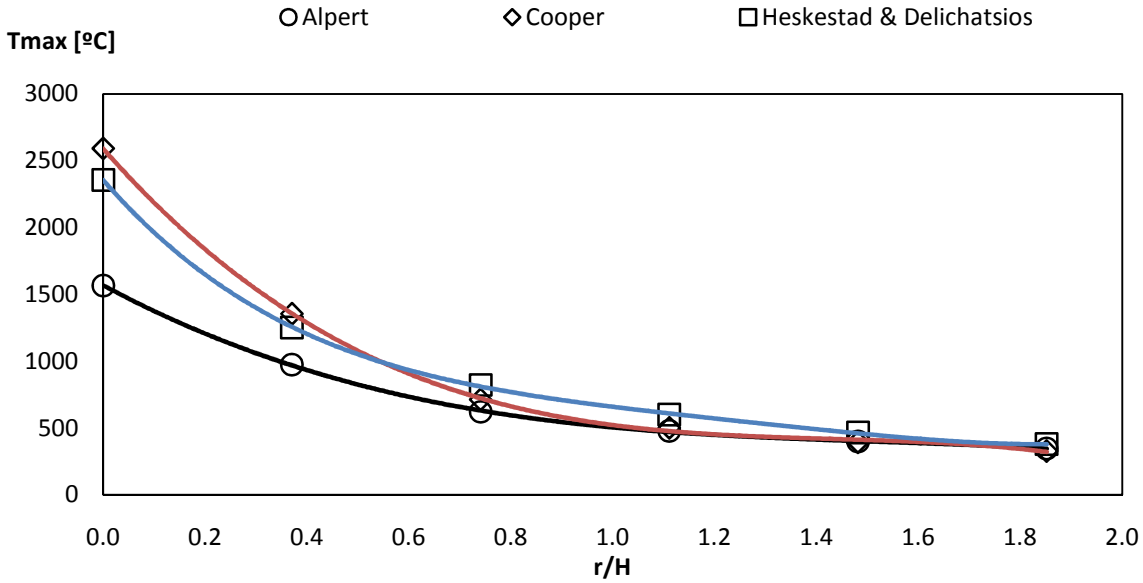

Figure 33- Comparison of the value of T_{max} from the correlative models for class 4,5

The results of Alpert and Cooper are close together for ratio r/H greater than 0.74. The following equations are based on the correlative results, which are the Cooper approximation for T_{max} (Eq 36), the Heskestad and Delichatsios approximation for T_{max} (Eq 37), and Alpert's approximation for T_{max} (Eq 38).

$$T_{max}= -682.5\left(\frac{r}{H}\right)^3+ 2935\left(\frac{r}{H}\right)^2 - 4319\left(\frac{r}{H}\right) + 2589 \quad (36)$$

$$R^2= 0.999$$

$$T_{max}= 466.5\left(\frac{r}{H}\right)^4 - 2366\left(\frac{r}{H}\right)^3+ 4555\left(\frac{r}{H}\right)^2 - 435.2\left(\frac{r}{H}\right)+ 2355 \quad (37)$$

$$R^2= 0.999$$

$$T_{max}= - 273.3\left(\frac{r}{H}\right)^3+ 1252\left(\frac{r}{H}\right)^2 - 2042\left(\frac{r}{H}\right) + 1567 \quad (38)$$

$$R^2= 0.999$$

We conclude that the maximum temperature on a ceiling jet decreases with the ratio r/H and the values also increase with the energy of the fire event. A table of comparison with the differences between the values is presented in annex B.

4.5.5- Maximum velocity comparison for class 1

Figure 34 represents the variation of the maximum velocity with respect to the ratio of the radial position r/H. The maximum velocity decreases with the radial position, being the intermediate results achieved with Cooper correlative model.

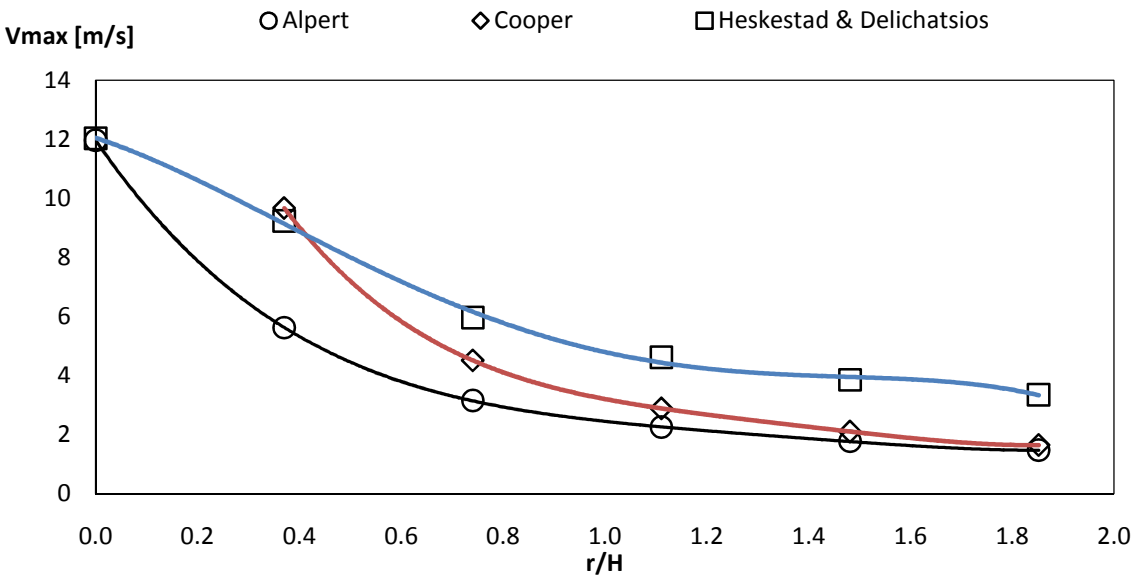

Figure 34- Comparison of the value of V_{max} from the correlative models for class 1

Taking Alpert's model as reference, the maximum velocity near the ceiling decreases with the ratio between the radial position and the height of the ceiling. The correlative models of Heskestad and Delichatsios and Alpert agree well for r/H equal to 0.0 (the plume zone) with relative difference between them equal to 0.5%. The Cooper correlative model for the plume is not presented. There is a good approximation between the model of Alpert and Cooper at r/H greater than 1.85, with relative difference between them below 12%. The best fitted approximation was calculated by $R^2 \approx 1$ coefficient. The following expressions are based on the correlative results which are the Cooper approximation for V_{max} (Eq 39), the Heskestad and Delichatsios approximation for V_{max} (Eq 40), and Alpert's approximation for V_{max} (Eq 41).

$$V_{max} = 4.831\left(\frac{r}{H}\right)^4 - 26.73\left(\frac{r}{H}\right)^3 + 55.74\left(\frac{r}{H}\right)^2 - 53.87\left(\frac{r}{H}\right) + 23.24 \quad (39)$$

$$R^2=1$$

$$V_{max} = -2.999\left(\frac{r}{H}\right)^4 + 11.04\left(\frac{r}{H}\right)^3 - 9.647\left(\frac{r}{H}\right)^2 - 5.653\left(\frac{r}{H}\right) + 12.05 \quad (40)$$

$$R^2=0.998$$

$$V_{max} = 2.3\left(\frac{r}{H}\right)^4 - 12.51\left(\frac{r}{H}\right)^3 + 25.77\left(\frac{r}{H}\right)^2 - 25.08\left(\frac{r}{H}\right) + 11.97 \quad (41)$$

$$R^2=1$$

4.5.6- Maximum velocity comparison for class 2

Figure 35 represents the variation of the maximum velocity with respect to the ratio of the radial position r/H. The maximum velocity for the plume zone does not agree between the

results of Alpert and Heskestad and Delichatsios, as reported in the previous fire event class. The correlative model of Cooper presents intermediate results.

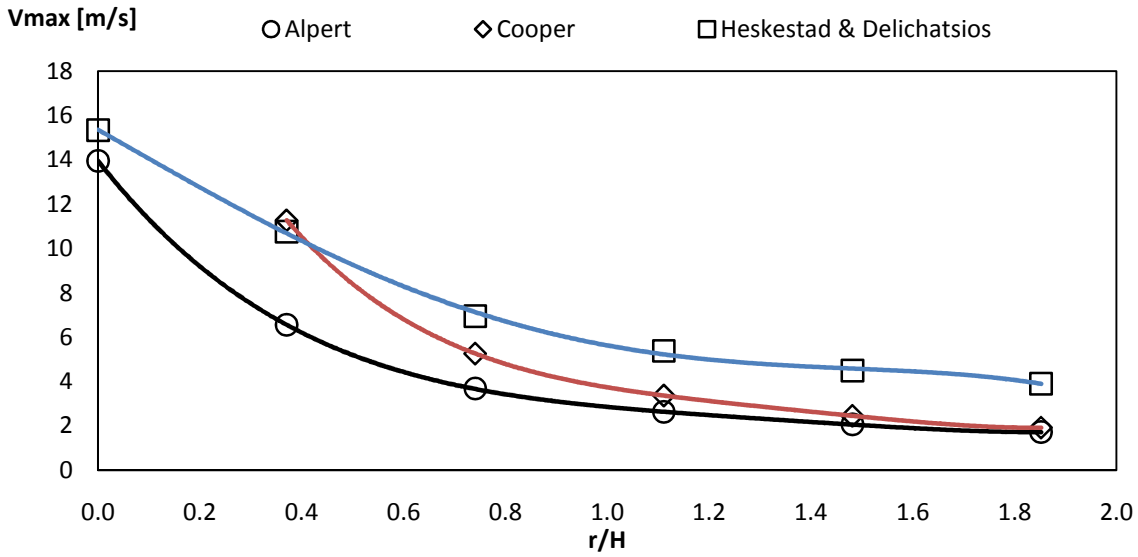

Figure 35- Comparison of the value of V_{max} from the correlative models for class 2

The results show that there is a divergence between the results of Alpert and Heskestad and Delichatsios with 4.4% of relative difference between them in the plume zone (r/H=0). There is a big difference between the two results (Alpert and Heskestad and Delichatsios) for ratios r/H greater than 0.37, with more than 60% of relative difference. The Cooper's model seems to approach the correlative Alpert's model for ratio r/H greater than 1.85, with relative difference between them below 12%.

The following equations are based on the results of V_{max} of car class two from correlative models and fit well the value of the maximum velocity with respect to r/H calculated by the $R^2 \approx 1$ coefficient which are: Cooper approximation for V_{max} (Eq42), the Heskestad and Delichatsios approximation for V_{max} (Eq 43), and Alpert's approximation for V_{max} (Eq 44).

$$V_{max} = 5.630\left(\frac{r}{H}\right)^4 - 31.16\left(\frac{r}{H}\right)^3 + 64.96\left(\frac{r}{H}\right)^2 - 62.79\left(\frac{r}{H}\right) + 27.09 \quad (42)$$

$$R^2=1$$

$$V_{max} = -2.043\left(\frac{r}{H}\right)^4 + 6.288\left(\frac{r}{H}\right)^3 - 0.944\left(\frac{r}{H}\right)^2 - 13.03\left(\frac{r}{H}\right) + 15.35 \quad (43)$$

$$R^2=0.999$$

$$V_{max}= 2.681\left(\frac{r}{H}\right)^4 - 14.59\left(\frac{r}{H}\right)^3 + 30.04\left(\frac{r}{H}\right)^2 - 29.23\left(\frac{r}{H}\right) + 13.95 \quad (44)$$

$$R^2=1$$

4.5.7- Maximum velocity comparison for class 3

Figure 36 depicts the variation of the maximum velocity with respect to the ratio of the radial position r/H. The maximum velocity decreases with the ratio r/H and the results from Cooper model agree with Alpert model for the higher values of r/H.

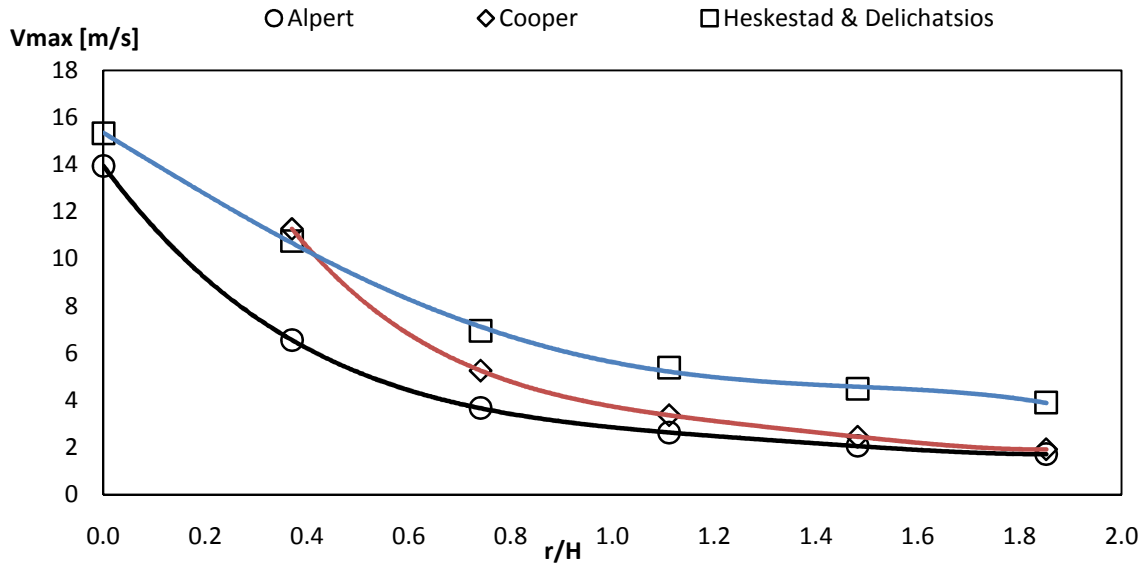

Figure 36- Comparison of the value of V_{max} from the correlative models for class 3

The relative difference between results from Heskestad and Delichatsios correlations and Alpert correlations reaches 9.9% for the ratio r/H=0.0 (plume zone). For the other radial positions, results are similar to the previous fire event car classes. An approximation based on the of fourth order polynomial is proposed to the maximum velocity using the best curve that fits well of the results for the maximum velocity with respect to r/H. The expressions are: Cooper approximation for V_{max} (Eq45), the Heskestad and Delichatsios approximation for V_{max} (Eq 46), and Alpert's approximation for V_{max} (Eq 47).

$$V_{max} = 5.630\left(\frac{r}{H}\right)^4 - 31.16\left(\frac{r}{H}\right)^3 + 64.96\left(\frac{r}{H}\right)^2 - 62.79\left(\frac{r}{H}\right) + 27.09 \quad (45)$$

$$R^2=1$$

$$V_{max} = -2.043\left(\frac{r}{H}\right)^4 + 6.288\left(\frac{r}{H}\right)^3 - 0.944\left(\frac{r}{H}\right)^2 - 13.03\left(\frac{r}{H}\right) + 15.35 \quad (46)$$

$$R^2 = 0.999$$

$$V_{max} = 2.681\left(\frac{r}{H}\right)^4 - 14.59\left(\frac{r}{H}\right)^3 + 30.04\left(\frac{r}{H}\right)^2 - 29.23\left(\frac{r}{H}\right) + 13.95 \quad (47)$$

$$R^2=1$$

4.5.8- Maximum velocity comparison for class 4 and 5.

Figure 37 represents the variation of the maximum velocity relative to the radial position, for a fire event of class 4 and 5. Similar conclusion regarding the correlative models can be made for this fire event.

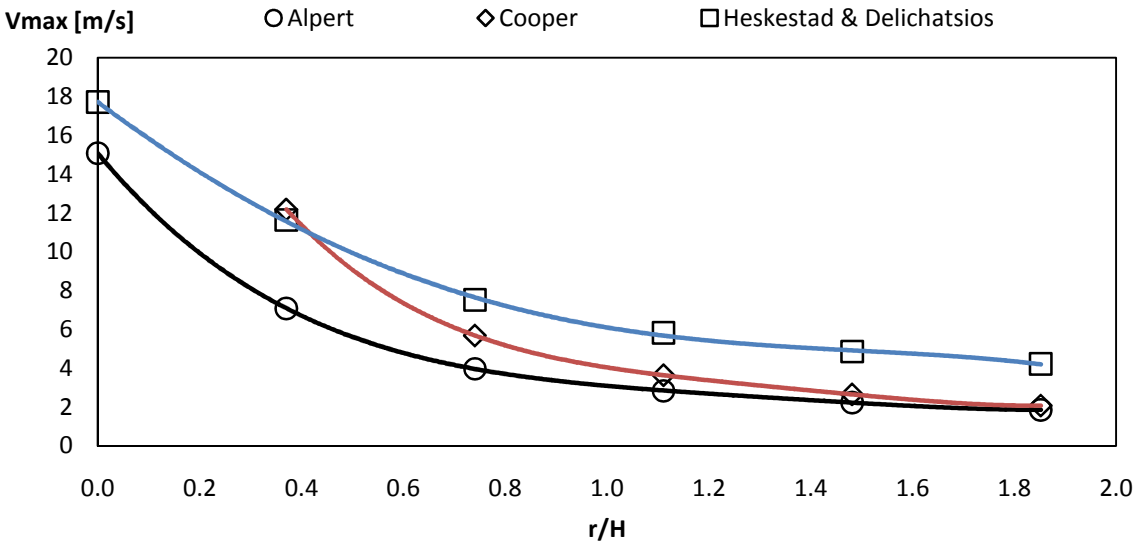

Figure 37- Comparison of the value of V_{max} from the correlative models for class 4,5

The results are similar to the previous fire car classes. Higher difference was detected for the plume zone between the correlative model of Heskestad and Delichatsios and Alpert correlative model. The relative difference achieved 17.4%.

The best fitted approximation to the proposed. Cooper approximation for V_{max} (Eq48), the Heskestad and Delichatsios approximation for V_{max} (Eq 49), and Alpert's approximation for V_{max} (Eq 50)

$$V_{max.} = 6.086\left(\frac{r}{H}\right)^4 - 33.68\left(\frac{r}{H}\right)^3 + 70.22\left(\frac{r}{H}\right)^2 - 67.87\left(\frac{r}{H}\right) + 29.28 \quad (48)$$

$$R^2=1$$

$$V_{max.} = -0.956\left(\frac{r}{H}\right)^4 + 1.129\left(\frac{r}{H}\right)^3 + 7.853\left(\frac{r}{H}\right)^2 - 19.64\left(\frac{r}{H}\right) + 17.72 \quad (49)$$

$$R^2=0.999$$

$$V_{max.} = 2.898\left(\frac{r}{H}\right)^4 - 15.77\left(\frac{r}{H}\right)^3 + 32.47\left(\frac{r}{H}\right)^2 - 31.59\left(\frac{r}{H}\right) + 15.08 \quad (50)$$

$$R^2=1$$

5- CFAST MODEL

Computer-based solutions to fire models are often used because of the complexity of fire phenomena and the cost a associated with experiments. Analytical models for predicting fire behaviour have been evolving since the 1960's. Different models divide the building into different numbers of control volumes, depending on the desired level of detail. The most common fire model, known as the zone model, generally uses two control volumes to describe a compartment: an upper layer and a lower layer [33]. A fairly realistic simulation can be done by a zone model under most conditions.

5.1- Definition of CFAST

CFAST is a computer program which helps engineers, fire investigators, architects and builders, safety officials to do a simulation of the impact of past or potential fires and smoke in a specific building environment, and the calculation of the evolving distribution of smoke, fire gases and temperature throughout compartments of a building during a fire. CFAST is one of fire codes known as zone model codes. It is a lumped-parameter code in which each room is divided into two lumped-parameter volumes, an upper layer and a lower layer, being the temperature within each layer consider uniform. CFAST can model a fire as either a source of heat or with a simple combustion model [9], which was developed by the National Institute of Standards and Technology (NIST). The zone model starts to solve the conservation of mass, the conservation of energy and the ideal gas law. CFAST is a two-zone fire model that can accommodate 30 compartments with multiple openings between the compartments. This two zone fire model has the capacity of predicting the environment in a multi-compartment structure subjected to a fire, where the transport of smoke and heat from zone to zone is dictated by empirical correlations [33]. The basic features of the software CFAST are the following: Simulation of the environment, Thermal properties, compartments, Wall vents, Ceiling/Floor vents, Mechanical ventilation, Definition of the fire, Detection / Suppression systems, Surface connections, and post processing of results.

5.2- The model

The model under analysis is the same that was used for the correlative models. Different fire events (car classes) were defined to determine temperature and velocity near the

ceiling of a fire induced ceiling jet. Different steps for doing this simulation are presented below with the specification of all data for each input parameter. The fire event of a class 3 is presented as an example.

5.2.1- Simulation environment

The initial conditions for the simulation of a fire event in CFAST are going to be presented. The simulation times was set to 4200s, being the text output interval time defined to 50s, and spreadsheet output interval defined to 10s. The time defined for the smoke view output interval was set to 10s. The maximum time step was set to default. The initial ambient temperature was defined to 20°C and the initial values for ambient atmospheric pressure inside and outside the compartment was defined to be 101325 Pa. The humidity inside the compartment was considered equal to 50%.

5.2.2- Thermal properties

Two materials were defined for the compartment, which are steel and concrete. Steel material was used for the definition of the target and concrete for the definition of the slab and walls. The thermal properties for both of these two materials are presented above (see Table 2). In this part we have some critical notes about CFAST considering the properties of the materials used. In CFAST the specific heat of steel is assuming to be constant C_p but in reality the specific heat depends on temperature. The same observation about the thermal conductivity λ for steel can be done.

About the second material using for the slab (concrete) we have also some critical notes about the use of its properties in CFAST. The Thermal conductivity of concrete is not constant, as is assuming in CFAST λ= 0.002 [kW/(m °C)].

5.2.3- Compartments

The compartment name that we proposed is OPEN_ CAR_ PARKING, the geometry was assumed that the width (X) =10m with absolute position equal to 0m and the depth(Y)= 10m with absolute Y coordinate equal to 0m and the height (Z)= 3m with absolute Floor Height equal to 0m, using concrete for the ceiling and walls and floor. In this simulation we

assume that conditions in the compartment like the flow characteristics are normal (two zone model), see Figure 38

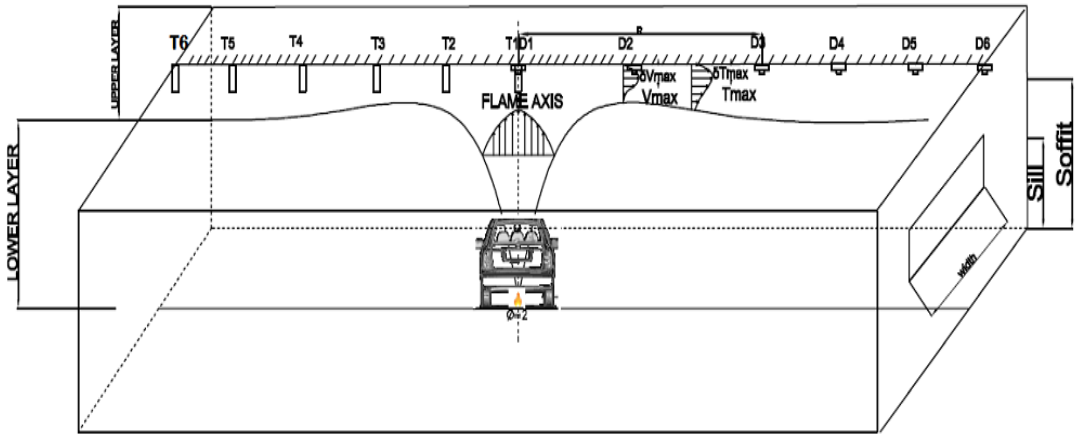

Figure 38- The geometry of our case of fire compartment

5.2.4- Wall vents

The wall vents are defined using the definition of two more external compartments. The geometry of the vents were defined to be coincident to the dimensions of the left and right surfaces of the main compartment, using a sill dimension equal to 0m, a soffit dimension equal to 3m and a width corresponding to 10m. The vents were considered fully open during the simulation. No Ceiling/Floor Vents and Mechanical Ventilation were considered in the model.

5.2.5- Fires

The fire source of the event is located in the centre of the compartment, above the ground in 0.3m. The time of ignition (Ignition Criterion) was considered equal to 0s, without ignition target. The total simulation time was set to 4200s. The values of the HRR were defined for each car class, see Table 1.

5.2.6- Defining targets

Six targets were define (OPEN_ CAR_ PARKING) for getting the local temperature of the hot gases in the plume zone and ceiling jet. These targets were made of steel, using thin

plate shape (high section factor), with the normal vector corresponding to X direction. Table 15 of annex C presents the different parameters for each target and their positions.

5.2.7- Defining the fire detectors

Six detectors were defined on the ceiling of the compartment, defined as heat alarms. The activation temperature was defined to be 100°C. The radial positions of the detectors are defined in table 15 of annex C.

5.2.8- Output results

The compartment was divided into a grid. The size of the grid was tested before simulation to decide the number of divisions. This convergence test was done and the number of divisions was defined to be 50 (16 grids for the hot layer and 34 grids for the cold layer) (see Figure 39). Different simulation were done for the five car classes (1, 2, 3, 4, 5) and the results of each car class are presented in the annex C in form of tables. The graphical results of the different CFAST simulations for the temperature and the velocity versus time are plotted in Figure 40 and Figure 41. The temperature and velocity of hot gases near the ceiling have the highest values when time equals to 25 min. The results for T_{max} and V_{max} depend on the ratio r/H and are represented by Figure 42, Figure 43 and Figure 44, Figure 45.

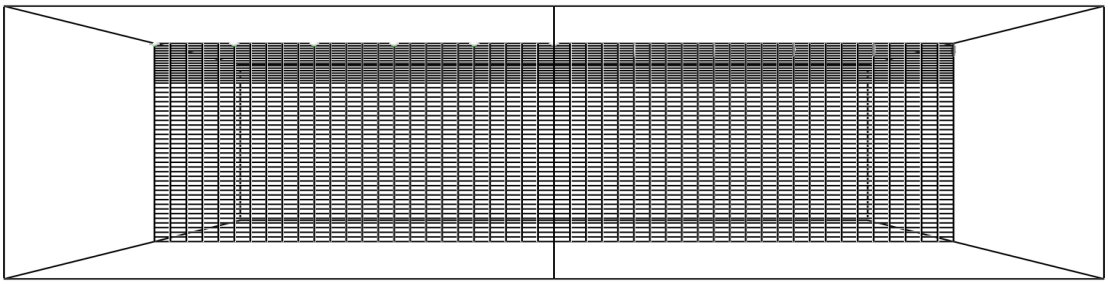

Figure 39- Grid size of the compartment

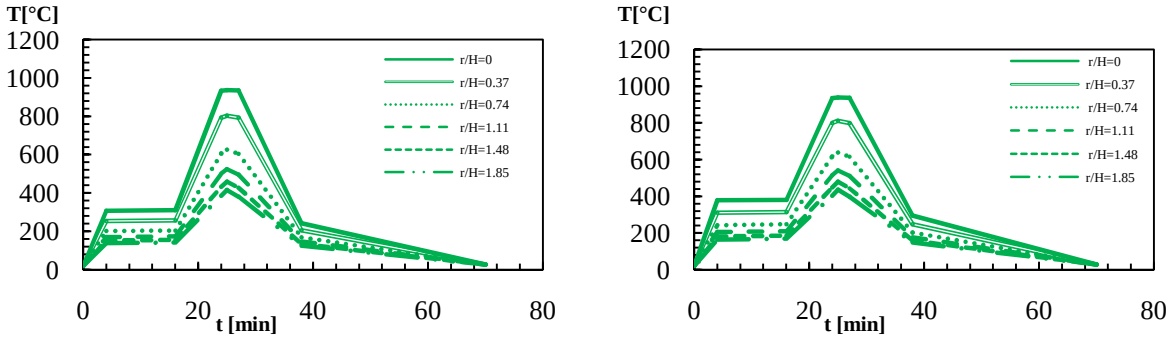

Class 1 Class2

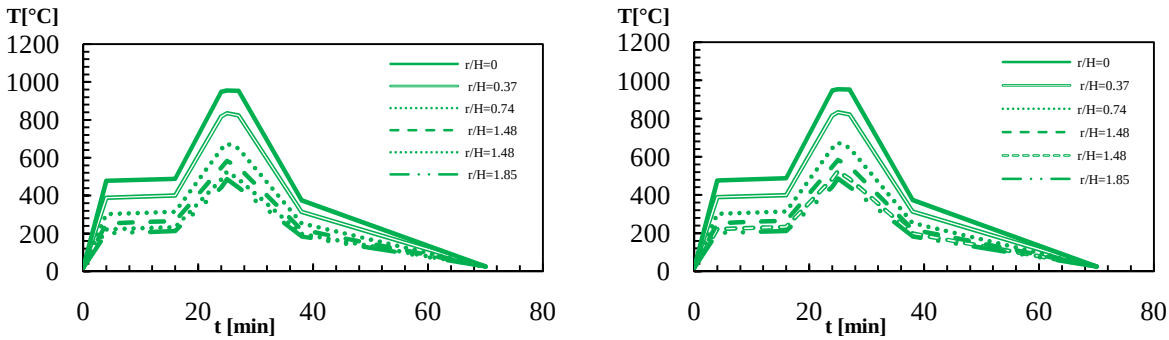

Class3 Class4,5

Figure 40- Results of temperature from CFAST simulation

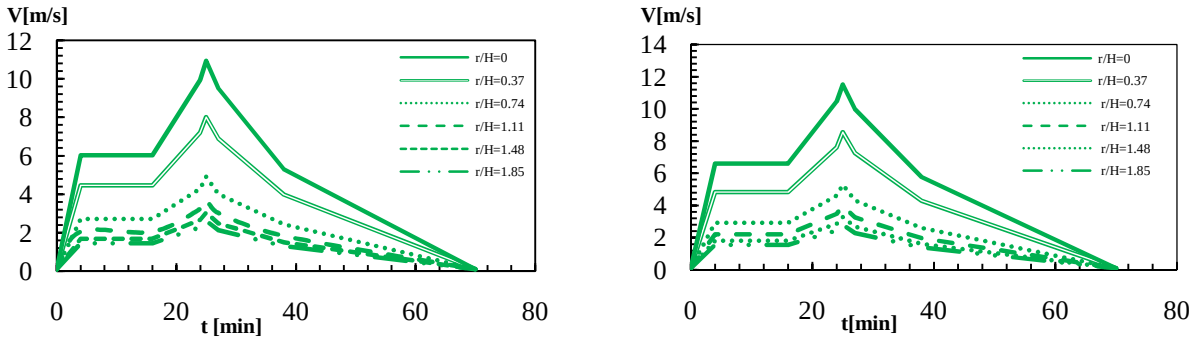

Class1

Class2

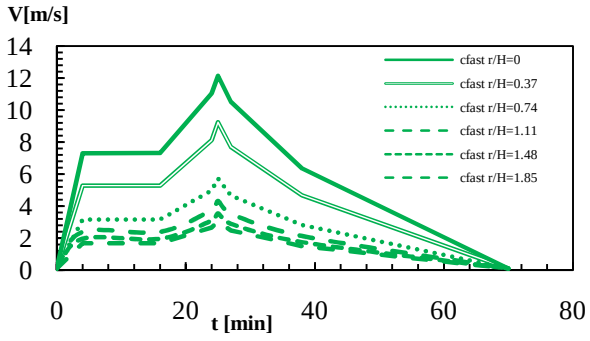

Class3

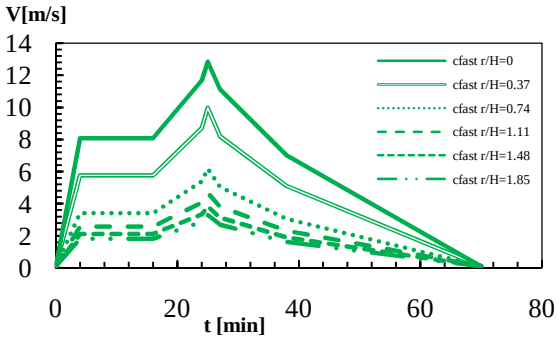

Class4,5

Figure 41-Results of velocity from CFAST simulation

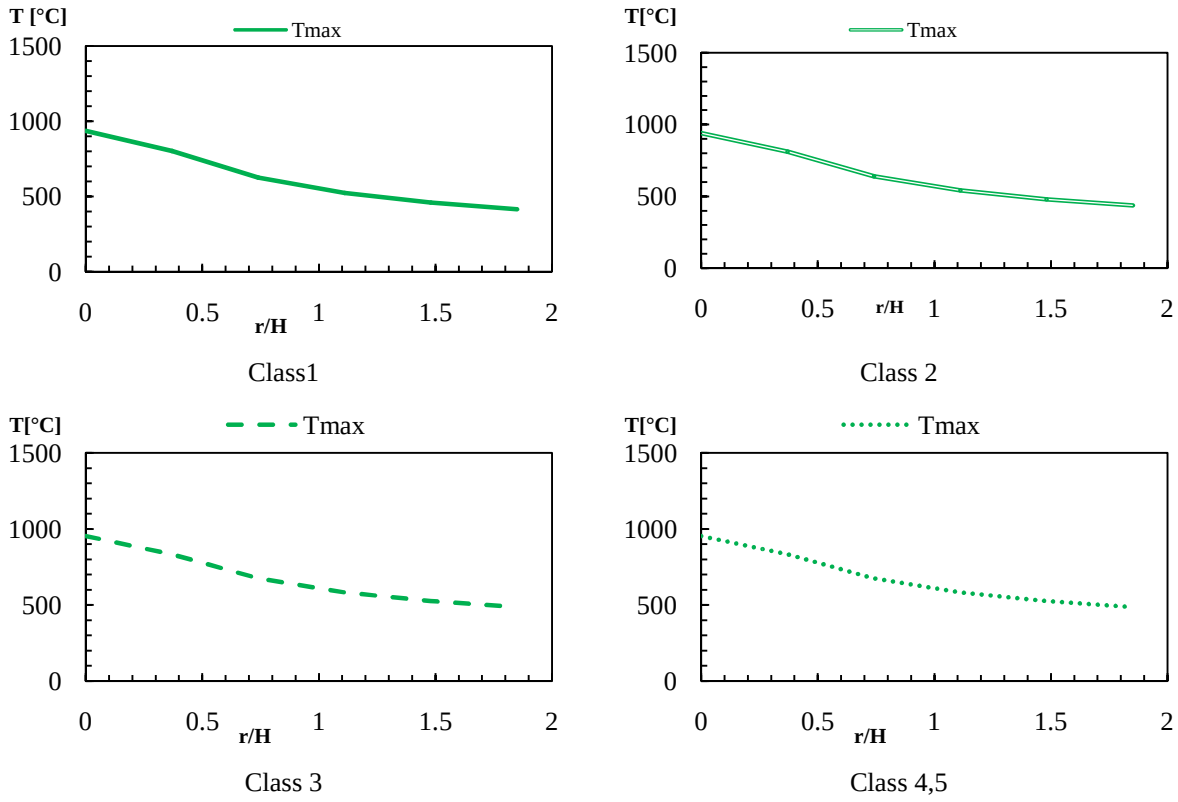

Figure 42- Results of T_{max} from CFAST simulation

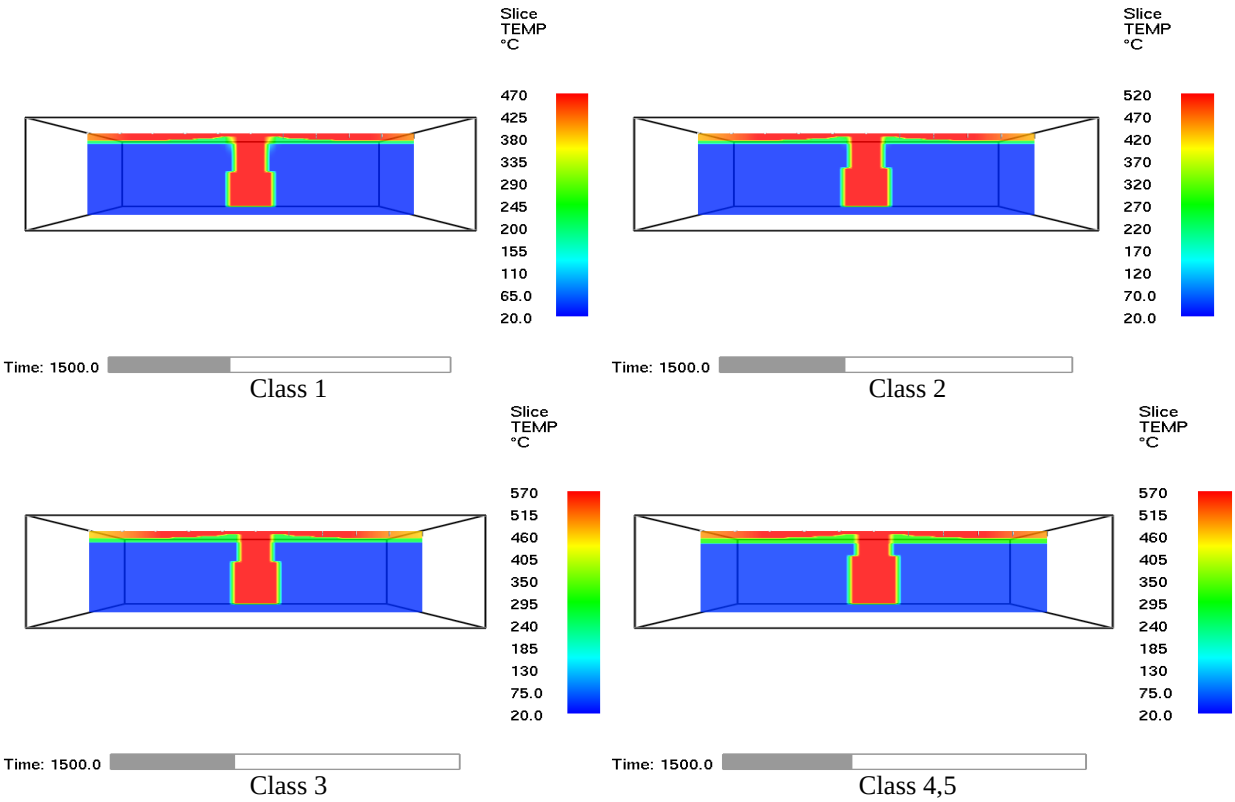

Figure 43- CFAST simulation for T_{max}

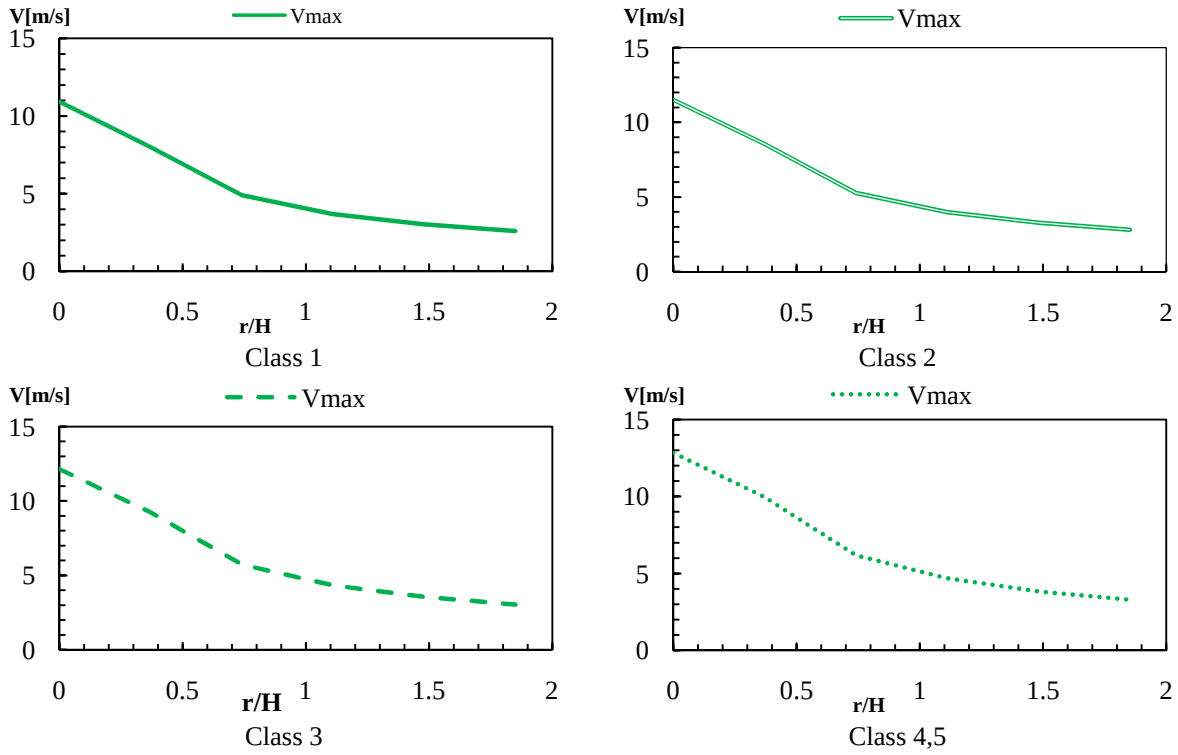

Figure 44- Results of V_{max} from CFAST simulation

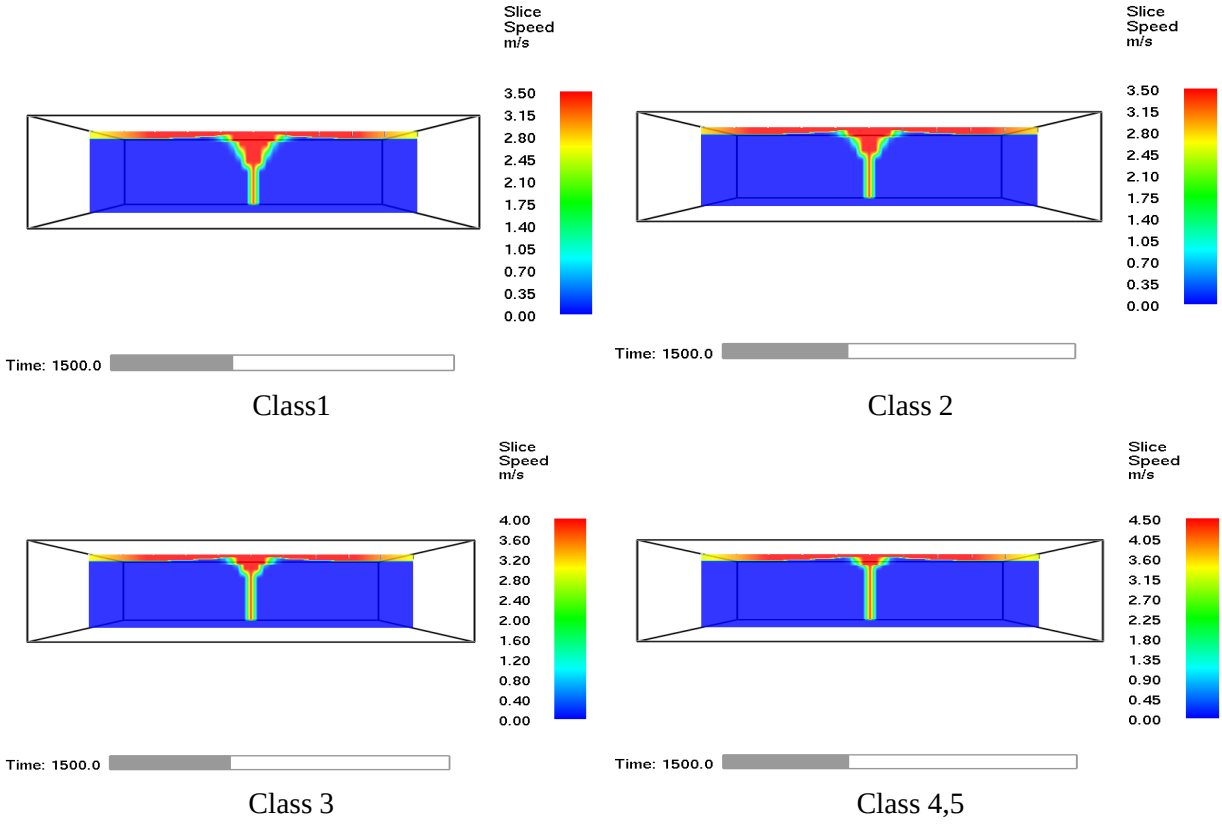

Figure 45- CFAST simulation for V_{max}

5.3- Comparison of results

A comparison of the maximum temperature and velocity between the correlative models and numerical simulation from CFAST is presented for all car classes. The difference between results is presented in table 17 of annex C.

5.3.1- Maximum temperature comparison for class 1

Figure 46 represents the comparison between correlative models and two zone model. The maximum temperature calculated by CFAST agrees well with the Alpert results for the plume zone, but is in general agreement with the correlative model from Heskestad and Delichatsios for the other radial positions.

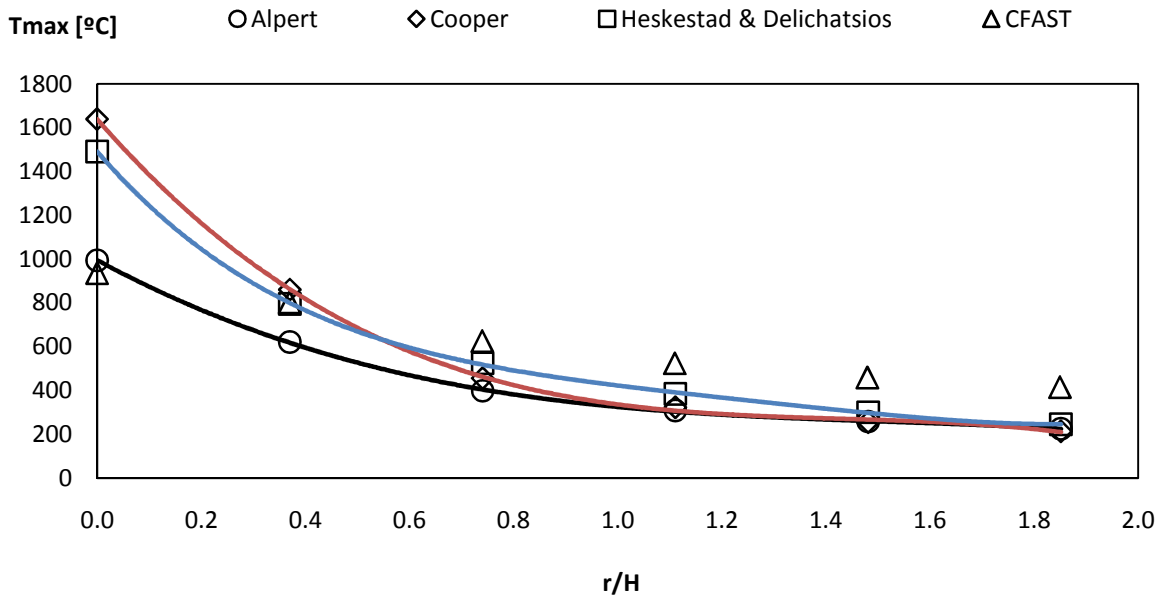

Figure 46- Comparison of T_{max} for class one

The maximum temperature decreases with the ratio r/H, for both types of results (correlative and CFAST). There is a good agreement between CFAST results and Alpert's model when the ratio r/H equals to 0 with relative difference of 5.9%. The difference between CFAST and Cooper's model for r/H is greater than 0.37 is 7.3%. In general the correlative models under predict the T_{max}.

5.3.2- Maximum temperature comparison for class 2

Figure 47 represents the comparison between correlative models and two zone model for class two. It seems that there is a relative difference of 18.4% between the Alpert's model and CFAST results in the plume zone unlike the results of class one with. There is always a good approximation between CFAST results and the correlative model from Heskestad and Delichatsios for the other radial positions.

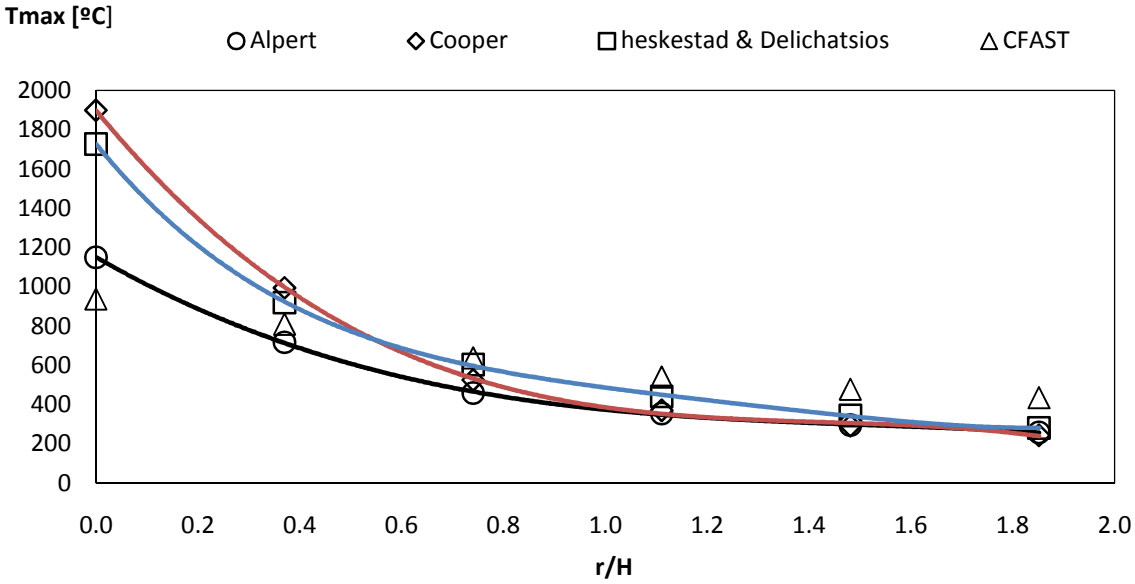

Figure 47- Comparison of T_{max} for class two

Also it is important to note that the relative difference between CFAST and Cooper is higher for the radial r/H=0.37 when compared to previous class one. In general there is always an approximation between results from the correlative models and CFAST simulation when the ratio r/H is greater than 0.74.

5.3.3- Maximum temperature comparison for class 3

Figure 48 represents the comparison between correlative models and two zone model for class three. The maximum temperature calculated by CFAST agrees well with the Alpert results when the ratio r/H equals to 0.37 with relative deference between them 0.3%.

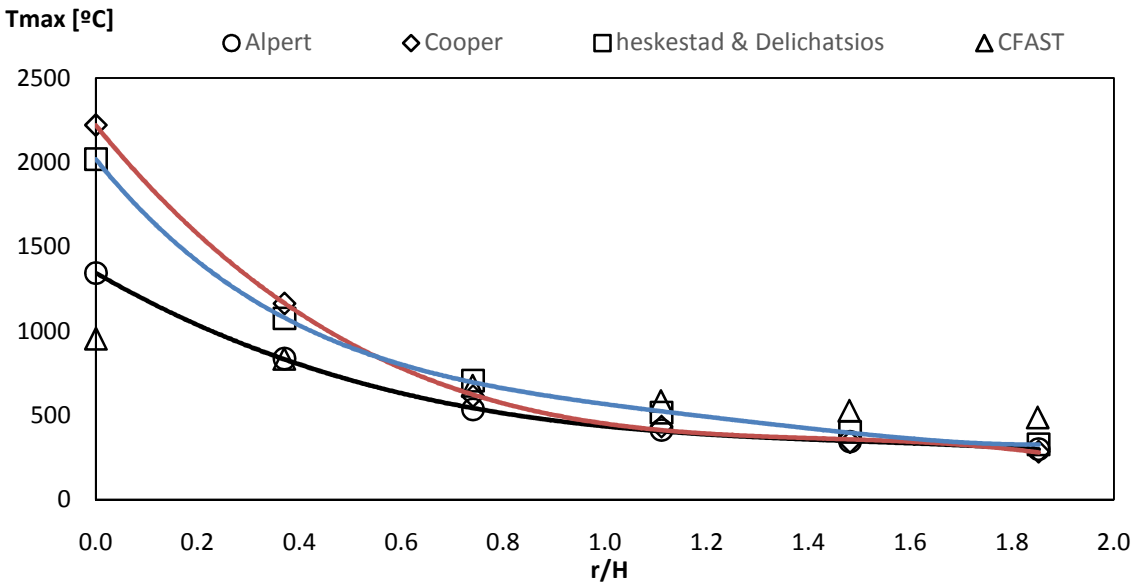

Figure 48- Comparison of T_{max} for class three

There is a better agreement between results from Heskestad and Delichatsios correlation and CTAST results for r/H greater than 1.1 with a maximum relative difference of 11%. The correlative models results approximate well with results from CFAST simulation, when the ratio of r/H is greater than 0.74, as the previous cases.

5.3.4- Maximum temperature comparison for class 4 and 5

Figure 49 represents the comparison between correlative models and two zone model for vehicle class four and five. The relative difference between Alpert's model and CFAST results is 14.5%, when the ratio r/H is equal to 0.37. The best region where all correlative models agree well with CFAST results is on the ratio r/H greater than 0.74.

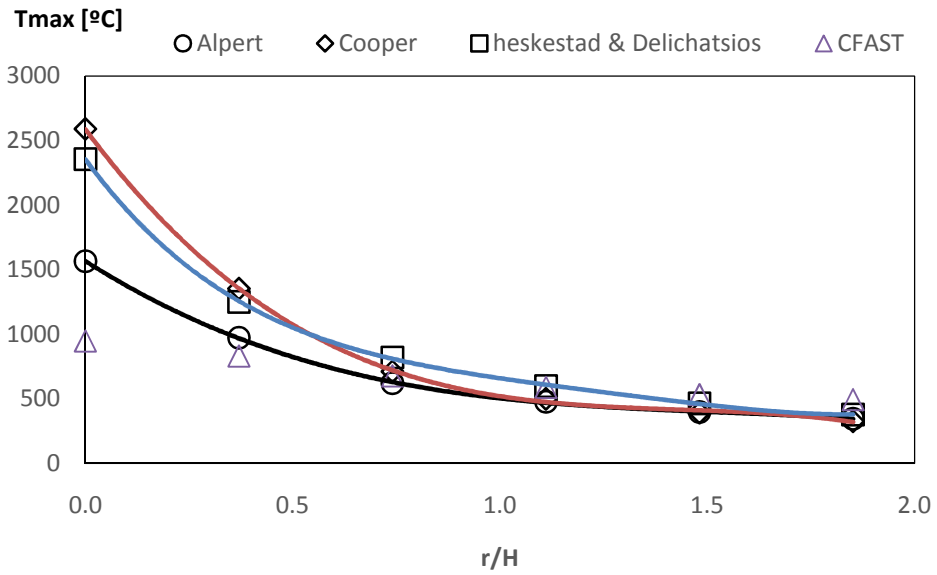

Figure 49- Comparison of T_{max} for class 4,5

There is a good agreement between results from Heskestad and Delichatsios models and CFAST simulation when the ratio r/H is equal to 1.1 with relative difference between them equal to 1.3%. There is a very big difference between the correlative models and CFAST on the plume zone.

As general observation from the comparison between the results from the correlative models and CFAST results for the maximum temperature near the ceiling for all the car categories is that: when the ratio r/H is greater than 0.74 the correlations and CFAST results agree very well. The maximum temperature decreases with the ratio r/H, for both types of results (correlative and CFAST). The difference between results is presented in tables 21, 22, 23 and 24 of annex C.

5.3.5- Maximum velocity comparison for all car classes

Figure 50 represents the comparison results for maximum velocity between CFAST and the correlative models. The difference between these results is qualitatively similar for all car classes. The maximum velocity decreases with the ratio of r/H for both results (correlative and numerical).

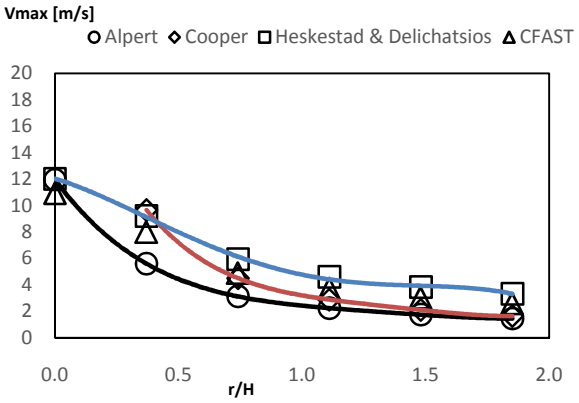

Class 1

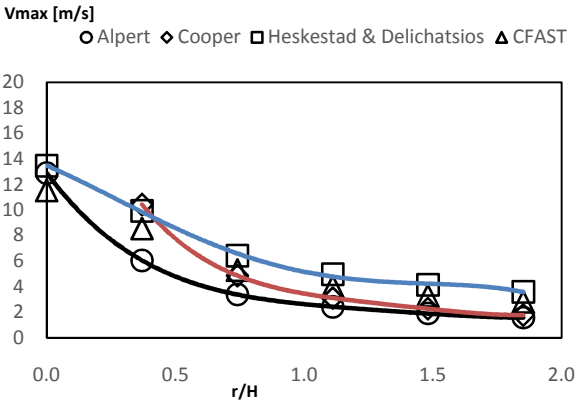

Class 2

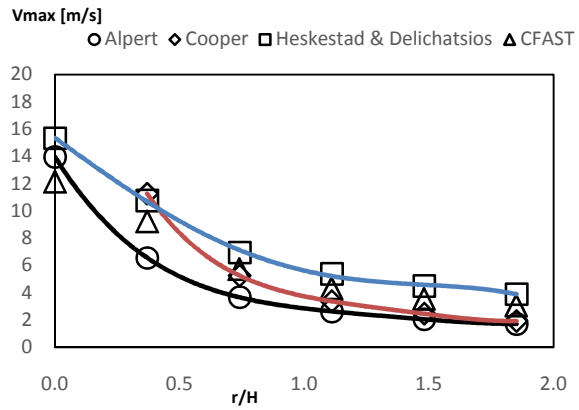

Class 3

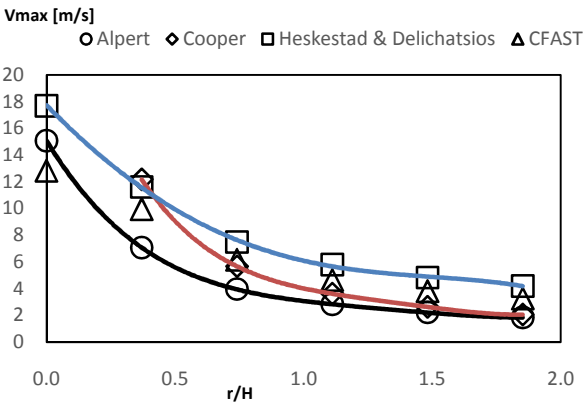

Class4,5

Figure 50- Comparison of V_{max} for all car classes

There is a good agreement between the results from the correlative models and the numerical simulation of CFAST when the ratio of r/H is greater than 1.1. A good approximation was also achieved between Alpert models and CFAST results for the plume zone. Cooper's model and CFAST results agree well when 0.5≤r/H≤1.0. The Heskestad and Delichatsios models agree with CAFST numerical results for the ratio r/H greater than 1.48. The difference between results is presented in tables 25, 26, 27 and 28 of annex C.

6- FLUENT MODEL

ANSYS is an US Computer-aided engineering software. ANSYS Fluent is one of two types of software to simulate fires. FDS software (Fire Dynamic Simulator) which is specially prepared for modelling and simulation of fire, and CFD software (Computational Fluid Dynamic) which may be adapted to any fluid mechanics problem. ANSYS Fluent is a CFD software used by engineers for design and analysis. Is the most-powerful computational fluid dynamics (CFD) software tool available with the broad physical modelling capabilities needed to model flow, turbulence, heat transfer, and chemical reactions.

6.1- Equations to be solved

A set of equations which are incorporated into a Finite Element method for solving fluid flow problems, are presented on the following

6.1.1- Continuity equation

In any closed system the conservation of mass must be satisfied. Mass must not be created or destroyed. The equation governing this principle is known as the continuity equation [34] and is shown below in equation 52.

$$\frac{\partial_\rho}{\partial_t} + \nabla.(\rho V) = 0 \tag{52}$$

where ρ id the density, t is the time and ∇ is Del operator$= \frac{\partial}{\partial_x}i + \frac{\partial}{\partial_y}j + \frac{\partial}{\partial_z}k$, then V is the vector of velocity $= V_x i + V_y j + V_z k$. This equation can be expanded.

$$\frac{\partial_\rho}{\partial_t} + \frac{\partial_\rho V_x}{\partial_x} + \frac{\partial_\rho V_y}{\partial_y} + \frac{\partial_\rho V_z}{\partial_z} = 0 \tag{53}$$

6.1.2- Navier-stokes equation

The Navier-Stokes equations are a collection of the 3 dimensional momentum equations for any Newtonian fluid. In fluid dynamics, a Newtonian fluid is one in which the stresses at each point in the fluid are linearly proportional to the strain rates at that point. These equations ensure that in any

system, the momentum is conserved. This means that the total force generated by the momentum transfer in each direction must be balanced by the rate of change of momentum in each direction. The Navier-Stokes equation is provided below [34] for the Z component. The other directions in space also apply.

$$\frac{\partial \rho V_z}{\partial t} + \frac{\partial (\rho V_x V_z)}{\partial x} + \frac{\partial (\rho V_y V_z)}{\partial y} + \frac{\partial (\rho V_z V_z)}{\partial z} = \rho g_z - \frac{\partial P}{\partial z} + R_z + \frac{\partial}{\partial x}\left(\mu_e \frac{\partial V_z}{\partial x}\right) + \frac{\partial}{\partial y}\left(\mu_e \frac{\partial V_z}{\partial y}\right) + \frac{\partial}{\partial z}\left(\mu_e \frac{\partial V_z}{\partial z}\right) + T_z \quad (54)$$

Where g_z is components of acceleration due to gravity that exists only in this direction. R_z is distributed resistance, μ_e is the effective viscosity of the fluid, T_z refers to viscous loss terms.

The final form of the Navier-Stokes equations for an incompressible flow without gravity acting in the y direction and with no distributed resistances is given in equation 55 [34].

$$\frac{\partial \rho V_z}{\partial t} + \frac{\partial (\rho V_X V_z)}{\partial x} + \frac{\partial (\rho V_y V_z)}{\partial y} + \frac{\partial (\rho V_z V_z)}{\partial z} = -\frac{\partial P}{\partial z} + \frac{\partial}{\partial x}(\mu_e \frac{\partial V_z}{\partial x}) + \frac{\partial}{\partial y}(\mu_e \frac{\partial V_z}{\partial y}) + \frac{\partial}{\partial z}(\mu_e \frac{\partial V_z}{\partial z}) \quad \text{Eq 55}$$

6.1.3- Energy equation

The first law of thermodynamics requires that the energy of a system be conserved. The three-dimensional energy equation for fluid flow is provided below [34].

$$\frac{\partial}{\partial t}(\rho C_p T) + \frac{\partial}{\partial x}(\rho v_x C_p T) + \frac{\partial}{\partial y}(\rho v_y C_p T) + \frac{\partial}{\partial z}(\rho v_z C_p T) = \frac{\partial}{\partial x}\left(K_{xx} \frac{\partial T}{\partial x}\right) + \frac{\partial}{\partial y}\left(K_{yy} \frac{\partial T}{\partial y}\right) + \frac{\partial}{\partial z}(K_{zz} \frac{\partial T}{\partial z}) + Q_V \quad \text{Eq 56}$$

Where ρ is density, Cp is specific heat, $V_{x;y;z}$ refers to the velocity in x, y, z directions and T represents the temperature, $K_{xx;yy;zz}$ is thermal conductivity in x, y, z directions, Q_V is the volumetric heat source, if exists.

6.2- The model

The model represents the fire compartment with 3m of height and 10m of depth and 10m of width. The fire event is located in the middle of this compartment, considering a burning car with an equivalent pool fire with a diameter of 2m.

Figure 51 shows the mesh of a fire event with a class 1 car vehicle, burning in the centre of a fire compartment with the overall dimension of 10x10x3 m^3. This compartment assumes the use of symmetry boundary conditions, allowing to model only one quarter of the full compartment. This compartment has two openings on the left side and right side, a concrete slab on the bottom and top floor and a concrete wall in the front and rear façade. The Thermal load is defined by the Heat Released Rate. Three types of boundary conditions were applied (fixed wall with thermal conduction through thickness, pressure out let and symmetry). The solution method monitors the residuals for all variables and assumes the convergence of the solution for continuity (residual less than 0.01), velocity components (residual less than 0.001), energy (residual less than 0.00001), turbulence parameters (residual less than 0.001) and radiation parameters (residual less than 0.000001).

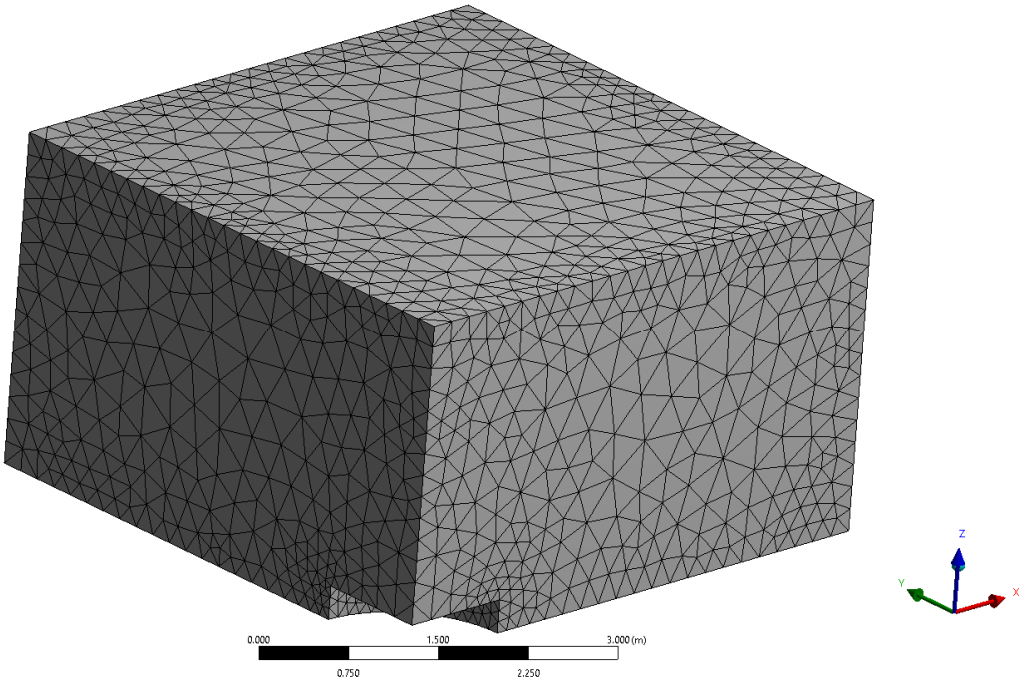

Figure 51- Mesh of the model

6.2.1- Material models

Two different materials models are defined. The fluid zone materialise defined by air and the solid material is represented by concrete. The thermal properties of the air are presented in . All the material properties were defined by piecewise linear approximation from a set of data points.

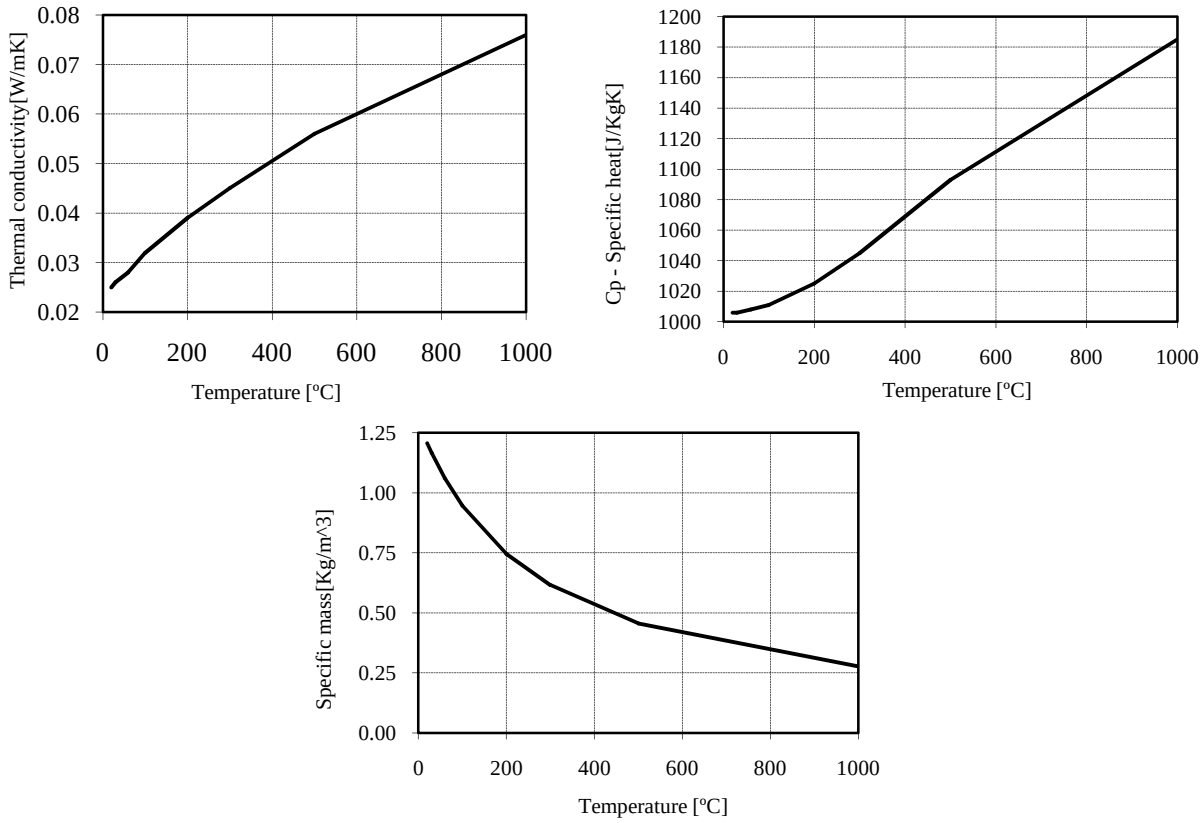

Figure 52- Properties of the Air

The specific density of concrete was specified by a UDF (User Defined Function), being the other two material properties defined by piecewise linear approximation from a set of data points. Table 3 represents the thermal properties of the concrete based on the data points.

Table 3- Properties of concrete based on data points

Points	Temperature °C	Temperature K	C_p(dry,u=3.0%) J/kgK	Density kg/m3	Diffusivity $m2/s$
1	20	293	900	2300	9.4E-07
2	100	373	900	2300	8.5E-07
3	101	374	2020	2300	3.8E-07
4	115	388	2020	2300	3.7E-07
5	200	473	1000	2254	6.9E-07
6	300	573	1050	2220	5.8E-07
7	400	673	1100	2185	5.0E-07
8	500	773	1100	2165	4.4E-07
9	600	873	1100	2145	3.9E-07
10	700	973	1100	2125	3.5E-07
11	800	1073	1100	2105	3.1E-07
12	900	1173	1100	2084	2.9E-07
13	1000	1273	1100	2064	2.7E-07
14	1100	1373	1100	2044	2.7E-07
15	1200	1473	1100	2024	2.7E-07

The specific heat *c*p(θ) of concrete considers moisture content of 3,0 % of concrete weight [35].

6.2.2- Boundary condition

A symmetry boundary condition in X negative and Y negative was assumed. It was also considered that there is a stationary wall boundary condition, an opening with zero pressure was consider for the pressure out let boundary, assuming $T_\infty = 20°C$ and radiation ε=1. The concrete material was modelled by stationary wall (wall thermal conductivity) and slabs, both with thickness of 0.3m. The thermal part of this boundary considered convection α=9[w/m^2k] of a surface not directly exposes to the fire, with $T_\infty = 20°C$.

6.2.3- Heat flux

The heat flux is equal to the ratio of HRR/ Surface [w/m^2]. The heat flux was applied in the top surface representing the car and was defined by User Defined Function (UDF) for car class 1. An adiabatic lateral surface was defined on the cylindrical zone. The surface of car is equal to 3.141593 [m^2] , corresponding to the diameter of 2m. The numerical values of the heat flux for car class 1used in our simulation are presented in Table 4

Table 4- HRR and heat flux of class 1

		class 1	class 1
Time	Time	Heat flux	HRR
min	S	W/m^2	W
0	0	0	0
4	240	281386	884000
16	960	281386	884000
24	1440	1105809	3474000
25	1500	1668580	5242000
27	1620	904637	2842000
38	2280	201172	632000
70	4200	0	0

6.3- Discussion of results

6.3.1- Velocity results from ANSYS fluent simulation

Figure 53 shows the graphical results of velocity amplitude for car class 1 depending of the targets positions.

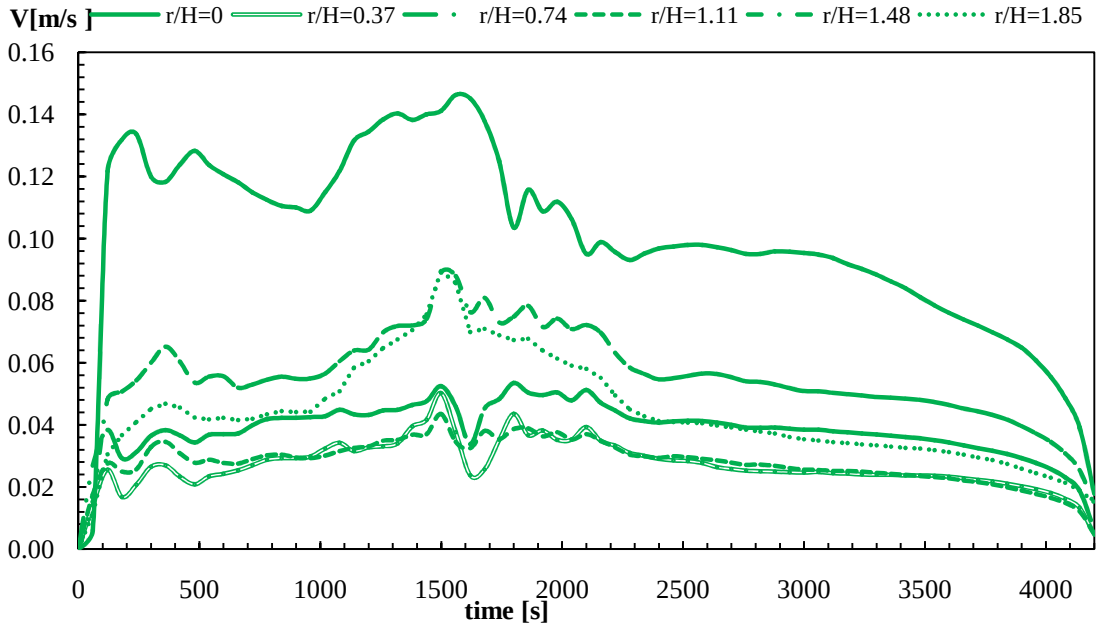

Figure 53- Results of velocity from ANSYS fluent simulation of car class 1

The results of velocity show that the highest values is when the ratio r/H is equal to zero (plume zone). The second target presents smaller results, probably due to mesh definition or due to the fact to be included in the transition zone between plume and ceiling jet. The numerical results for V_{max} for all car classes are presented in table 30 of annex D.

6.3.2-Temperature results from ANSYS fluent simulation

Figure 54 represents the results of temperature from the numerical simulation using ANSYS fluent. This graphs show the time evolution of the temperature for different radial targets.

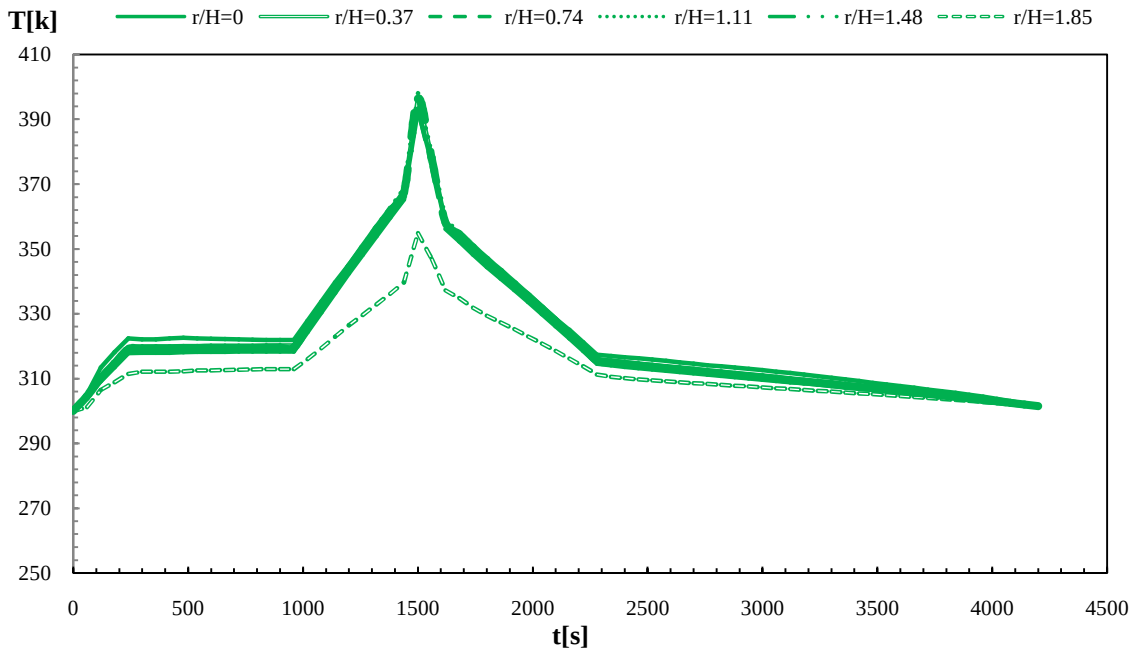

Figure 54- Results of temperature from ANSYS fluent simulation of car class 1

Figure 55 shows the results of the CFD simulation when t=25 minutes(1500s), and also represents the model and the grid size.

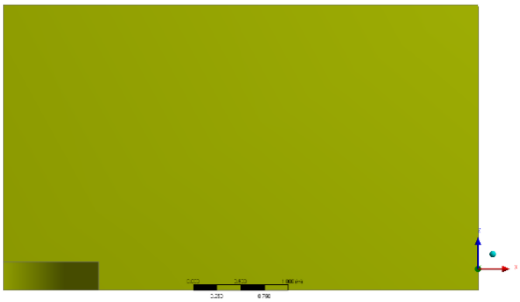

a) The model

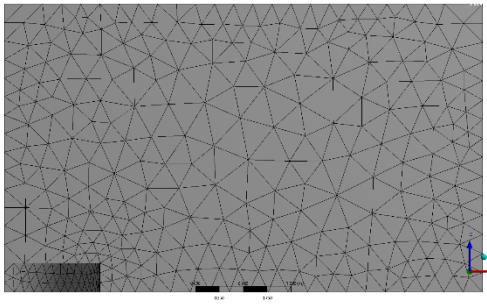

b) Grid size

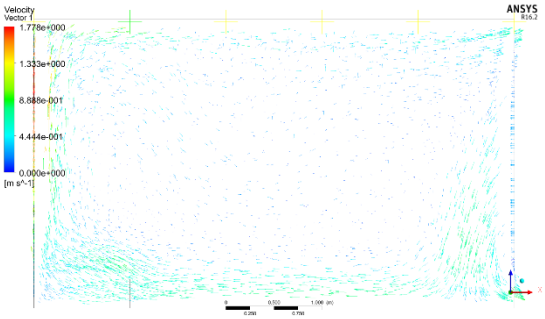

Vector total velocity for t=1500 s

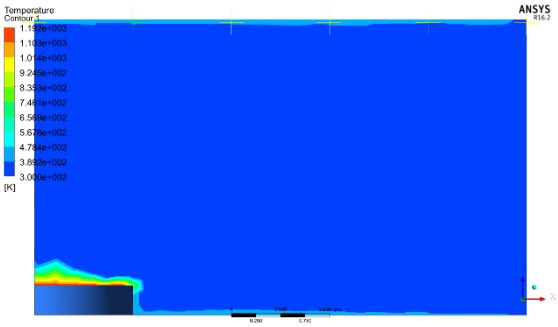

Temperature for t=1500 s

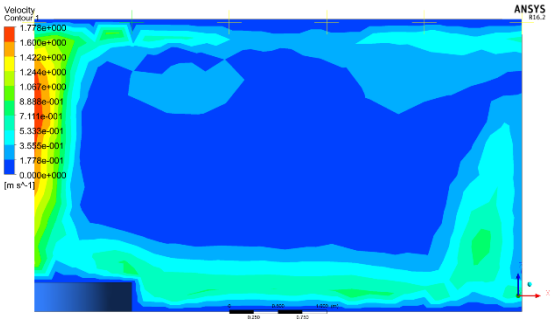

Amplitude total Velocity for t=1500 s

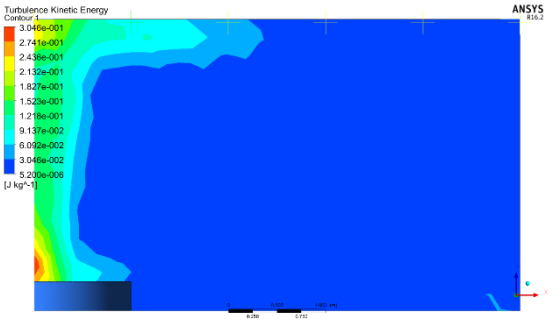

Turbulence Kinetic energy for t=1500 s

Figure 55- Model and results of CFD simulation for t=25 min

The Fluent model is running without solving the equation for species, even though the results are qualitatively in accordance to expectation. The low level of temperature and velocity is related to the boundary condition that were defined. The residuals for the continuity equation was not achieved (0.01) and the mass flow rate did not converge. Higher flow rate should be expected, and consequently higher values for temperature and velocity would also be expected on the hot layer.

7- CONCLUSIONS

This work presented a study about the thermal and dynamic characteristics of a fire-induced ceiling-jet in open car parks.

A burning car is localised in compartment with unconfined ceiling jet using a specific dimensions of the car and of the fire, using six targets on the ceiling to get results for the maximum temperature and velocity of the hot gases near the ceiling. This results were calculated with simple correlative models (Alpert, Cooper, Heskestad and Delichatsios), and with two numerical models: zone model (CFAST) and the software ANSYS fluent.

The comparison of the results between the correlative models, CFAST and ANSYS fluent showed an agreement between these results in specific radial positions, taking on consideration that each one of the software has a different way of doing calculations. Correlative results are usually define from experimental results and the numerical models are based on different equations.

The confrontation between correlative, two zone and CFD models can improve the knowledge state on the ceiling-jets and probably helps the fire engineers to enhance the performance of the fire protection devices.

For technical purposes regarding fire engineering, it would be interesting to perform a Computational Fluid Dynamics (CFD) calculation, where turbulent Navier-Stokes equations are solved using either RANS or LES approaches. Here, both dynamic and thermal characteristics of the flow in the beneath of the ceiling can be predicted with respect to heat release rate (HRR) and $\dot{m}$ mass sources.

REFERENCES

[1] R. L. ALPERT, Calculation of Response Time of Ceiling-Mounted Fire Detectors, paper (76th Annual Meeting of the National Fire Protection Association), pp 181-195, May 18, 1972.

[2] Gunnar Heskestad, Michael. Delichatsios, The Initial Convective Flow In Fire, Symposium (International) on Combustion, volume 17, issue 1, pp 1113-1123, 1979.

[3] Nora H. Jason, An Investigation of Fire Impingement on A Horizontal Ceiling, report discusses research (U.S. Department of Commerce National Bureau of Standards Center for Fire Research Washington), DC 20234, NBS-GCR-81-304, pp 1-78, December 1981.

[4] Leonard Y. Cooper, A Buoyant Source in The Lower of Two Homogeneous Stably Stratified Layers,twentieth symposium (international) on combustion, pp. 1567-1573, 1984.

[5] Robert P. Schifiliti, Use of Fire Plume Theory in The Design and Analysis of Fire Detector and Sprinkler Response, Master thesis, pp 1-119, January 1986.

[6] V.Motevalli and C. Ricciuti, Characterization of the Confined Ceiling Jet in the Presence of an Upper Layer in Transient and Steady-State Conditions, final report, pp 1-148, August 1990 - July 1991.

[7] V.Motevalli, and Marks, Characterizing The Unconfined Ceiling Jet Under Steady-state Conditions: A Reassessment, Fire Safety journal Science3, pp 301-312, Doi 10.3801/IAFSS.FSS.3-301, January 1991.

[8] David D. Evans, ceiling jet flows, SFPE Handbook of Fire Protection Engineering, 2nd Edition, Chapter 4, Section 2, pp 2/32-2/39, 1995.

[9] Jason E. Floyd, Comparison of CFAST and FDS for Fire Simulation with the HDR T51 and T52 Tests, paper, pp 1-112, March 2002.

[10] Kevin Mc Grattan, Simo Hostikka, Randall McDermott, Jason Floyd, Craig Weinschenk Kristopher Overho, Fire Dynamics Simulator User's Guide, FDS Version 6.0.1, SVN Repository Revision: 17529, November 26, 2013.

[11] Xiaobo Yao, characterization of fire induced flow transport along ceilings using salt-water modelling, requirements for the degree of Doctor, pp 1-152, 2006.

[12] R. L. ALPERT, Fire-induced Ceiling-jet Revisited, fifth FireSeat event, pp 1-22, 9th November 2011.

[13] Johansson, Nils, Wahlqvist, Jonathan, VanHees, Patrick, simple ceiling jet correlation derived from numerical experiments, thirteenth international interflam conference, pp 61-72, 2013.

[14] Ying Zhen Li, HaukurIngason, Fire-induced ceiling jet characteristics in tunnels under different ventilation conditions, report, pp 1-69, 2015.

[15] T Hara, S Kato, Numerical Simulation of Fire Plume-Induced Ceiling Jets Using the Standard k -ε Model, journal of Fire Technology, 42, pp.131–160, Doi: 10.1007/s10694-006-7504-y, 2006.

[16] Bj*ö*rn Karlsson and James G. Quintiere, Enclosure Fire Dynamics, book, TH9195. K37, 693. 82-dc21, 1991.

[17] L. H. HU, R. HUO and H. B. WANG and R. X. YANG, experimental and numerical studies on longitudinal smoke temperature distribution upstream and downstream from the fire in a road tunnel, Journal of Fire Sciences, doi: 10.1177/0734904107062357, pp 23-43, 2007.

[18] ECCS, Fire Safety in Open Car Parks, Modern Fire Engineering, Technical Committee 3, nº75, European Convention for Constructional Steelwork, Brussels, Belgium, 1993.

[19] C. Haremza, A. Santiago and L. Simões da Silva, Design of Steel and Composite open car parks under fire, Advanced Steel Construction Vol. 9, No. 4, pp. 321-339, 2013.

[20] EN 1991-1-2 (2002), Eurocode 1: Actions on structures, Part 1-2: General actions - Actions on structures exposed to fire, European committee for standardization, November 2002 .

[21] Cansortium Steel prost, Fire guideline Design and Examples, demo project Fp7, STEELPROST - Innovative Fire Protective Coatings For Steel Structures, ISBN 978-989-99226-2-4, CMM. Portuguese association for steel and composite construction, October 2015.

[22] Walter W. Jones, State of The Art In Zone Modelling of Fires, International Fire Protection Seminar, 9th. Engineering Methods for Fire Safety, pp 89-126, May 25-26, 2001, Munich, Germany, ISBN 3-89288-133-2.

[23] L. Y. Cooper, A. Woodhouse, The Buoyant Plume-Driven Adiabatic Ceiling Temperature Revisited, journal of Heat Transfer, pp 8228-26, Vol. 108, November 1986

[24] Bin Zhao & Joël Kruppa, Structural Behaviour of an Open Car Park Under Real Fire Scenarios, Second International Workshop « Structures in Fire » Christchurch, March 2002.

[25] Nils Johansson, Jonathan Wahlqvist & Patrick Van Hees, Simple Ceiling jet Correlation Derived from Numerical Experiments, Proceedings of the 13th International Interflam Conference, pp.61-72, 01/01/2013.

[26] Yuguang Li, Assessment of Vehicle Fires in New Zealand Parking Buildings, master thesis of Engineering in fire engineering, Research Report 04/2, May 2004

[27] James G. Quintiere, Fundamentals of Fire Phenomena, Chap 11, Compartment Fires, ISBN: 978-0-470-09113-5, March 2006.

[28] W. K. Chow, Numerical Studies on the Transient Behaviour of a Fire Plume and Ceiling Jet, Mathl. Comput. Modelling Vol. 17, No 9, pp. 71-79, MAY1993.

[29] Cooper Fire, The Fire Installers Mate, A guide to fire alarm systems design BS 5839 Part 1, 2002.

[30] David D. Evans, ceiling jet flows, SFPE Handbook of Fire Protection Engineering, 2nd Edition, Chapter 4, Section 2, pp 2/32-2/39, 1995.

[31] Gunnar Heskestad, Michael. Delichatsios, Update: The Initial Convective Flow in Fire, Fire Safety Journal, volume 15, issue 6, pp 471-475, 1989.

[32] Gunnar Heskestad, Michael. Delichatsios, The Initial Convective Flow In Fire, Symposium (International) on Combustion, volume 17, issue 1, pp 1113-1123, 1979.

[33] Richard D. Peacock, CFAST – Consolidated Fire and Smoke Transport, Version 7, Volume 4: Configuration Management, November 2015.

[34] Nathaniel Michael Knop, Thermal analysis of a fireplace using ANSYS, Graduate Theses and Dissertations, Paper 10496, 2009.

[35] EN 1992-1-2, Eurocode 2: Design of concrete structures - Part 1-2: General rules - Structural fire design, European committee for standardization, December 2004.

Annex A: Information about fire scenarios

Table1- Definition of car categories (classes)

Type	Category1	Category 2	Category 3	Category 4	Category 5
Peugeot	106	306	406	605	806
Renault	Twingo-Clio	Mégane	Laguna	Safrane	Espace
Citroën	Saxo	ZX	Xantia	XM	Evasion
Ford	Fiesta	Escort	Mondeo	Scorpion	Galaxy
Opel	Corsa	Astra	Vectra	Omega	Frontera
Fiat	Punto	Bravo	Tempra	Croma	Ulysse
Volkswagen	Polo	Golf	Passat	//	Sharan

Table 2- Car mass, mass of combustible materials, theoretical energy of combustion

Class	Car mass [kg]	Mass of combustible materials [kg]	theoretical energy of combustion
1	850	200	6000
2	1000	250	7500
3	1250	320	9500
4	1400	400	12000
5	1400	400	12000

Table3- Rough Measure of Energy Released or Generated from Various Sources[15]

BURNING OF OBJECTS	HRR
A burning cigarette	5 W
A typical light bulb	60W
A human being at normal exertion	60W
A burning wastepaper basket	100 kW
A burning $1m^2$ pool of gasoline	2.5 MW
Burning wood pallets, stacked to the height of 3 m	7 MW
Burning polystyrene jars, in cartons, 2 m^2, 4.9 m high	30–40 MW
Output from a typical reactor at a Nuclear Power Plant	500–1000 MW

Annex B: Results from correlative models

The numerical values of the maximum temperature and velocity of the gases near the ceiling getting from the correlative models of burning car (all classes) with data of L_f and Z_0 are shown below

1- Alpert's results

Table 4- T_{max} and V_{max} getting form Alpert's correlations

	Class 1		Class 2		Class3		Class4		Class5	
	$L_f[m]$	$Z_0[m]$	$L_f[m]$	$Z_0[m]$	$L_f[m]$	$Z_0[m]$	$L_f[m]$	$Z_0[m]$	$L_f[m]$	$Z_0[m]$
	5.2	0.51	5.86	0.75	6.64	1.03	7.49	1.33	7.49	1.33
r/H	$T_{max}[°c]$	$V_{max}[\frac{m}{s}]$	$T_{max}[°c]$	$V_{max}[\frac{m}{s}]$	$T_{max}[°c]$	$V_{max}[\frac{m}{s}]$	$T_{max}[°c]$	$V_{max}[\frac{m}{s}]$	$T_{max}[°c]$	$V_{max}[\frac{m}{s}]$
0.00	994	11.98	1150	12.90	1343	13.96	1566	15.09	1566	15.09
0.37	621	5.62	718	6.06	837	6.55	974	7.08	974	7.08
0.74	399	3.16	460	3.40	535	3.68	621	3.98	621	3.98
1.11	309	2.25	355	2.42	413	2.62	479	2.84	479	2.84
1.48	259	1.77	297	1.91	344	2.06	399	2.23	399	2.23
1.85	226	1.47	259	1.58	299	1.71	346	1.85	346	1.85

2- Cooper's results

Table5- T_{max} and V_{max} getting form Cooper's correlations

	Class 1		Class 2		Class3		Class4		Class5	
	$L_f[m]$	$Z_0[m]$	$L_f[m]$	$Z_0[m]$	$L_f[m]$	$Z_0[m]$	$L_f[m]$	$Z_0[m]$	$L_f[m]$	$Z_0[m]$
	5.2	0.51	5.86	0.75	6.64	1.03	7.49	1.33	7.49	1.33
r/H	$T_{max}[°c]$	$V_{max}[\frac{m}{s}]$	$T_{max}[°c]$	$V_{max}[\frac{m}{s}]$	$T_{max}[°c]$	$V_{max}[\frac{m}{s}]$	$T_{max}[°c]$	$V_{max}[\frac{m}{s}]$	$T_{max}[°c]$	$V_{max}[\frac{m}{s}]$
0.00	1640	0.00	1900	0.00	2220	0.00	2591	0.00	2591	0.00
0.37	861	9.67	996	10.42	1162	11.27	1355	12.19	1355	12.19
0.74	457	4.51	527	4.86	613	5.26	713	5.69	713	5.69
1.11	323	2.89	372	3.11	432	3.37	501	3.64	501	3.64
1.48	255	2.11	293	2.27	340	2.45	394	2.65	394	2.65
1.85	213	1.65	244	1.77	283	1.92	327	2.07	327	2.07

3- Heskestad and Delichatsios's results

Table6- T_{max} and V_{max} getting form Heskestad and Delichatsios correlations

	Class 1		Class 2		Class3		Class4		Class5	
	$L_f[m]$	$Z_0[m]$	$L_f[m]$	$Z_0[m]$	$L_f[m]$	$Z_0[m]$	$L_f[m]$	$Z_0[m]$	$L_f[m]$	$Z_0[m]$
	5.2	0.51	5.86	0.75	6.64	1.03	7.49	1.33	7.49	1.33
r/H	$T_{max}[°c]$	$V_{max}[\frac{m}{s}]$	$T_{max}[°c]$	$V_{max}[\frac{m}{s}]$	$T_{max}[°c]$	$V_{max}[\frac{m}{s}]$	$T_{max}[°c]$	$V_{max}[\frac{m}{s}]$	$T_{max}[°c]$	$V_{max}[\frac{m}{s}]$
0.00	1492	12.04	1728	13.47	2019	15.34	2356	17.71	2356	17.71
0.37	796	9.24	920	9.95	1074	10.76	1251	11.64	1251	11.64
0.74	524	5.97	605	6.43	705	6.96	820	7.52	820	7.52
1.11	384	4.62	443	4.98	515	5.39	598	5.82	598	5.82
1.48	301	3.86	346	4.15	401	4.49	465	4.86	465	4.86
1.85	246	3.35	282	3.61	326	3.91	378	4.22	378	4.22

4- Maximum temperature comparison between correlative models

A percentages of error between the results of the maximum temperature from the correlative models, taking the Alpert's results as reference are presented in Tables below :

Table 7- Comparison between correlative models for T_{max} of class 1

r/H	Alpert T_{max}[°C]	Cooper T_{max}[°C]	Error [%]	Heskestad T_{max}[°C]	Error [%]
0	994	1640	|64.9|	1492	|50.1|
0.37	621	861	|38.6|	796	|28.1|
0.74	399	457	|14.5|	524	|31.4|
1.11	309	323	|4.6	384	|24.3|
1.48	259	255	|1.3|	301	|16.2|
1.85	226	213	|5.4|	246	|8.8|

Table 8- Comparison between correlative models for T_{max} of class 2

r/H	Alpert T_{max}[°C]	Cooper T_{max}[°C]	Error [%]	Heskestad T_{max}[°C]	Error [%]
0	1150	1900	|65.1|	1728	|50.2|
0.37	718	996	|38.7|	920	|28.2|
0.74	460	527	|14.6|	605	|31.7|
1.11	355	372	|4.6|	443	|24.5|
1.48	297	293	|1.3|	346	|16.4|
1.85	259	244	|5.5|	282	|8.9|

Table 9- Comparison between correlative models for T_{max} of class 3

r/H	Alpert T_{max}[°C]	Cooper T_{max}[°C]	Error [%]	Heskestad T_{max}[°C]	Error [%]
0	1343	2220	|65.3|	2019	|50.3|
0.37	837	1162	|38.9|	1074	|28.3|
0.74	535	613	|14.7|	705	|31.9|
1.11	413	432	|4.6|	515	|24.8|
1.48	344	340	|1.3|	401	|16.5|
1.85	299	283	|5.6|	326	|9.0|

Table 10- Comparison between correlative models for T_{max} of class 4,5

r/H	Alpert T_{max}[°C]	Cooper T_{max}[°C]	Error [%]	Heskestad T_{max}[°C]	Error [%]
0	1566	2591	|65.4|	2356	|50.4|
0.37	974	1355	|39.0|	1251	|28.4|
0.74	621	713	|14.8|	820	|32.0|
1.11	479	501	|4.7|	598	|24.9|
1.48	399	394	|1.3|	465	|16.7|
1.85	346	327	|5.6|	378	|9.1|

5- Maximum velocity comparison between correlative models

A percentages of error between the results of the maximum velocity from the correlative models ,taking the Alpert's results as reference are presented in Tables below :

Table 11- Comparison between correlative models for V_{max} of class 1

r/H	Alpert $V_{\max}[\frac{m}{s}]$	Cooper $V_{\max}[\frac{m}{s}]$	Error [%]	Heskestad $V_{\max}[\frac{m}{s}]$	Error [%]
0	11.98			12.04	|0.5|
0.37	5.62	9.67	|72.0|	9.24	|64.2|
0.74	3.16	4.51	|43.0|	5.97	|89.1|
1.11	2.25	2.89	|28.3|	4.62	|105.4|
1.48	1.77	2.11	|18.8|	3.86	|117.7|
1.85	1.47	1.65	|12.0|	3.35	|127.8|

Table 12- Comparison between correlative models for V_{max} of class 2

r/H	Alpert $V_{\max}[\frac{m}{s}]$	Cooper $V_{\max}[\frac{m}{s}]$	Error [%]	Heskestad $V_{\max}[\frac{m}{s}]$	Error [%]
0	12.90			13.47	|4.4|
0.37	6.06	10.42	|72.0|	9.95	|64.2|
0.74	3.40	4.86	|43.0|	6.43	|89.1|
1.11	2.42	3.11	|28.3|	4.98	|105.4|
1.48	1.91	2.27	|18.8|	4.15	|117.7|
1.85	1.58	1.77	|12.0|	3.61	|127.8|

Table 13- Comparison between correlative models for V_{max} of class 3

r/H	Alpert $V_{\max\,[\frac{m}{s}]}$	Cooper $V_{\max\,[\frac{m}{s}]}$	Error [%]	Heskestad $V_{\max\,[\frac{m}{s}]}$	Error [%]
0	13.96			15.34	|9.9|
0.37	6.55	11.27	|72.0|	10.76	|64.2|
0.74	3.68	5.26	|43.0|	6.96	|89.1|
1.11	2.62	3.37	|28.3|	5.39	|105.4|
1.48	2.06	2.45	|18.8|	4.49	|117.7|
1.85	1.71	1.92	|12.0|	3.91	|127.8|

Table 14- Comparison between correlative models for V_{max} of class 4,5

r/H	Alpert $V_{\max\,[\frac{m}{s}]}$	Cooper $V_{\max\,[\frac{m}{s}]}$	Error [%]	Heskestad $V_{\max\,[\frac{m}{s}]}$	Error [%]
0	15.09			17.71	|17.4|
0.37	7.08	12.19	|72.0|	11.64	|64.2|
0.74	3.98	5.69	|43.0|	7.52	|89.1|
1.11	2.84	3.64	|28.3|	5.82	|105.4|
1.48	2.23	2.65	|18.8|	4.86	|117.7|
1.85	1.85	2.07	|12.0|	4.22	|127.8|

Annex C: Results from CFAST simulation

1- Positions of targets and heat alarm in CFAST simulation

The following tables show the position of each one of six targets and heat alarms which are situated on the ceiling, from these positions results of temperature and velocity were calculated for each radial position.

Table 15- Data of the six targets in the compartment

Target Number	Compartment	X position[m]	Y position[m]	Z position[m]
Targ 1	OPEN_ CAR_ PARKING	5	5	2.9
Targ 2	OPEN_ CAR_ PARKING	6	5	2.9
Targ 3	OPEN_ CAR_ PARKING	7	5	2.9
Targ 4	OPEN_ CAR_ PARKING	8	5	2.9
Targ 5	OPEN_ CAR_ PARKING	9	5	2.9
Targ 6	OPEN_ CAR_ PARKING	10	5	2.9

Table 16- Data of the six heat alarms in compartment

N° of heat alarm	Compartment	Position X [m]	Position Y [m]	Position Z [m]
Heat alarm 1	OPEN_ CAR_ PARKING	5	5	2.97
Heat alarm 2	OPEN_ CAR_ PARKING	4	5	2.97
Heat alarm 3	OPEN_ CAR_ PARKING	3	5	2.97
Heat alarm 4	OPEN_ CAR_ PARKING	2	5	2.97
Heat alarm 5	OPEN_ CAR_ PARKING	1	5	2.97
Heat alarm 6	OPEN_ CAR_ PARKING	0	5	2.97

Another simulation was done using Copper for the material of targets and heat alarms to verify if there was any difference in results, when compared to steel material. The results with copper and steel agree well and are presented on the following tables:

Table17- comparison between temperature of targets and sensors using Copper material

t	Tar 1	Tar 2	Tar 3	Tar 4	Tar 5	Tar 6	Sen 1	Sen 2	Sen 3	Sen 4	Sen 5	Sen 6	E 1	E 2	E 3	E 4	E 5	E 6
min	°C	°C	°C	°C	°C	°C	°C	°C	°C	°C	°C	°C	%	%	%	%	%	%
0	20	20	20	20	20	20	20	20	20	20	20	20	0	0	0	0	0	0
4	419	355	281	238	210	190	406	355	281	238	210	190	3	0	0	0	0	0
16	425	361	288	244	216	196	412	361	288	244	216	196	3	0	0	0	0	0
24	940	832	657	553	486	439	940	832	657	553	486	439	0	0	0	0	0	0
25	945	843	679	582	519	475	945	843	679	582	519	475	0	0	0	0	0	0
27	934	833	655	551	482	435	934	833	655	551	482	435	0	0	0	0	0	0
38	334	290	239	210	190	177	325	290	239	210	190	177	3	0	0	0	0	0
70	32	32	32	32	32	32	32	32	32	32	32	32	0	0	0	0	0	0

Table18- comparison between temperature of targets and sensors using Steel material

t	Tar 1	Tar 2	Tar 3	Tar 4	Tar 5	Tar 6	Sen 1	Sen 2	Sen 3	Sen 4	Sen 5	Sen 6	E 1	E 2	E 3	E 4	E 5	E 6
min	°C	°C	°C	°C	°C	°C	°C	°C	°C	°C	°C	°C	%	%	%	%	%	%
0	20	20	20	20	20	20	20	20	20	20	20	20	0	0	0	0	0	0
4	417	354	281	238	210	191	404	354	281	238	210	191	3	0	0	0	0	0
16	427	354	290	247	219	199	413	354	290	247	219	199	3	0	0	0	0	0
24	949	841	666	563	496	449	949	841	666	563	496	449	0	0	0	0	0	0
25	955	854	690	593	530	486	955	854	690	593	530	486	0	0	0	0	0	0
27	951	841	662	557	489	441	951	841	662	557	489	441	0	0	0	0	0	0
38	315	271	220	191	171	158	306	271	220	191	171	158	3	0	0	0	0	0
70	26	26	26	26	26	26	26	26	26	26	26	26	0	0	0	0	0	0

Where t is the time in minutes, Tar is the abbreviation for the target, Sen the abbreviation for the sensor, and E refers to the error calculated between the surrounding gas temperature of the sensor and the surrounding gas temperature of the target.

2- Maximum temperature from CFAST numerical simulation

for the maximum surrounding gas temperature derived from CFAST simulation for all car classes are presented in next table.

Table 19 - results of CFAST simulation for maximum temperature

r/H	Class 1 T_{max} [°C]	Class 2 T_{max} [°C]	Class 3 T_{max} [°C]	Class 4 T_{max} [°C]	Class 5 T_{max} [°C]
0	935.87	939.16	953.85	949.30	949.30
0.37	802.67	810.67	834.15	833.29	833.29
0.74	625.18	639.45	674.65	678.69	678.69
1.11	523.83	541.68	583.57	590.42	590.42
1.48	459.24	479.37	525.52	534.16	534.16
1.85	414.92	436.63	485.70	495.56	495.56

3- Maximum velocity from CFAST numerical simulation

In the following table the results of maximum velocity from CFAST simulation for all car classes are presented

Table 20- results of CFAST simulation for maximum temperature

r/H	Class 1 V_{max} [m/s]	Class 2 V_{max} [m/s]	Class 3 V_{max} [m/s]	Class 4 V_{max} [m/s]	Class 5 V_{max} [m/s]
0	10.93	11.52	12.13	12.85	12.85
0.37	8.01	8.55	9.23	9.97	9.97
0.74	4.91	5.29	5.72	6.18	6.18
1.11	3.71	4.00	4.32	4.67	4.67
1.48	3.04	3.28	3.55	3.83	3.83
1.85	2.61	2.81	3.04	3.29	3.29

4- Maximum temperature comparison between the correlations and CFAST

A relative deference between results of each one of the correlative models and CFAST simulation for the maximum temperature in each radial position containing all vehicles classes are shown in the tables below.

Table21- Comparison of T_{max}between correlative models and CFAST for class 1

r/H	CFAST T_{max}[°C]	Alpert T_{max}[°C]	Error %	Cooper T_{max}[°C]	Error %	Heskestad T_{max}[°C]	Error %
0	935.87	994	|5.9|%	1640	|75.2|%	1492	|59.4|%
0.37	802.67	621	|29.2|%	861	|7.3|%	796	|0.9|%
0.74	625.18	399	|56.8|%	457	|27.0|%	524	|16.2|%
1.11	523.83	309	|69.5|%	323	|38.3|%	384	|26.6|%
1.48	459.24	259	|77.6|%	255	|44.4|%	301	|34.6|%
1.85	414.92	226	|83.9|%	213	|48.6|%	246	|40.8|%

Table22- Comparison of T_{max}between correlative models and CFAST for class 2

r/H	CFAST T_{max}[°C]	Alpert T_{max}[°C]	Error %	Cooper T_{max}[°C]	Error %	Heskestad T_{max}[°C]	Error %
0	939.16	1150	|18.4|%	1900	|102.3|%	1728	|84.0|%
0.37	810.67	718	|12.9|%	996	|22.8|%	920	|13.5|%
0.74	639.45	460	|39.1|%	527	|17.7|%	605	|5.4|%
1.11	541.68	355	|52.4|%	372	|31.4|%	443	|18.3|%
1.48	479.37	297	|61.5|%	293	|38.9|%	346	|27.9|%
1.85	436.63	259	|68.8|%	244	|44.0|%	282	|35.5|%

Table23- Comparison of T_{max}between correlative models and CFAST for class 3

r/H	CFAST T_{max}[°C]	Alpert T_{max}[°C]	Error %	Cooper T_{max}[°C]	Error %	Heskestad T_{max}[°C]	Error %
0	953.85	1343	|40.8|%	2220	|132.8|%	2019	|111.7|%
0.37	834.15	837	|0.3|%	1162	|39.3|%	1074	|28.7|%
0.74	674.65	535	|20.8|%	613	|9.1|%	705	|4.5|%
1.11	583.57	413	|29.3|%	432	|26.0|%	515	|11.8|%
1.48	525.52	344	|34.5|%	340	|35.4|%	401	|23.7|%
1.85	485.70	299	|38.4|%	283	|41.8|%	326	|32.8|%

Table24- Comparison of T_{max}between correlative models and CFAST for class 4,5

r/H	CFAST T_{max}[°C]	Alpert T_{max}[°C]	Error %	Cooper T_{max}[°C]	Error %	Heskestad T_{max}[°C]	Error %
0	949.30	1566	|39.4|%	2591	|173.0|%	2356	|148.2|%
0.37	833.29	974	|14.5|%	1355	|62.6|%	1251	|50.2|%
0.74	678.69	621	|9.2|%	713	|5.1|%	820	|20.9|%
1.11	590.42	479	|23.3|%	501	|15.1|%	598	|1.3|%
1.48	534.16	399	|33.9|%	394	|26.3|%	465	|12.9|%
1.85	495.56	346	|43.0|%	327	|34.0|%	378	|23.7|%

5- Maximum velocity comparison between the correlations and CFAST

A relative deference between results of each one of the correlative models and CFAST simulation for the maximum velocity in each radial position containing all vehicles classes are shown in the tables below:

Table25- Comparison of V_{max}between correlative models and CFAST for class 1

r/H	CFAST V_{max}[m/s]	Alpert V_{max}[m/s]	Error %	Cooper V_{max}[m/s]	Error %	Heskestad V_{max}[m/s]	Error %
0	10.93	11.98	|9.5|%			12.04	|10.1|%
0.37	8.01	5.62	|29.8|%	9.67	|72.0|%	9.24	|15.3|%
0.74	4.91	3.16	|35.7|%	4.51	|43.0|%	5.97	|21.6|%
1.11	3.71	2.25	|39.3|%	2.89	|28.3|%	4.62	|24.6|%
1.48	3.04	1.77	|41.8|%	2.11	|18.8|%	3.86	|26.8|%
1.85	2.61	1.47	|43.6|%	1.65	|12.0|%	3.35	|28.5|%

Table26- Comparison of V_{max}between correlative models and CFAST for class 2

r/H	CFAST V_{max}[m/s]	Alpert V_{max}[m/s]	Error %	Cooper V_{max}[m/s]	Error %	Heskestad V_{max}[m/s]	Error %
0	11.52	12.90	|12.0|%			13.47	|17.0|%
0.37	8.55	6.06	|29.2|%	10.42	|21.8|%	9.95	|16.3|%
0.74	5.29	3.40	|35.7|%	4.86	|8.0|%	6.43	|21.6|%
1.11	4.00	2.42	|39.3|%	3.11	|22.1|%	4.98	|24.6|%
1.48	3.28	1.91	|41.8|%	2.27	|30.8|%	4.15	|26.8|%
1.85	2.81	1.58	|43.6|%	1.77	|36.8|%	3.61	|28.5|%

Table27- Comparison of V_{max}between correlative models and CFAST for class 3

r/H	CFAST V_{max}[m/s]	Alpert V_{max}[m/s]	Error %	Cooper V_{max}[m/s]	Error %	Heskestad V_{max}[m/s]	Error %
0	12.13	13.96	|15.1|%			15.34	|26.5|%
0.37	9.23	6.55	|29.0|%	11.27	|22.2|%	10.76	|16.7|%
0.74	5.72	3.68	|35.7|%	5.26	|8.0|%	6.96	|21.6|%
1.11	4.32	2.62	|39.3|%	3.37	|22.1|%	5.39	|24.6|%
1.48	3.55	2.06	|41.8|%	2.45	|30.8|%	4.49	|26.8|%
1.85	3.04	1.71	|43.6|%	1.92	|36.8|%	3.91	|28.5|%

Table28- Comparison of V_{max}between correlative models and CFAST for class 4,5

r/H	CFAST $V_{max}[m/s]$	Alpert $V_{max}[m/s]$	Error %	Cooper $V_{max}[m/s]$	Error %	Heskestad $V_{max}[m/s]$	Error %
0	12.85	15.09	|17.4|%			17.71	|37.9|%
0.37	9.97	7.08	|29.0|%	12.19	|22.2|%	11.64	|16.7|%
0.74	6.18	3.98	|35.7|%	5.69	|8.0|%	7.52	|21.6|%
1.11	4.67	2.84	|39.3|%	3.64	|22.1|%	5.82	|24.6|%
1.48	3.83	2.23	|41.8|%	2.65	|30.8|%	4.86	|26.8|%
1.85	3.29	1.85	|43.6|%	2.07	|36.8|%	4.22	|28.5|%

Annex D: Results from ANSYS fluent simulation

Table 29 represents the values of the maximum velocity of car class one from CFD simulation and Table 30 represents the values of the maximum temperature near the ceiling of car class one from CFD simulation.

Table 29- Maximum velocity from ANSYS fluent

Target position r/H	V_{max} [m/s]
0	0.131
0.37	0.050
0.74	0.052
1.11	0.043
1.48	0.089
1.85	0.090
0	0.131

Table 30- Maximum temperature from ANSYS fluent

Target position r/H	T_{max} [K]
0	392.90
0.37	396.56
0.74	396.34
1.11	397.99
1.48	393.21
1.85	354.85
0	392.90